[American Journal of Science, Vol. 319, September, 2019, P. 582-630, DOI 10.2475/07.2019.03]

FORMATION AND OROGEN-PARALLEL TRANSPORT OF THE DADEVILLE COMPLEX, ALABAMA, USA: IMPLICATIONS FOR THE TACONIAN OROGENY IN THE SOUTHERN APPALACHIANS

CHONG MA*,†, DANE S. VanDERVOORT**, MARK G. STELTENPOHL*, and JOSHUA J. SCHWARTZ***

ABSTRACT. The Taconian orogeny in the southern Appalachians has not been fully understood due to a lack of connections among the various Ordovician lithotectonic units. Zircon U-Pb ages obtained by laser ablation-sector field-inductively coupled plasma-mass spectrometry from arc-related meta-igneous rocks comprising the Dadeville Complex in the Alabama Inner Piedmont (southeastern USA) indicate continuous arc magmatism at *ca.* 465 to 454 Ma following an earlier phase at *ca.* 480 Ma. These meta-igneous rocks, in conjunction with literature data, are interpreted to represent remnants of the Taconian-aged Dadeville arc, which formed on a rifted Laurentian crustal block. Metamorphic overgrowths on zircons from the meta-igneous rocks of the Dadeville Complex and a schist of the uppermost Emuckfaw Group, along with zircons from a felsic melt in the Agricola Schist (metasedimentary cover of the Dadeville arc), reveal a regional metamorphic event at *ca.* 408 to 394 Ma. Dominant 1300 to 900 Ma zircons in the Agricola Schist suggest that the Dadeville Complex sedimentary rocks were primarily sourced from Laurentia.

The depocenters of the Taconian bentonites and clastic wedge and the location of peak Taconian metamorphism, based on literature data, suggest that the locus of the Taconian orogeny in the southern Appalachians was located at the Tennessee embayment. Early Devonian metamorphism/magmatism, Taconian arc rocks, and detrital zircon provenances are shared by the Dadeville Complex at the Alabama promontory and Taconian assemblages at the Tennessee embayment, which, in conjunction with the southwest-directed extrusion/shear structures found in the Inner Piedmont and uppermost eastern Blue Ridge from North Carolina to Alabama, suggest that the Dadeville arc and its companion back-arc basin originally formed in the Tennessee embayment and were subsequently transported to the Alabama promontory along orogen-parallel shear zones likely associated with the Acadian-Neoacadian transpressional convergence. This study provides a palinspastic view of the original Taconian orogeny in the southern Appalachians.

Key words: zircon U-Pb geochronology, southern Appalachian orogen, original Taconic orogen

INTRODUCTION

Subduction of oceanic plates and amalgamation of crustal masses were likely occurring along most parts of the eastern Laurentian and western Baltic margins during the Middle Ordovician. The representative magmatic-metamorphic-depositional events are described as the Taconian (or Taconic) orogeny in the North American Appalachians (for example, van Staal and others, 2007; Hatcher, 2010; Pollock and others, 2012) and (ultra)high-pressure metamorphism of the Seve Nappe Complex in the Scandinavian Caledonides (for example, Brueckner and others, 2004; Majka and others, 2014; Klonowska and others, 2017). Although this continental-scale convergence of lithosphere is well-constrained in the Caledonides and in parts of the

* Department of Geosciences, Auburn University, Auburn, Alabama 36849, U.S.A.
** Geologic Investigations Program, Geological Survey of Alabama, Tuscaloosa, Alabama 35401, U.S.A.
*** Department of Geological Sciences, California State University Northridge, Northridge, California 91330, U.S.A.
† Corresponding author: macmachong@gmail.com

northern and central Appalachians, it is less so in the southern Appalachians of the southeastern USA.

The Taconian orogeny (~470–445 Ma) is classically known as the first major Paleozoic orogenic event prior to the Acadian-Neoacadian (~404–345 Ma) and Alleghanian (~325–260 Ma) orogenies that collectively created the Appalachian Mountain chain of eastern North America (Hatcher, 2010; Hatcher and others, 2017). The Taconian orogen is best preserved in the northern Appalachians as a system of allochthons containing remnant Cambrian–Middle Ordovician continental and oceanic arcs and sedimentary rocks that were accreted to eastern Laurentia during the late Cambrian to Ordovician (for example, Karabinos and others, 1998; van Staal and others, 2007), and in the central Appalachians as Cambrian–Ordovician continental slope and deep-water sedimentary rocks that were polydeformed and accreted during the Middle to Late Ordovician (for example, Wise and Ganis, 2009; Codegone and others, 2012).

In the southern Appalachians, the Taconian event and its associated effects are recorded by sedimentary sequences containing bentonites in the foreland (for example, Thomas, 1977; Tucker, 1992), high-grade metamorphism in the western Blue Ridge (for example, Corrie and Kohn, 2007; Dickson and others, 2019), granulite- and eclogite-facies metamorphism (for example, Moecher and others, 2004; Miller and others, 2010) and bimodal volcanism in the eastern Blue Ridge (for example, Tull and others, 2007; Holm-Denoma and Das, 2010), and granitic plutonism in the Inner Piedmont (fig. 1) (for example, Sagul, ms, 2016; Huebner and others, 2017; Tull and others, 2018). The tectonic setting for the formation of these assemblages of Ordovician rocks in a regional context, however, remains elusive. Thus, addressing this question will facilitate our understanding of the Taconian orogen in the southern Appalachians, and help elucidate the geodynamics of the eastern Laurentian margin during this period.

In the southernmost Appalachians, a medium- to high-grade Taconian arc fragment composed of volcanic-arc related felsic gneisses, mafic-ultramafic meta-igneous bodies, amphibolites, and schists has recently been recognized in the Inner Piedmont Dadeville Complex of Alabama and western Georgia (fig. 1B) (for example, VanDervoort and others, 2017; Tull and others, 2018). This Taconian arc has been interpreted to have formed within the Alabama promontory along the attenuated Laurentia margin, outboard of the Pine Mountain window (fig. 1B) (Farris and others, 2017; Tull and others, 2018). Herein we report new zircon U-Pb data from meta-igneous and metasedimentary rocks of the Dadeville Complex and adjacent eastern Blue Ridge, which, in conjunction with literature data and contextual regional geology, indicates that the Taconian arc of the Dadeville Complex originally formed at the Tennessee embayment and was later transported southwestward to the Alabama promontory possibly during the Acadian-Neoacadian orogeny. This interpretation integrates regional magmatic, metamorphic, structural, and stratigraphic data from the Inner Piedmont, Blue Ridge, and the foreland basin in order to advance our understanding of the formation and evolution of the Taconian orogen in the southern Appalachians.

GEOLOGIC BACKGROUND

Regional Geology

Evidence of the Taconian event is recorded in the southern Appalachians by a variety of rocks preserved across the orogen. In the foreland, the extensive easterly-derived Blount clastic wedge in the Valley and Ridge of Tennessee, Georgia, and Alabama (Thomas, 1977; Hatcher, 1989; Bayona and Thomas, 2006) contains multiple bentonite layers, such as the ~455 to 448 Ma Deicke and Millbrig bentonites, that document evidence of late Middle to early Late Ordovician volcanism (fig. 1A)

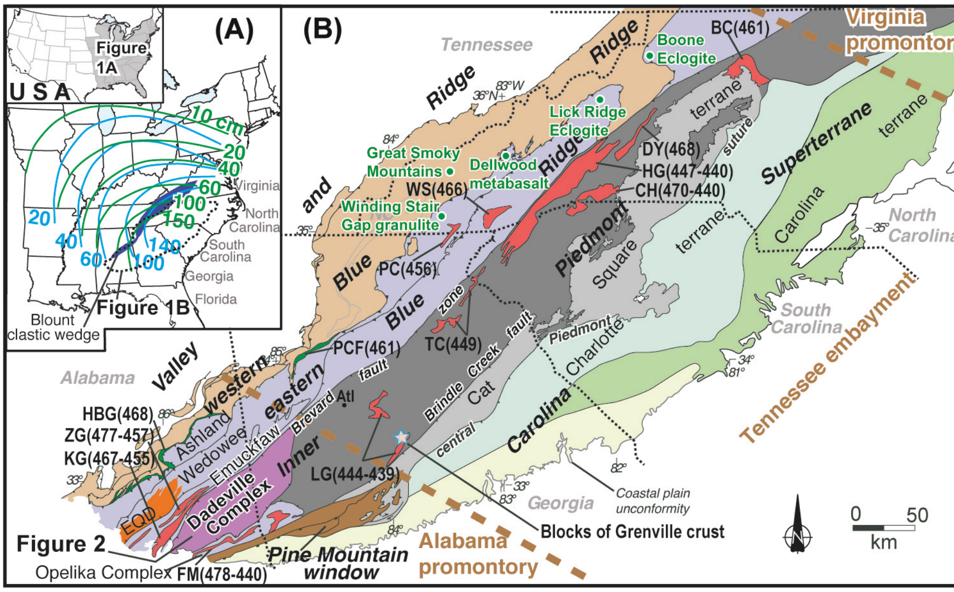

Fig. 1. (A) Thickness contours of the Ordovician Millbrig (blue) and Deicke (green) bentonites (Huff and others, 1996) along with distribution of the Blount clastic wedge (Ettensohn, 2004; Bayona and Thomas, 2006). (B) General geologic map of the southern Appalachian orogen (modified from Merschat and others, 2010; Hibbard and others, 2012; and Huebner and others, 2017). The locations of the Tennessee embayment and Virginia and Alabama promontories (in brown) are from Thomas (2006). Ordovician igneous rocks and ages (Ma): BC = Brooks Crossroads Granite, CH = Caesar's Head Granite, DY = Dysartsville Tonalite, FM = Farmville Metagranite, HG = Henderson Gneiss, HBG = Hillabee Greenstone, KG = Kowaliga Gneiss, LG = Lithonia Gneiss, PC = Persimmon Creek Gneiss, PCF = Pumpkinvine Creek Formation, TC = Toccoa Granite, WS = Whiteside Granite, ZG = Zana Gneiss (Miller and others, 2006; Tull and others, 2007; Holm-Denoma and Das, 2010; Hawkins and others, 2013; Sagul, ms, 2016; Huebner and others, 2017). EQD = Elkahatchee Quartz Diorite. Blocks of Grenville crust (star) are from Huebner and others (2017).

(Tucker, 1992; Haynes, 1994; Huff and others, 1996; Min and others, 2001). Detrital zircons from some units of the Blount clastic wedge contain significant ~460 Ma populations indicative of a Taconian source (for example, the Colvin Mountain Sandstone: Guerrero and others, 2016). In the hinterland, Taconian-aged peak metamorphism is documented by garnets in the western Blue Ridge of eastern Tennessee (Dickson and others, 2019); by overgrowths in monazite at Great Smoky in the western Blue Ridge of eastern Tennessee and western North Carolina (Corrie and Kohn, 2007); and by the Lick Ridge eclogite and Winding Stair Gap granulite in the eastern Blue Ridge of western North Carolina (fig. 1B) (Moecher and others, 2004; Miller and others, 2010).

Middle to Late Ordovician volcanism is documented by the bimodal meta-igneous rocks in the eastern Blue Ridge of Alabama and Georgia, such as the Hillabee Greenstone and Pumpkinvine Creek Formation, which yield back-arc basin geochemistry along with positive $\varepsilon Nd_{(i)}$ values for basaltic rocks and negative $\varepsilon Nd_{(i)}$ and $\varepsilon Hf_{(i)}$ values for some of the felsic rocks (for example, Tull and others, 2007; Holm-Denoma and Das, 2010). These volcanic rocks are linked with metasedimentary sequences of the eastern Blue Ridge in Alabama and Georgia (that is, the Wedowee-Emuckfaw-Dahlonega basin) and are collectively interpreted to represent an Early to Middle Ordovician back-arc basin (Tull and others, 2014, 2018).

Extensive Ordovician magmatism is documented by a variety of granitoid plutons in the eastern Blue Ridge and Inner Piedmont, which are commonly characterized

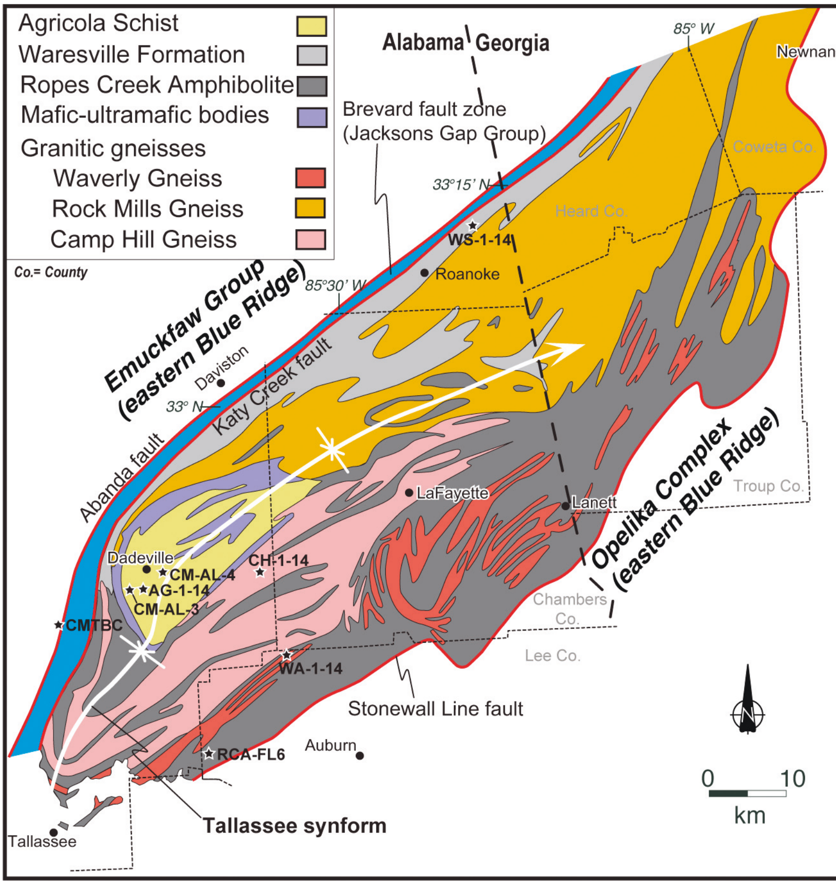

Fig. 2. Geologic map of the Dadeville Complex with sample locations (stars), modified after Bentley and Neathery (1970) and Osborne and others (1988). See figure 1 for map location.

by enriched large-ion lithophile elements and depleted high field-strength elements (fig. 1B) (for example, McDowell and others, 2002; Miller and others, 2006; Sagul, ms, 2016; Huebner and others, 2017; Tull and others, 2018). Of these plutons, those in the Persimmon Creek Gneiss and Dadeville Complex contain mafic rocks and have been interpreted to be remnants of a Taconian arc (for example, McDowell and others, 2002; Barineau and others, 2015; VanDervoort and others, 2015, 2017; Tull and others, 2018).

Dadeville Complex

Remnants of an Ordovician arc (for example, VanDervoort and others, 2015; Tull and others, 2018) are recognized in the allochthonous Dadeville Complex in the southernmost Appalachian Inner Piedmont of Alabama and western Georgia. The Dadeville Complex is a klippe of amphibolite- to granulite-facies metamorphosed volcanic, plutonic, and sedimentary rocks, which currently lies in the core of the shallowly northeast-plunging Tallassee synform and is separated from the structurally lower eastern Blue Ridge lithologies by the Brevard fault zone to the northwest and the Stonewall Line fault to the southeast (fig. 2) (Bentley and Neathery, 1970; Sears and others, 1981; Neilson and Stow, 1986; Higgins and others, 1988; Spell and Norrell, 1990; Steltenpohl and others, 1990). The eastern Blue Ridge is composed of continental margin siliciclastics (the Ashland Group) and Early—Middle Ordovician back-arc sequences (the Wedowee-Emuckfaw Groups and Opelika Complex in Alabama, fig. 1B) that were metamorphosed at middle- to upper-amphibolite facies (Steltenpohl, 2005; Tull and others, 2007; Holm-Denoma and Das, 2010; Tull and others, 2014; Barineau and others, 2015). These lithologies are intruded by Middle Ordovician–Mississippian-aged granitoids (for example, Steltenpohl and others, 2013; Sagul, ms, 2016).

The most prominent unit of the Dadeville Complex is the structurally lowest Ropes Creek Amphibolite, which consists of layered to massive amphibolite, lesser amounts of felsic and metasedimentary rocks, and minor ultramafic bodies (Bentley and Neathery, 1970; Neilson and Stow, 1986). The Ropes Creek Amphibolite is intruded by the Waverly Gneiss that consists of biotite-hornblende quartzofeldspathic gneiss containing thin layers of amphibolite, calc-silicate rock, garnet-bearing quartzite, and muscovite schist (fig. 2) (Osborne and others, 1988). Along the northwest margin of the Dadeville Complex, the Waresville Formation is characterized by fine-grained felsic schist, banded amphibolite, and metaquartzite that are interlayered at the centimeter to meter scale (fig. 2) (Bentley and Neathery, 1970). Two granitic gneiss batholiths, the Camp Hill Gneiss in the south and the Rock Mills Gneiss in the north, are present in the Dadeville Complex, as are two suites of mafic-ultramafic bodies, the Doss Mountain suite of olivine-bearing metanorite and metaorthopyroxenite and the Slaughters suite of metagabbro (fig. 2) (Neilson and Stow, 1986). The Camp Hill Gneiss is a well-foliated, low-potassium, biotite-rich trondhjemitic gneiss containing local amphibolite blocks and lenses, and the Rock Mills Gneiss (also known as the Chattasofka Creek Gneiss in Alabama and Franklin Gneiss in Georgia) is a strongly peraluminous, high-potassium, weak- to well-foliated leucogranitic gneiss containing local amphibolite bodies (Bentley and Neathery, 1970; Osborne and others, 1988; Neilson and others, 1997; VanDervoort, ms, 2016; Harstad, ms, 2017; Tull and others, 2018). The structurally highest unit, the Agricola Schist, is strongly deformed and is composed of biotite ± muscovite ± garnet ± sillimanite schist interlayered with thin (from 10 cm to <1 m) amphibolite (Bentley and Neathery, 1970; Osborne and others, 1988; Steltenpohl and others, 1990; Tull and others, 2014). The Agricola Schist is locally migmatitic and the Ropes Creek Amphibolite locally contains melts of tonalite and/or veins of plagiogranite (for example, Hall and Salpas, 1990; Tull and others, 2018).

Major element compositions of the meta-igneous rocks comprising the Dadeville Complex reveal that the mafic-ultramafic rocks are low-potassium tholeiites and the felsic rocks are generally peraluminous in composition (Neilson and Stow, 1986; Stevens and Tull, 2017; Tull and others, 2018). Trace element compositions show that the felsic assemblages are enriched in Rb, Ba, and Pb and are relatively depleted in Nb and Ta (Tull and others, 2018), and that the mafic-ultramafic assemblages, including the Ropes Creek Amphibolite and Doss Mountain-Slaughters suites, have trace element signatures characteristic of relatively enriched Rb, Ba, Th, U, Pb and depleted Nb, Ta, Zr, Hf (Stow and others, 1984; Tull and others, 2018). In addition, whole-rock Sm-Nd and zircon Lu-Hf isotopic data demonstrates that the Ropes Creek Amphibolite and Camp Hill Gneiss have depleted isotopic ratios ($\varepsilon Hf_{(i)} > 0$) whereas that the Rock Mills Gneiss and the Doss Mountain-Slaughters suites have evolved isotopic ratios ($\varepsilon Hf_{(i)}$ and $\varepsilon Nd_{(i)} < 0$) (Tull and others, 2018).

Recent zircon U-Pb data give crystallization ages of ~450 to 440 Ma for the Camp Hill Gneiss and Ropes Creek Amphibolite and 456 ± 9 Ma for the Chattasofka Creek Gneiss (that is, Rock Mills Gneiss) (Tull and others, 2018). A Rb-Sr whole-rock isochron age of 462 ± 4 Ma (MSWD = 1.9) was previously reported for the Franklin Gneiss (that is, Rock Mills Gneiss) in western Georgia (Seal and Kish, 1990). The ~450 to 440 Ma ages are interpreted as minimum estimates of the timing of magmatism due to possible lead loss as indicated by ~400 Ma and younger dates from the Camp Hill Gneiss and Ropes Creek Amphibolite (Tull and others, 2018). U-Pb dating of detrital zircons has shown dominant age populations of ~1200 to 900 Ma and ~500 to 440 Ma in the Agricola Schist and age populations clustered at ~1440 Ma, ~1130 Ma, ~940 Ma, and ~585 to 475 Ma in the metasedimentary rocks found near the base of the Ropes Creek Amphibolite (Tull and others, 2018).

The Dadeville Complex was metamorphosed at upper amphibolite- to lower granulite-facies conditions, as suggested by pressure-temperature estimates of up to 700 to 800 °C and 8 to 10 kbar reported for the Ropes Creek Amphibolite and Agricola Schist (Drummond and others, 1997). The high-grade metamorphism is also indicated by sillimanite-grade ductile shear zones within the Dadeville Complex (that is, the Dadeville and Agricola shear zones) that exhibit subhorizontal, northeast-trending stretching lineations postdating the peak metamorphism on the basis of overprinting relationships of mineral assemblages (Bittner and Neilson, 1990). These metamorphic conditions are distinctively higher than those documented in the underlying eastern Blue Ridge (for example, Goldberg and Steltenpohl, 1990; Tull and others, 2018).

U-Pb GEOCHRONOLOGY

Analytical Methods

Zircons were extracted following standard methods including pulverizing hand samples with a jaw crusher and disk mill, sieving, and separations by Frantz magnetic barrier separator and heavy liquids. Zircons were handpicked under a binocular microscope, mounted in epoxy, polished to half thickness, and imaged by a cathodoluminescence (CL) detector attached to a FEI Quanta 600 Scanning Electron Microscope. U-Pb analyses were performed using laser ablation-sector field-inductively coupled plasma-mass spectrometry at California State University, Northridge. New Wave/Lambda Physik and Teledyne Analyte G2 193 nm excimer lasers with a beam diameter of ~25 to 40 μm were utilized for zircon ablation. Sample aerosol was transported with He carrier gas through Teflon-lined tubing, where it was mixed with Ar gas before introduction to the plasma torch. Isotopes measured include ^{202}Hg, ^{204}(Pb+Hg), ^{206}Pb, ^{207}Pb, ^{208}Pb, ^{232}Th, ^{235}U, and ^{238}U. Analyses were conducted in a 40-second time resolved analysis mode. Each zircon analysis consisted of a 10-second integration on peaks with the laser on but not ablating (for backgrounds), 20 seconds of integrations with the laser firing on sample, and a 5 to 10 second delay to purge the previous sample and move to the next sample. Approximate depth of the ablation pit was ~20 to 30 μm. The primary standard, 91500 (1065 ± 5 Ma: Wiedenbeck and others, 1995), was analyzed every 5 to 10 analyses to correct for in-run fractionation of Pb/U and Pb isotopes. Secondary zircon standards, R33 (419.3 ± 0.4 Ma: Black and others, 2004), Temora-2 (416.8 ± 0.3 Ma: Black and others, 2004), and/or Plešovice (337.2 ± 0.4 Ma: Sláma and others, 2008) were analyzed within run to assess reproducibility of the data. Analyses of 91500, R33, Temora-2, and Plešovice during collection of unknown data presented here give weighted average ^{206}Pb/^{238}U ages of 1063 ± 4 Ma, 422.5 ± 2.9 Ma, 421.5 ± 3.1 Ma, and 339.2 ± 2.3 Ma, respectively. Corrections for minor amounts of common Pb in zircons were made using an age-appropriate Pb isotopic composition of Stacey and Kramers (1975) and measured ^{207}Pb/^{206}Pb and ^{238}U/^{206}Pb ratios following the methods of Tera and Wasserburg (1972). Analyses interpreted as having ~5 percent or greater contribution from common Pb were discarded from further consideration.

All the U-Pb ages were calculated and/or plotted using ^{206}Pb/^{238}U ages for grains younger than 1000 Ma (^{206}Pb/^{238}U age) and using ^{207}Pb/^{206}Pb ages for grains older than 1000 Ma (^{206}Pb/^{238}U age). For detrital zircons, a 10 percent discordance filter was applied and those grains with Th/U<0.1 (Appendix table A1) are not included in the age spectra. All the ages are reported with 2σ errors in the text and figures. Sample locations are shown in figure 2; GPS coordinates, sample descriptions, and full tabulations of the isotopic data are given in the Appendix in table A1.

Results

Zircons from four meta-igneous samples (RCA-FL6, fig. 3A; WS-1-14, fig. 3B; WA-1-14, fig. 3C; CH-1-14, fig. 3D) from the major units comprising the Dadeville Complex in Alabama were analyzed in order to constrain the timing of magmatism. Zircons from a felsic layer (CM-AL-3, fig. 3E) in the Agricola Schist were analyzed in order to constrain the timing of local magmatism and minimum depositional age of the Agricola Schist protoliths. Detrital zircons from three metasedimentary samples were dated to identify the sedimentary provenances of the Agricola Schist (fig. 3F) and uppermost Emuckfaw Group (fig. 3G) protoliths. Moreover, as metamorphic overgrowths of varying thickness (mostly ~5–30 μm) generally occur in subhedral/anhedral zircons, rare large (>40 μm) overgrowths were also dated in order to constrain the timing of metamorphism. Age data and CL images of representative zircons are shown in figures 4 and 5, and the results for individual samples are described below.

Zircons from a fine- to medium-grained, biotite-hornblende quartzofeldspathic gneiss (sample RCA-FL6) in the Ropes Creek Amphibolite are generally subhedral to anhedral and show oscillatory zoning in CL images (fig. 4A). Thirty-two of 39 analyses yield an error-weighted average $^{206}Pb/^{238}U$ age of 457.6 ± 5.1 Ma (MSWD = 0.7, fig. 4A). Zircons from a strongly foliated, very fine-grained, chlorite-sericite-biotite-hornblende schist in the Waresville Formation (sample WS-1-14) are generally subhedral and show oscillatory zoning in CL images (fig. 4B). Nineteen of 20 analyses give an error-weighted average $^{206}Pb/^{238}U$ age of 464.8 ± 3.8 Ma (MSWD = 1.7, fig. 4B). A moderately foliated, medium-grained, muscovite-hornblende-biotite quartzofeldspathic gneiss in the Waverly Gneiss (sample WA-1-14) contains zircons with oscillatory zoning in the interiors and a few relatively wide (~40–50 μm) metamorphic overgrowths (fig. 4C). Twenty-seven analyses were obtained in grain interiors and yield an error-weighted average $^{206}Pb/^{238}U$ age of 453.9 ± 6.5 Ma (MSWD = 1.4, fig. 4C). Analyses in the overgrowth domains of zircons from sample WA-1-14 have distinctively higher uranium contents (246–945 ppm, table A1) than that of the zircon interiors (<150 ppm, mostly <50 ppm, table A1). Five of 9 analyses of these overgrowths yield an error-weighted average $^{206}Pb/^{238}U$ age of 402.4 ± 11.5 Ma (MSWD = 1.9, fig. 4C). Zircons from a strongly foliated, medium- to coarse-grained, hornblende-muscovite-biotite granitic gneiss of the Camp Hill Gneiss (sample CH-1-14) also show oscillatory zoning in the interiors (fig. 4D). Twelve of 20 analyses yield an error-weighted average $^{206}Pb/^{238}U$ age of 480 ± 6.0 Ma (MSWD = 2.9, fig. 4D).

The felsic layer from the Agricola Schist (sample CM-AL-3) contains two types of zircons: medium to highly luminescent anhedral grains with uranium concentrations of <200 ppm (table A1), and dark subhedral grains with uranium concentrations of >3000 ppm (fig. 4E, table A1). Two of the medium to highly luminescent zircons are dated to be 901 ± 62 Ma and 912 ± 140 Ma, while 17 of the 22 high-uranium zircons yield an error-weighted average $^{206}Pb/^{238}U$ age of 393.7 ± 8.1 Ma (MSWD = 0.5, fig. 4E). There is no correlation between age and uranium concentration for the dark zircons.

Zircon grains from three samples were dated to reveal detrital zircon age-populations within metasedimentary rocks of the Dadeville Complex and its adjacent terrane: two from the Agricola Schist, and one from the uppermost Emuckfaw Group of the eastern Blue Ridge that has been overprinted by crystal-plastic shearing along the Brevard fault zone. The sample from the uppermost Emuckfaw Group (fig. 2) is a

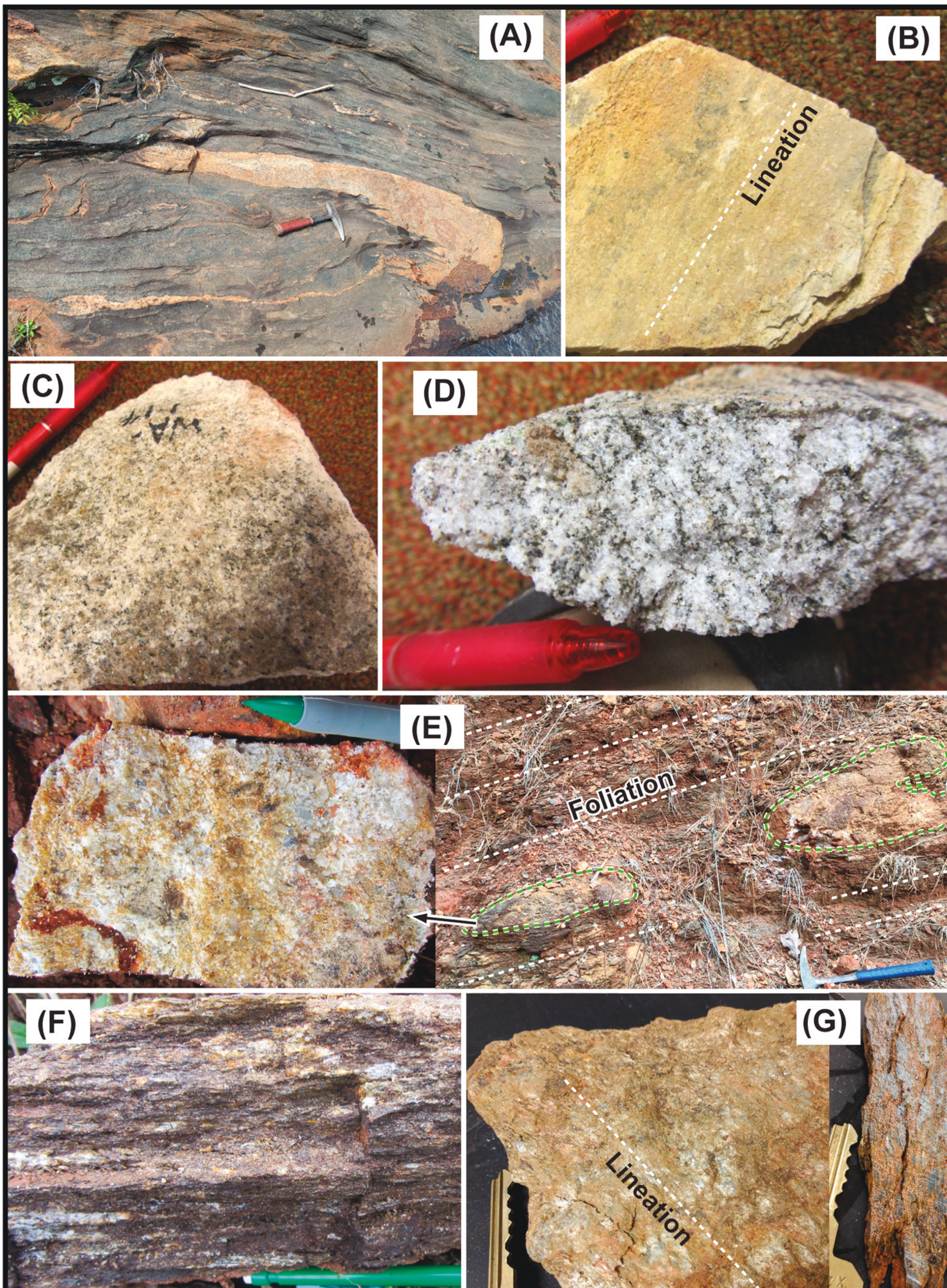

Fig. 3. Outcrops or hand specimens of the rocks analyzed in the current study. (A) Deformed felsic layer intruded in the Ropes Creek Amphibolite. (B) Fine-grained felsic schist from the Waresville Formation. (C) Felsic layer from the Waverly Gneiss. (D) Foliated granitic gneiss of the Camp Hill Gneiss. (E) Felsic boudins in the Agricola Schist (right) and hand specimen of a felsic boudin (left). (F) Typical fabrics of the Agricola Schist. (G) Strongly sheared button schist of the Emuckfaw Group immediately beneath the Brevard fault zone; view of foliation plane (left) and perpendicular to foliation (right). Hammer, pen, and key for scales.

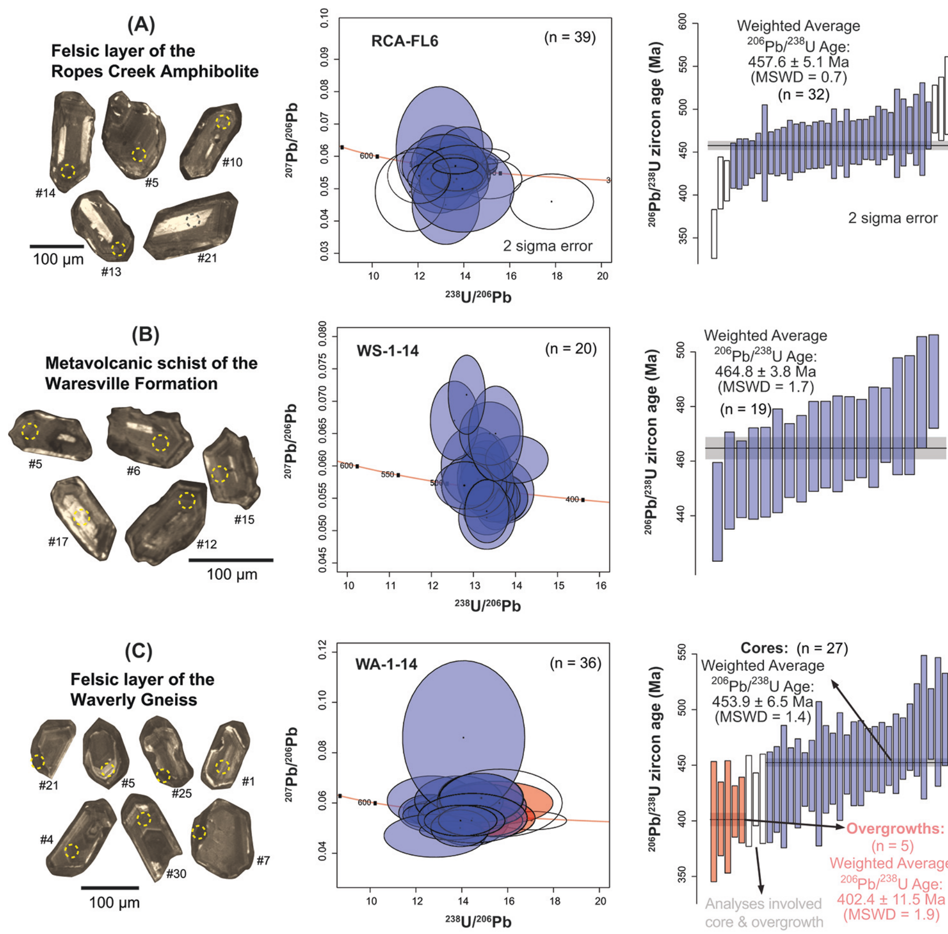

Fig. 4. Representative cathodoluminescence images and U-Pb ages of zircons from meta-igneous samples of the Dadeville Complex: (A) felsic layer of Ropes Creek Amphibolite, (B) Waresville Formation, (C) felsic layers of Waverly Gneiss, (D) Camp Hill Gneiss, (E) felsic boudin of Agricola Schist. For each sample, data are plotted on Tera-Wasserburg diagrams and weighted averages are calculated using IsoplotR (Vermeesch, 2018). n = number of analyses.

garnet-chlorite-muscovite-biotite schist exhibiting a strong S-C fabric (fig. 3G). Zircons from this sample display a strong metamorphic overprint, as shown by the common metamorphic overgrowths (fig. 5A) and high degree of discordance for a large portion of the data (table A1). Thirty-six analyses were performed in the interiors of zircons and 21 of them passed the discordance filter and give a Precambrian age population that discontinuously ranges from 2576 ± 67 Ma to 628 ± 56 Ma. Analyses made in the overgrowths of zircons define a Paleozoic population centered at about 408 Ma (weighted average = 408.2 ± 6.6 Ma, MSWD = 1.49, fig. 5A).

Both samples of the Agricola Schist are described as a medium- to coarse-grained muscovite-garnet-biotite schist. One hundred and one of 144 analyses of zircons from sample CM-AL-4 passed the discordance filter and yield ages ranging continuously within error from 1337 ± 88 Ma to 662 ± 28 Ma with an outlier of 466 ± 70 Ma (table A1). The detrital zircons from this sample are characteristic of a dominant 1300 to 900 Ma source (fig. 5B). One hundred and thirty-seven of 160 analyses of zircons from

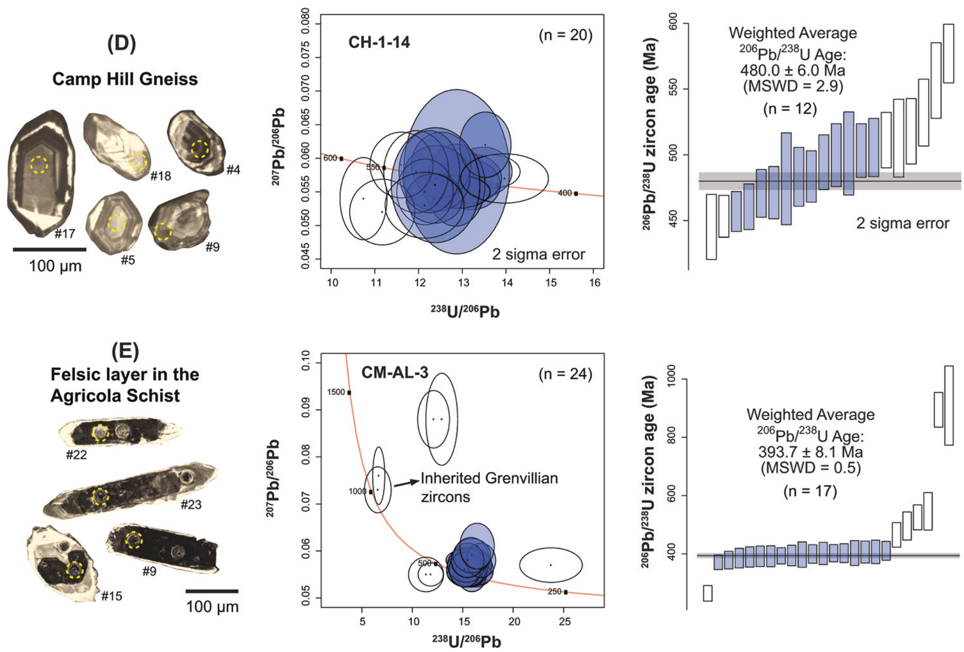

Fig. 4. (continued).

sample AG-1-14 passed the discordance filter and give ages ranging continuously within error from 1382 ± 43 Ma to 622 ± 16 Ma with four outliers of 2776 ± 50, 1605 ± 55, 493 ± 13, and 461 ± 18 Ma (table A1). Zircons from this sample are dominated by a 1300 to 850 Ma source (fig. 5C).

DISCUSSION

Nature of the Taconian Arc in the Dadeville Complex

The bulk of the Dadeville Complex (>50%) is composed of metamorphosed mafic and intermediate volcanic and volcanoclastic rocks (Bentley and Neathery, 1970; Sears and others, 1981; Neilson and Stow, 1986) that are intercalated with andesitic, dacitic, and/or granitic gneisses, minor metasedimentary rocks, and local mafic and ultramafic intrusive bodies (Neathery, 1968; Sears and others, 1981; Higgins and others, 1988). These lithologies, in combination with previously reported elemental, isotopic, and geochronologic data, indicate that the Dadeville Complex contains a Taconian-aged (for example, VanDervoort and others, 2015) volcanic arc terrane, herein termed the Dadeville arc, that was developed along the southeastern Laurentian margin (Farris and others, 2017; Tull and others, 2018).

The extensive Ropes Creek Amphibolite is interpreted to represent arc volcanism as part of the Dadeville arc (Tull and others, 2018). Because the Japan arc and Japan Sea back-arc basin system has been proposed to be the present-day analogy of the Taconian orogen in the southern Appalachians (Tull and others, 2012; Barineau and others, 2015), we compare trace element compositions of basaltic rocks between the Ropes Creek Amphibolite, the Japan frontal/rear arc, and the Japan Sea back-arc basin in figure 6. The enriched Rb, Ba, Th, U, and Pb and depleted Nb, Ta, Zr, and Hf of the basaltic rocks of the Ropes Creek Amphibolite (Stow and others, 1984; Tull and others,

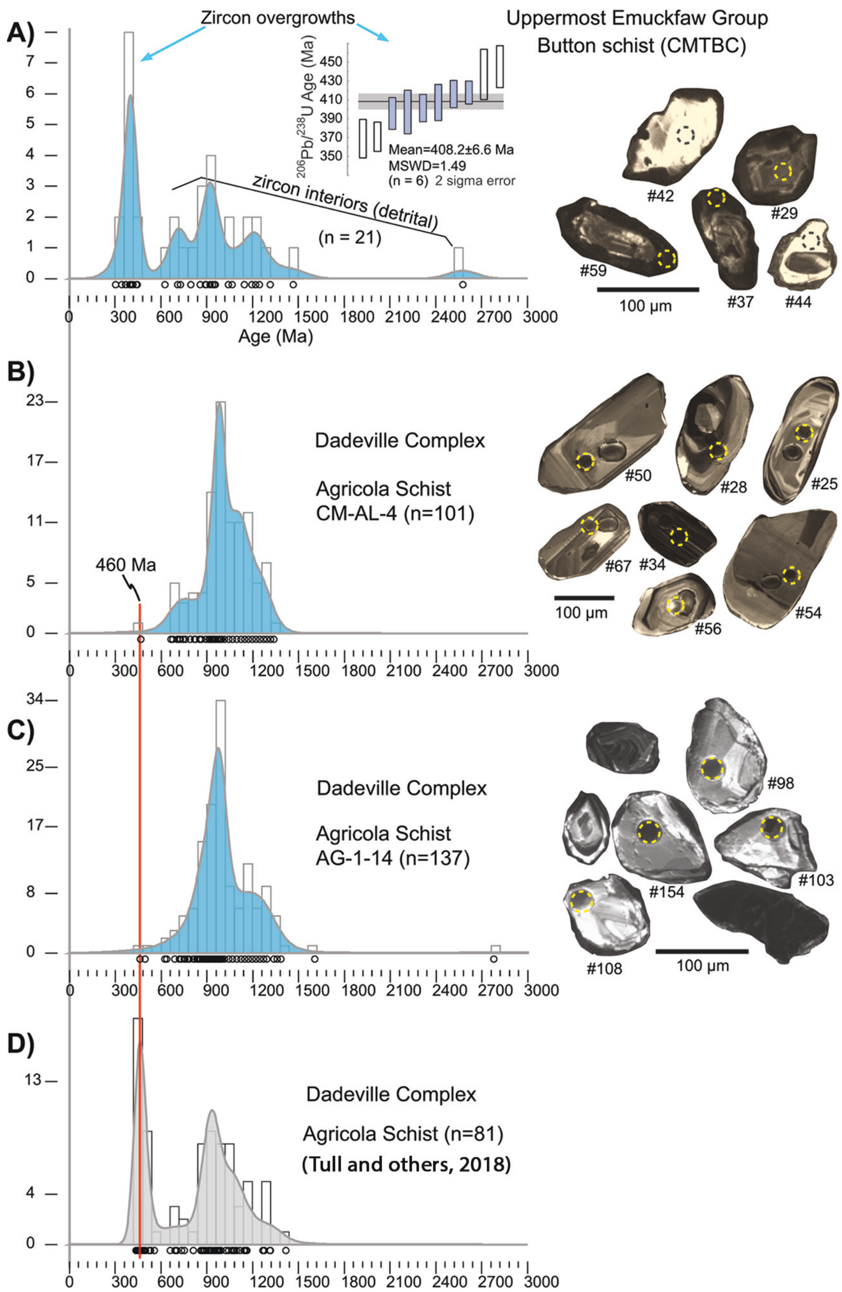

Fig. 5. Kernel density estimation and histogram (bin size = 60 Ma) plots (Vermeesch, 2012) of detrital zircon U-Pb data of the button schist from the uppermost Emuckfaw Group of the eastern Blue Ridge (A) and Agricola Schist of the Dadeville Complex (B, C), compared to those of the Agricola Schist reported by Tull and others (2018) (D). Representative cathodoluminescence images of zircons are shown to the right. Ages <1000 Ma are $^{206}Pb/^{238}U$ dates and ages >1000 Ma are $^{207}Pb/^{206}Pb$ dates. Circles under each plot are the ages without errors; n = number of analyses.

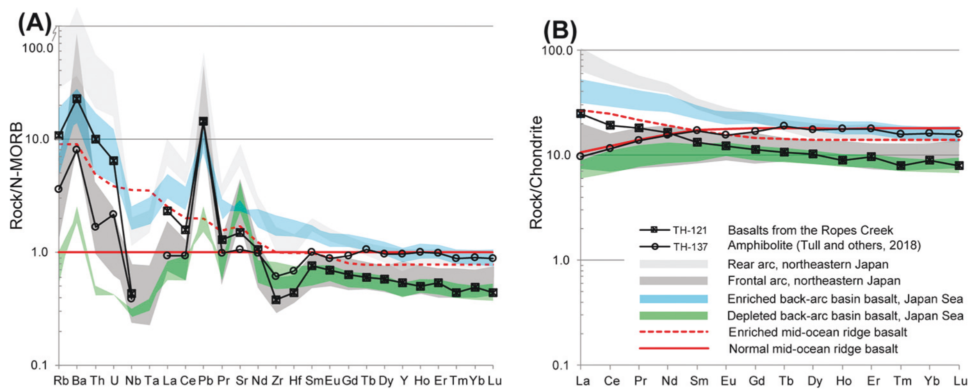

Fig. 6. Trace element abundances of basaltic rocks from the Ropes Creek Amphibolite (Tull and others, 2018) compared with those of frontal/rear arc basalts from northeastern Japan (Kimura and Yoshida, 2006) and back-arc basin basalts from the Sea of Japan (Hirahara and others, 2015). (A) Spider diagram of trace elements normalized to normal mid-oceanic ridge basalt (N-MORB). (B) Rare earth elements normalized to chondrite. The normalizing values and the enriched mid-oceanic ridge basalt data are from Sun and McDonough (1989).

2018) are most consistent with the frontal arc basalts in northeastern Japan (fig. 6A), although the light rare earth element abundances of some Ropes Creek Amphibolite are depleted relative to the heavy rare earth elements (fig. 6B). The significant depletions of Zr and Hf relative to Sm and high enrichment of Ba relative to Th observed in the Ropes Creek Amphibolite are commonly found in mantle-derived arc basalts (for example, Hochstaedter and others, 2001). Moreover, depleted-mantle components are suggested in the sources of some the Ropes Creek Amphibolite lithologies, as evidenced by zircon $\varepsilon Hf_{(i)}$ values of +12 to +5 of a felsic layer and whole-rock $\varepsilon Nd_{(i)}$ values of up to +7 for some basaltic rocks (Tull and others, 2018). The Ropes Creek Amphibolite, therefore, likely represents volcanic rocks formed proximal to the frontal arc of the Dadeville arc and originated from magmas involved depleted-mantle components and subduction zone fluids.

Tull and others (2018) reported zircon $\varepsilon Hf_{(i)}$ values of +6 to 0 for the Camp Hill Gneiss and −1 to −13 for the Rock Mills Gneiss, which indicates a source magma with a depleted-mantle component for the Camp Hill Gneiss that formed at 480 ± 6 Ma (fig. 4D) and an evolved magma with a significant crustal component for the Rock Mills Gneiss that formed at 456 ± 9 Ma (Tull and others, 2018). These two granitic batholiths, therefore, document the evolution of Dadeville arc magmatism from older, more primitive magmas to younger, more evolved magmas during the construction of the arc. This interpretation is consistent with the fact that the Camp Hill Gneiss is low-potassium and low-Al_2O_3, whereas the Rock Mills Gneiss is high-potassium and strongly peraluminous (Bentley and Neathery, 1970; Osborne and others, 1988; Neilson and others, 1997; Tull and others, 2018). The evolving felsic magmatism was probably accompanied by evolving ultramafic/mafic magmas, as indicated by the negative $\varepsilon Nd_{(i)}$ values (−4 to −9) in the Doss Mountain and Slaughters suites (Tull and others, 2018). The nature of the Dadeville arc, therefore, is consistent with a continental margin arc formed by various interaction between depleted-mantle and evolved crustal components (probably Grenvillian, Tull and others, 2018).

U-Pb dates of the volcanic and plutonic rocks from the Dadeville Complex define the timing of magmatic phases responsible for partial construction of the Dadeville arc. The meta-igneous rocks dated in the current study (fig. 7) consist of granitic gneisses and metavolcanics collected from the type localities of the major constitute

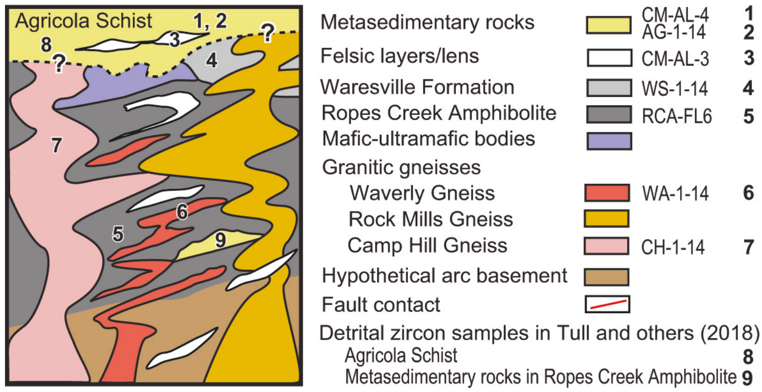

Fig. 7. Schematic crustal column of the Dadeville Complex showing the spatial relationships of the dated rocks discussed in the text.

units of the Dadeville Complex in Alabama (Bentley and Neathery, 1970). The weighted mean ages of 457.6 ± 5.1 Ma for the felsic intrusion in the Ropes Creek Amphibolite, 464.8 ± 3.8 Ma for the felsic metatuff from the Waresville Formation, and 453.9 ± 6.5 Ma for the felsic layer of the Waverly gneiss (figs. 4A, 4B, 4C) all overlap within error. These magmatic ages are compatible with the 456 ± 9 Ma date from the Rock Mills Gneiss (Tull and others, 2018) and, based on the current dataset, ~465 to 454 Ma is considered to represent the main magmatic phase of the preserved components of the Dadeville arc. The older age of 480 ± 6 Ma of the Camp Hill Gneiss (fig. 4D) is interpreted to represent an early magmatic pulse associated with the arc construction. The zircon U-Pb ages of ~450 to 440 Ma in Tull and others (2018) are interpreted to represent the waning stage of the Dadeville arc magmatism.

A regional metamorphic event at about 408 to 394 Ma is revealed in the current study by new zircon U-Pb data from the Dadeville Complex and the adjacent eastern Blue Ridge. This metamorphic event is represented by (1) overgrowths on zircons from the Waverly Gneiss (402.4 ± 11.5 Ma, figs. 2 and 4C) and from a button-schist collected from the uppermost Emuckfaw Group (408.2 ± 6.6 Ma, figs. 2 and 5A), and (2) felsic melts (393.7 ± 8.1 Ma, figs. 2 and 4E) locally preserved in the Agricola Schist. Zircon overgrowths with ages of ~400 Ma have also been reported for some other meta-igneous rocks of the Dadeville Complex (Tull and others, 2018, their fig. 8).

Deposition and Provenance of the Sedimentary Cover of the Dadeville Arc

The detrital zircon age-spectra of the Agricola Schist reported in the current study (figs. 5B and 5C) indicate that the sedimentary cover of the Dadeville arc was sourced primarily from provenances containing Grenville-aged (1300−900 Ma) zircons. Detrital zircon data of the Agricola Schist in Tull and others (2018) show a similar 1300 to 900 Ma population and an additional grouping of 500 to 440 Ma centered at ~460 Ma (fig. 5D). The youngest population of detrital zircons in the available dataset, therefore, defines a maximum depositional age of ~460 Ma (figs. 5B, 5C, and 5D). The zircon crystallization age (394 ± 8 Ma, fig. 4E) of the felsic layer in the Agricola Schist provides a minimum constraint on the depositional age. The protoliths of the Agricola Schist, therefore, were likely deposited between ~460 Ma and ~394 Ma. Apparently, future work is needed to further constrain the depositional age of the Agricola Schist protoliths.

During the Middle Ordovician–Early Devonian, southeastern Laurentia was likely featured by an active convergent margin with marginal basins fed by detritus from

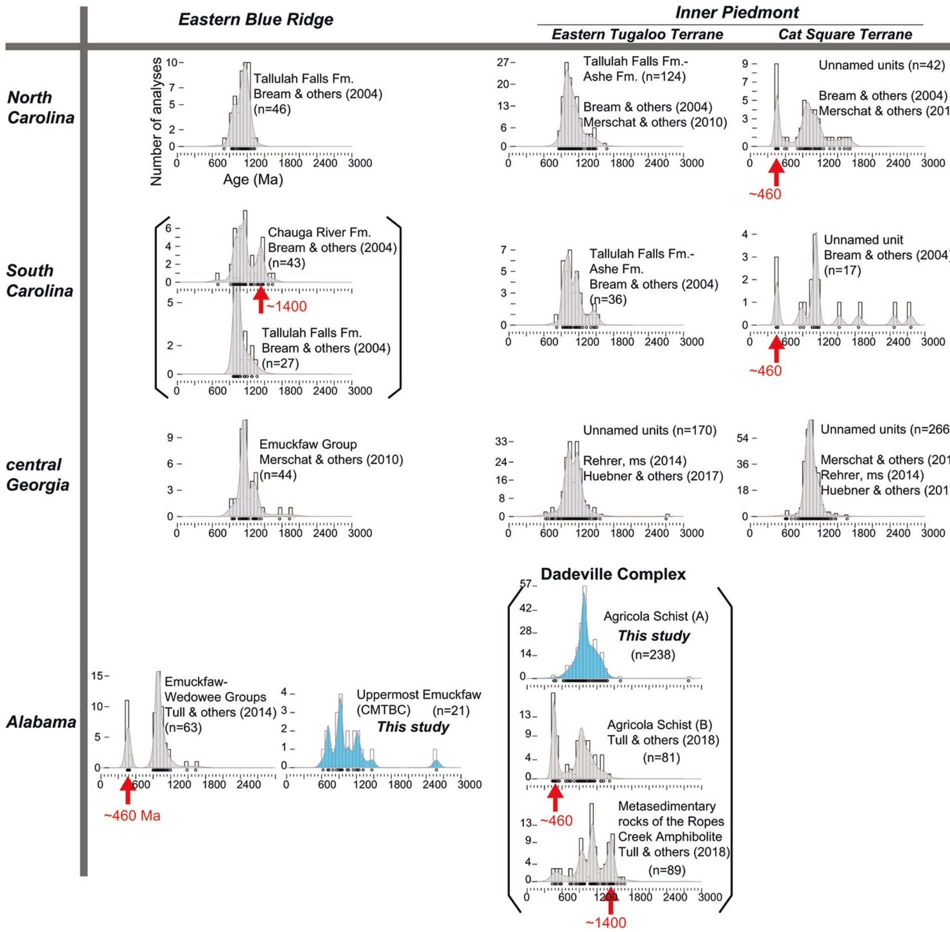

Fig. 8. Published detrital zircon data for metasedimentary rocks in the eastern Blue Ridge, Tugaloo terrane, and Cat Square terrane from North Carolina, South Carolina, central Georgia, and Alabama. Data sources: Bream and others, 2004; Merschat and others, 2010; Rehrer, ms, 2014; Tull and others, 2014; Huebner and others, 2017; Tull and others, 2018, and the current study. Data plotted the same way as figure 5. Distinctive age groups are marked by red arrows. Fm. = Formation.

Laurentia and Taconian terranes (for example, Drake and others, 1989). In this tectonic setting, the 1300 to 900 Ma detrital zircons of the Agricola Schist were likely sourced from the Grenville orogen in southeastern Laurentia or recycled from (meta)sedimentary rocks containing Grenville-aged zircons. The early Paleozoic zircons that cluster at ~460 Ma were likely derived from igneous rocks comprising the Dadeville arc and/or other igneous rocks coeval with those 480 to 440 Ma plutons currently exposed in the Inner Piedmont and eastern Blue Ridge from Virginia to Alabama (fig. 1B) (McDowell and others, 2002; Bream, ms, 2003; Miller and others, 2006; Sinha and others, 2012; Sagul, ms, 2016; Huebner and others, 2017).

Orogen-Parallel Transport of the Dadeville Arc

The Ordovician rocks described in the Geologic Background show the current distribution of a variety of lithotectonic elements associated with the Taconian orogeny in the southern Appalachians. A complete understanding of the Taconian orogeny in this region, however, requires a palinspastic view of all the key Ordovician lithologies associated with this event.

Published data and those from the current study have collectively shown that the Dadeville Complex is composed of a Taconian magmatic arc assemblage (that is, the Dadeville arc) and a sedimentary cover (now the Agricola Schist). The ~465 to 454 Ma age range is considered to represent the main phase of magmatic construction of the Dadeville arc; an early phase of magmatism at ~480 Ma (fig. 4D) and a waning stage at 450 to 440 Ma (Tull and others, 2018) appear to bracket a more comprehensive evolution of the arc. On the basis of the geometry and kinematics of high-temperature shear zones and folds in the Inner Piedmont of North Carolina, South Carolina, and Georgia (Merschat and others, 2005), in conjunction with conditions and timing of regional metamorphism within the context of transpressional accretion of the Carolina superterrane onto Laurentian/Taconian components, Hatcher and Merschat (2006) suggested that the Dadeville Complex was extruded southwestward along the bottom of a tectonically-forced orogenic channel during the Acadian-Neoacadian orogeny. This interpretation is consistent with the Dadeville Complex as a gently northeast-plunging, recumbent sheath fold possibly formed during the Acadian-Neoacadian (Steltenpohl and others, 2013), which was overprinted by the Alleghanian orogeny to form the Tallassee synform (Bentley and Neathery, 1970). Estimates of 200 to 400 km of southwest-directed displacement were made for the Inner Piedmont (Merschat and others, 2005; Merschat and Hatcher, 2007; Huebner and others, 2017), which is of the magnitude necessary to palinspastically restore the Dadeville Complex to the Tennessee embayment (fig. 1B). In the regional context of the Ordovician geology of the southern Appalachians, our new geochronologic data and tectonic analysis support that the Dadeville arc may have formed in the vicinity of the Tennessee embayment during the Taconian orogeny prior to being transported to the Alabama promontory as a result of the subsequent orogenic processes during the Acadian-Neoacadian orogeny.

Ordovician bentonites and coeval clastic wedges preserved in the Appalachian foreland provide supporting evidence for the original locus of the Taconian orogeny in the southern Appalachians. Thickness distribution patterns of the Deicke and Millbrig bentonites (fig. 1A), the two thickest (up to 1.4–1.5 m) bentonite layers, indicate that the depocenter of these ash deposits and their associated volcanic vents were located in the region of the Tennessee embayment (fig. 1B) (Haynes, 1994; Huff and others, 1996). The Deicke and Millbrig bentonites have been dated to be 454.5 ± 0.5 Ma and 453.1 ± 1.3 Ma, respectively, by zircon U-Pb (Tucker, 1992), and to be 450 ± 2 Ma and 448 ± 2 Ma, respectively, by biotite $^{40}Ar/^{39}Ar$ (Min and others, 2001). These two layers of bentonites, thus, record volcanism coeval with the late-stage magmatism of the Dadeville arc.

The late Middle to early Late Ordovician Blount clastic wedge was deposited in the foreland basin as the Taconian orogeny was active in the hinterland (for example, Ettensohn, 2004; Thomas, 2006). Remnants of the Blount clastic wedge are now preserved throughout the foreland from the Virginia promontory to the Alabama promontory (fig. 1B); the thickness pattern suggests that the depocenter for this clastic wedge was also located in the Tennessee embayment (Bayona and Thomas, 2006).

Moreover, Taconian peak metamorphism is recorded in the Blue Ridge in the Tennessee embayment region (fig. 1B) by: (1) the ~459 Ma high-pressure eclogite at Lick Ridge that likely represents metamorphosed oceanic basalts (Miller and others, 2010); (2) the 470 to 460 Ma retrograded eclogites (metabasalts) at Boone and Dellwood (Anderson and Moecher, 2009); (3) the ~458 Ma granulite-facies metamorphism recorded in rocks at Winding Stair Gap (Moecher and others, 2004); (4) the 450 ± 5 Ma high-grade metamorphism and deformation at the Great Smoky Mountains (Corrie and Kohn, 2007); and (5) the garnet Sm-Nd age of 449 ± 12 Ma from a clinoamphibole-garnet-chlorite schist in western Blue Ridge (Dickson and others, 2019). The available pressure-temperature estimates of these metamorphosed rocks (ranging from 7 to 19 kbar and 625 to 875 °C: Adams and others, 1995; Abbott and Greenwood, 2001; Moecher and others, 2004; Anderson and Moecher, 2009; Miller and others, 2010), which are surrounded by accretionary complexes containing ophiolite fragments (for example, Peterson and others, 2009; Raymond and others, 2016), suggest subduction of oceanic rocks in a back-arc oceanic basin to >50 km depth followed by exhumation to shallower crustal levels (for example, Miller and others, 2010).

In short, published evidence for Taconian volcanism and plate convergence at the latitude of the Tennessee embayment is compelling in the Blue Ridge, foreland, and cratonic interior, where the Taconian rocks were not significantly translated along the orogen-parallel strike-slip faults during the subsequent Acadian-Neoacadian and Alleghanian orogenies (Merschat and others, 2005; Hatcher and others, 2017). This suggests that the locus of the Taconian orogeny in the southern Appalachians was located at the Tennessee embayment. The Dadeville arc, therefore, might be palinspastically restored to the Tennessee embayment based on the lines of evidence presented above. The following data further support such a connection between the Dadeville arc and those Taconian lithotectonic elements found in the Tennessee embayment.

Evidence of Early Devonian regional metamorphism and magmatism at ~408 to 394 Ma is recorded by zircon overgrowths in meta-igneous rocks of the Dadeville Complex (fig. 4C) and in metasedimentary rocks from the Emuckfaw Group collected along the Brevard fault zone (fig. 5A), and by zircons from a felsic layer in the Agricola Schist (fig. 4E). Metamorphism and magmatism at ~408 to 394 Ma are not reported elsewhere in the Alabama Appalachians, but are evident in the eastern Blue Ridge of the Carolinas and northeastern Georgia. The supporting data include: (1) metamorphic overgrowths of Taconian monazites at ~400 Ma during prograde metamorphism in the Great Smoky Mountains (fig. 1B) (Kohn and Malloy, 2004; Corrie and Kohn, 2007); (2) a titanite closure date of 394 ± 4 Ma from a partially amphibolitized eclogite in Lick Ridge (fig. 1B) (Miller and others, 2010); (3) a garnet overgrowth Sm-Nd age of 411 ± 12 Ma (Dickson and others, 2019) from a migmatitic gneiss in the Winding Stair Gap area (fig. 1B); and (4) the ~404 to 377 Ma Spruce Pine plutonic suite from the Ashe Metamorphic Suite of the eastern Blue Ridge (Swanson and Veal, 2010). These data collectively indicate burial of some of the Blue Ridge and Inner Piedmont rocks at amphibolite-facies or higher conditions at the beginning of the Acadian orogeny in the Tennessee embayment (see also Merschat and others, 2005; Merschat and Hatcher, 2007; Huebner and others, 2017).

The detrital zircon age-spectra of the Dadeville Complex also suggest a connection to the Tennessee embayment. There are two distinctive features for the Dadeville Complex metasedimentary rocks: (1) the protoliths of the Agricola Schist appear to be deposited in an environment where it could receive detrital zircons of ~1300 to 1000 Ma and ~460 Ma; and (2) the metasedimentary rocks near the base of the Ropes Creek Amphibolite received detrital zircons of ~1400 Ma in addition to Grenvillian and Taconian grains (Tull and others, 2018). Compilation of published detrital zircon data from the eastern Blue Ridge as well as the Tugaloo terrane and Cat Square terrane of the Inner Piedmont of North Carolina, South Carolina, central Georgia, and Alabama is presented in figure 8. In the Carolina segment, the Chauga River Formation of the Tugaloo terrane (deposited prior to the ~448 Ma Henderson gneiss, Huebner and others, 2017) contains detrital zircons dominated by ~1400 Ma and ~1300 to 1000 Ma, and the metasedimentary rocks of the Cat Square terrane (deposited after ~430 Ma, Bream and others, 2004; Merschat and others, 2010; Huebner and others, 2017) includes zircons dominated by ~1300 to 1000 Ma and ~460 Ma. This suggests that the detrital zircon sources required for the sedimentary protoliths of the Dadeville Complex were available in the Tennessee embayment.

In addition, remnants of a Taconian arc are proposed to be preserved as the Persimmon Creek Gneiss (fig. 1B) in the Tennessee embayment region. Zircons from this mafic-felsic igneous complex were crystallized at ~468 to 458 Ma and contain ~1.4 Ga and ~1.2 to 1.0 Ga inherited cores (McDowell and others, 2002; Miller and others, 2006). Trace elements and Nd-Sr-O isotopic compositions indicate an arc origin for the Persimmon Creek Gneiss (McDowell and others, 2002).

In summary, the depocenters of the late Middle to early Late Ordovician bentonites and the coeval Blount clastic wedge in the foreland, and the subduction-related eclogite- and granulite-facies metamorphism at 470 to 460 Ma, jointly suggest that Taconian volcanism and plate convergence took place at the latitude of the Tennessee embayment. Data from the Dadeville Complex suggest that the Taconian Dadeville arc originally formed at the Tennessee embayment where detrital sources of ~1400 Ma, ~1300 to 1000 Ma, and ~460 Ma zircons were available. This interpretation is corroborated by the occurrence of Taconian arc remnants (Persimmon Creek Gneiss) in the Tennessee embayment, the ~408 to 394 Ma metamorphism and magmatism shared by a variety of rocks in the Dadeville Complex and the Tennessee embayment, and the southwest-directed channel-flow structures with estimated displacements of 200 to 400 km in the Inner Piedmont (Hatcher and Merschat, 2006; Merschat and Hatcher, 2007; Hatcher and others, 2017; Huebner and others, 2017).

The structures that accommodated the transport of the Dadeville Complex in Alabama, in addition to internal structures in the Dadeville Complex, are possibly preserved in the Brevard fault zone and the uppermost eastern Blue Ridge, that is, the Jacksons Gap Group (fig. 2) and Emuckfaw Group (fig. 1B), respectively. The structurally higher Dadeville Complex contains sillimanite-grade, top-to-the-southwest shear zones (Bittner and Neilson, 1990; Abrahams, ms, 2014). The structurally lower Jacksons Gap Group, however, is characterized by sillimanite-bearing, subhorizontally sheared rocks showing top-to-the-northeast displacement (fig. 9A) near Tallassee, Alabama (fig. 2). The similar metamorphic grade and ductile strain as well as compatible structural orientation suggest that these mylonitic rocks possibly formed coevally due to the same event. As coexistence of opposite kinematics across different structural levels indicates differential rates of ductile flow, extrusion tectonics (for example, Thompson and others, 1997), therefore, might have contributed to the transport of the Dadeville Complex at certain structural levels.

The main deformation responsible for the orogen-parallel transport of the Dadeville Complex, however, were probably the southwest-directed shearing primarily recorded in Alabama by the pervasive, dextrally sheared, southeast-dipping lithologies observed in the northeast-striking segment of the Jacksons Gap Group (Abrahams, ms, 2014) and the Emuckfaw Group (figs. 9B, 9C, and 9D). S-C-C' (schistosity-cisaillement-extensional crenulation cleavage) structures are widespread in the Emuckfaw Group (fig. 9B), Kowaliga Gneiss (fig. 9C), Zana Gneiss (fig. 9D), and the southeastern margin of the Elkahatchee Quartz Diorite (fig. 1B) (Steltenpohl and others, 2013). These highly sheared rocks define a ~10 km wide Acadian/Neoacadian ductile shear zone located just west of the Brevard fault zone (see also Steltenpohl and others, 2013). Similar structures occur continuously from Alabama to North Carolina along the Brevard fault zone and the adjacent eastern Blue Ridge (Merschat and others, 2005; Hatcher and Merschat, 2006).

A Palinspastic View of the Taconian Orogen in the Southern Appalachians

Palinspastic restoration of the Dadeville arc to the Tennessee embayment adjacent to the eastern Blue Ridge of North Carolina (fig. 1B) suggests that the accretionary

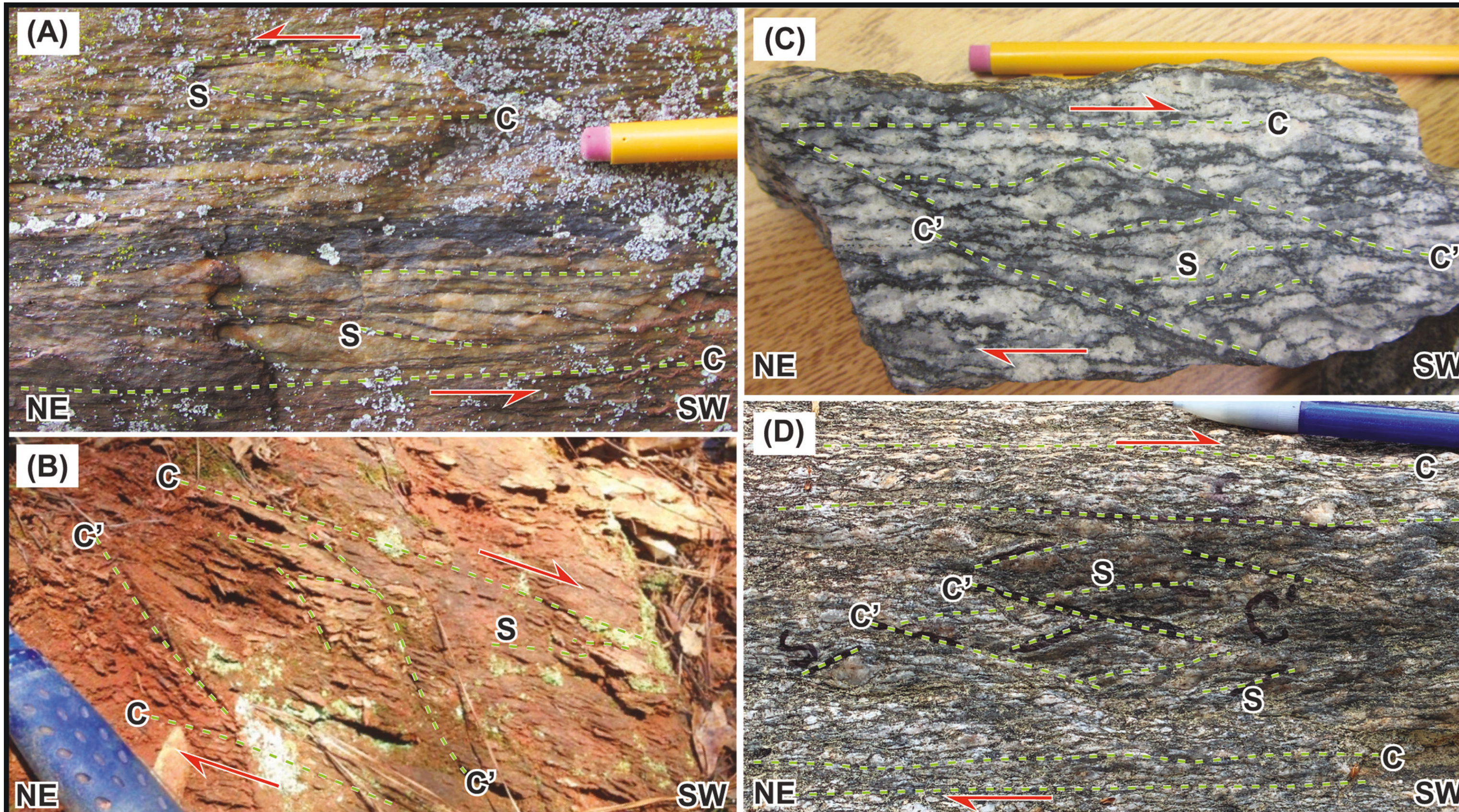

Fig. 9. Highly sheared rocks and representative structures beneath the Dadeville Complex. (A) Top-to-the-northeast, subhorizontal, sillimanite-bearing, mylonitic metaconglomerate of the Jacksons Gap Group defining the southernmost Brevard fault zone near Tallassee, Alabama. (B) S-C-C' structure in the button schist of the Emuckfaw Group. (C) S-C-C' structure in the Middle Ordovician Kowaliga Gneiss. (D) S-C-C' structure in the Middle Ordovician Zana Gneiss. Rocks in (B), (C), and (D) are all dextrally sheared, dip moderately to the southeast, and contain northeast trending subhorizontal stretching lineations. Pencil and hammer for scale.

complex represented by the Ashe Metamorphic Suite (for example, Stewart and others, 1997; Raymond and others, 2016) was a part of the companion back-arc basin of the Dadeville arc (see also Miller and others, 2006). This back-arc basin might continue into the original Wedowee-Emuckfaw-Dahlonaga basin as the latter currently extends to the Tennessee embayment (Tull and others, 2014). Occurrence of eclogites and metabasalts of oceanic affinities (for example, Stewart and others, 1997; Abbott and Greenwood, 2001; Collins, ms, 2011) and ophiolite fragments (for example, Peterson and others, 2009; Raymond and others, 2016) in the Ashe Metamorphic Suite indicates that this back-arc basin contains oceanic crust. It was, therefore, an oceanic back-arc basin that possibly formed due to rifting along the southeastern Laurentia margin (see also Stewart and others, 1997; Abbott and Greenwood, 2001; Miller and others, 2006; Anderson and Moecher, 2009). An oceanic back-arc basin is consistent with the positive $\varepsilon Nd_{(i)}$ values for some of the volcanic rocks in the region, such as the Pumpkinvine Creek Formation (fig. 1B) (Holm-Denoma and Das, 2010). The Dadeville arc, therefore, possibly formed as a volcanic arc built atop a continental crustal block that was rifted and separated from Laurentia by an oceanic back-arc basin. This is consistent with both positive and negative $\varepsilon Nd_{(i)}$ and $\varepsilon Hf_{(i)}$ values for some of the felsic-mafic rocks of the Dadeville Complex (Tull and others, 2018). Direct evidence for the continental crust is possibly preserved as zircon cores in Taconian arc granitic rocks such as the ~1.2 to 1.0 Ga inherited zircons in the Persimmon Creek Gneiss (fig. 1B) (McDowell and others, 2002), or, as gneissic bodies in Taconian plutons such as the ~1.1 Ga Snapping Shoals augen gneiss in the Lithonia Gneiss (fig. 1B) (Huebner and others, 2017).

On the basis of the data presented above, a regional model for the evolution of the Taconian Dadeville arc and its back-arc basin at the Tennessee embayment is described in figure 10. At the beginning of the Taconian orogeny in the southern Appalachians (fig. 10A), westward subduction of the Iapetus oceanic plate was likely on-going under a rifted crustal fragment of Laurentia and the associated oceanic back-arc basin at the latitude of the Tennessee embayment (for example, Hatcher, 1978; Hibbard and others, 2007; Anderson and Moecher, 2009). Between ~480 Ma and ~460 Ma (fig. 10B), magmatism was active in the Dadeville arc that was developed on the rifted continental block while some of the oceanic rocks of the back-arc basin were subducted to high-pressure conditions to form the eclogites that are currently preserved in the eastern Blue Ridge (for example, Stewart and others, 1997; Miller and others, 2006, 2010; Anderson and Moecher, 2009). Between ~460 Ma and ~440 Ma (fig. 10C), the Dadeville arc continued growing and the subducted back-arc basin lithosphere was possibly detached from the Laurentian margin that underwent attempted subduction. This potentially resulted in tectonic under-pressure above the subducting plate (for example, Majka and others, 2014), which facilitated buoyancy-driven exhumation of the continental crust that incorporated accretionary complexes and high-grade rocks such as the Lick Ridge eclogite and the Winding Stair Gap granulite (for example, Anderson and Moecher, 2009).

From ~480 Ma to ~440 Ma, multiple phases of plutonism and volcanism occurred in the oceanic back-arc basin and the neighboring continental crust. This is supported by the ~470 to 440 Ma granitic plutons (fig. 1B) containing enriched large-ion lithophile elements, depleted high field-strength elements, and negative $\varepsilon Hf_{(i)}$ and $\varepsilon Nd_{(i)}$ values in the Inner Piedmont and eastern Blue Ridge (for example, Sagul, ms, 2016; Huebner and others, 2017), and by the Ordovician basaltic rocks of back-arc basin signatures and positive/negative $\varepsilon Hf_{(i)}$ and $\varepsilon Nd_{(i)}$ values represented by the Wedowee-Emuckfaw-Dahlonega basin and its equivalents in the Tennessee embayment (Holm-Denoma and Das, 2010; Tull and others, 2014; Barineau and others, 2015). During the late-stage of the Taconian orogeny, the Deicke and Millbrig

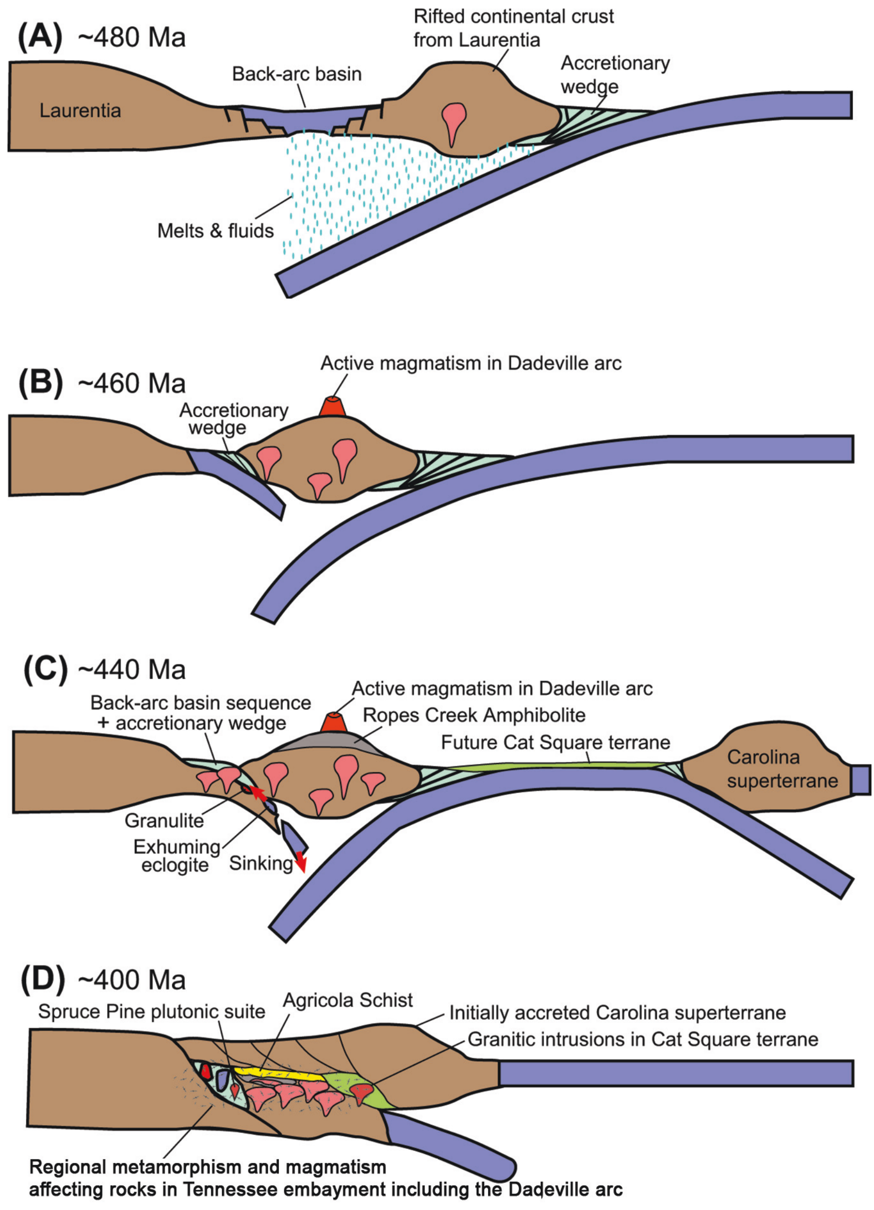

Fig. 10. Tectonic model for the formation and metamorphism of the Dadeville arc and associated back-arc in the Tennessee embayment region during and after the Taconian orogeny, prior to the orogen-parallel translation of Dadeville arc to Alabama promontory. (A) Westward subduction of oceanic crust under a rifted continental margin and back-arc basin (for example, Anderson and Moecher, 2009). (B) Partial subduction of the back-arc basin to high-pressure conditions (subduction direction is after Miller and others, 2006; Merschat and others, 2017) and active magmatism on the Dadeville arc. (C) Closure of the back-arc basin, exhumation of continental crust incorporating eclogites, and continued magmatism on the Dadeville arc. (D) Regional metamorphism affecting the Dadeville arc and eastern Blue Ridge rocks due to the tectonic burial by the approaching Carolina superterrane (Merschat and others, 2017).

bentonites were deposited in the foreland and sourced from the continental arc at the Tennessee embayment, as phenocryst mineralogy and geochemical data indicate that the parental magmas of the Deicke and Millbrig bentonites were dacitic to rhyolitic and involved a significant component of continental crust (Huff and others, 1992).

Around ~400 Ma (fig. 10D), the Dadeville Complex protoliths and parts of the Blue Ridge experienced regional metamorphism in the Tennessee embayment due to tectonic burial resulting from the initial accretion of the Carolina superterrane. Early phases of the ~404 to 377 Ma Spruce Pine plutonic suite in the Ashe Metamorphic Suite (Swanson and Veal, 2010) and the ~404 to 371 Ma granitoids in the Cat Square terrane (Huebner and others, 2017) likely formed in this tectonic setting. Subsequently, as the transpressional accretion of the Carolina superterrane onto the Laurentian/Taconian margin continued, the Dadeville arc and some of the eastern Blue Ridge rocks adjacent to the Brevard fault zone were likely transported at mid-crustal levels in a northeast-southwest orogenic channel that extended from the Tennessee embayment to the Alabama promontory by the time of peak Acadian-Neoacadian metamorphism at ~360 to 345 Ma (Merschat and others, 2005; Hatcher and others, 2017; Merschat and others, 2017). The northeast-trending Ordovician plutons discontinuously distributed in the Inner Piedmont (fig. 1B) might result from this mid-crustal ductile flow. Finally, due to the collision of Gondwana with Laurentia during the Alleghanian orogeny, the Blue Ridge-Inner Piedmont was transported further onto the Laurentian basement and platform rocks as a megathrust sheet (for example, Hatcher and others, 1989).

CONCLUSIONS

This study reports new zircon U-Pb geochronology data for constraining magmatism, metamorphism, and sedimentary provenance of the Dadeville Complex in the southernmost Appalachians and provides a new regional view of the original Taconian orogen. In combination with literature data, the following conclusions are proposed: (1) felsic meta-igneous rocks of the Dadeville Complex reveal the main phase of arc magmatism at *ca.* 465 to 454 Ma, an earlier phase at *ca.* 480 Ma, and a possible late phase at 450 to 440 Ma; (2) detrital zircons from the sedimentary cover of the Dadeville arc are dominated by Grenville-aged grains with secondary Taconian-aged zircons; (3) metamorphic zircon overgrowths and local melts in the Dadeville Complex and metamorphic zircon overgrowths in the adjacent Blue Ridge collectively define a metamorphic/magmatic event at about 408 to 394 Ma; (4) the Taconian Dadeville arc represented by the meta-igneous rock of the Dadeville Complex was likely built on a rifted Laurentian block; and (5) the Dadeville arc and the companion oceanic back-arc basin were likely transported at mid-crustal levels along the Brevard fault zone and the adjacent eastern Blue Ridge from the Tennessee embayment to the Alabama promontory due to the dextral transpression associated with the Acadian-Neoacadian orogeny.

ACKNOWLEDGMENTS

Berry (Nick) Tew, Sandy Ebersole, Irene Burgess, Seth Newton, Patrick O'Neil, and Gregory Guthrie of the Geological Survey of Alabama have read and improved the manuscript. John Hawkins and John Whitmore are thanked for collecting one of the samples. We also thank Meghann Decker, Mike Cho, and Zhan Peng at California State University Northridge for assistance with the U-Pb analysis. This work was supported by an EDMAP grant awarded to Steltenpohl from the U.S. Geological Survey National Cooperative Geologic Mapping Program.

Reviews by Arthur Merschat, Nigel Kelly, and James Tull helped improve the manuscript.

TABLE A1

Sample descriptions, coordinates, and U-Pb isotopic data

Sample name	U (ppm)	Th/U	$^{238}U/^{206}Pb$	2 sigma abs	$^{207}Pb/^{206}Pb$	2 sigma abs	207/235 age Ma	1 sigma abs err Ma	206/238 age† Ma	1 sigma abs err Ma	207/206 age Ma	1 sigma abs err Ma	disc†† %
WS-1-14, Waresville Formation													
	33.19923°N, 85.29494°W; strongly foliated, very fine-grained, chlorite-sericite-biotite-hornblende schist												
ws_1_14_14	119	0.81	14.025	0.610	0.0607	0.0029	475.0	12.3	444.0	9.3	627.7	51.5	6.5
ws_1_14_0	249	1.22	13.736	0.453	0.0547	0.0027	444.2	10.7	453.0	7.2	399.0	55.3	-2.0
ws_1_14_8	90	0.69	13.736	0.566	0.0561	0.0040	453.4	15.1	453.0	9.0	455.3	79.1	0.1
ws_1_14_9	129	0.96	13.661	0.523	0.0554	0.0032	450.8	12.6	455.4	8.4	427.4	64.4	-1.0
ws_1_14_6	118	0.78	13.532	0.421	0.0551	0.0044	452.3	15.6	459.6	6.9	415.3	89.2	-1.6
ws_1_14_3	102	0.72	13.532	0.531	0.0653	0.0055	517.7	18.8	459.6	8.7	783.1	88.5	11.2
ws_1_14_12	217	1.14	13.514	0.493	0.0552	0.0032	453.4	12.5	460.2	8.1	419.3	64.7	-1.5
ws_1_14_10	81	0.70	13.387	0.591	0.0651	0.0042	520.8	15.9	464.4	9.9	776.6	67.8	10.8
ws_1_14_13	88	0.77	13.316	0.550	0.0517	0.0035	435.2	14.0	466.8	9.3	271.1	77.6	-7.3
ws_1_14_4	158	0.92	13.316	0.426	0.0526	0.0037	441.3	13.8	466.8	7.2	310.6	80.1	-5.8
ws_1_14_5	115	0.78	13.316	0.461	0.0530	0.0032	444.0	12.5	466.8	7.8	327.8	68.5	-5.1
ws_1_14_7	72	0.65	13.316	0.532	0.0566	0.0038	468.2	14.7	466.8	9.0	475.0	74.2	0.3
ws_1_14_15	70	0.67	13.316	0.496	0.0594	0.0036	486.6	13.8	466.8	8.4	580.8	65.8	4.1
ws_1_14_16	76	0.91	13.298	0.477	0.0592	0.0048	485.8	17.1	467.4	8.1	573.5	88.2	3.8
ws_1_14_1	84	0.73	13.106	0.395	0.0581	0.0036	484.2	13.3	474.0	6.9	532.6	67.8	2.1
ws_1_14_19	107	0.96	13.021	0.627	0.0572	0.0038	480.7	15.7	477.0	11.1	498.3	73.2	0.8
ws_1_14_18	81	0.76	12.987	0.624	0.0602	0.0047	501.6	18.1	478.2	11.1	609.8	84.4	4.7
ws_1_14_2	96	0.84	12.837	0.363	0.0709	0.0047	574.7	15.8	483.6	6.6	953.6	67.8	15.9
ws_1_14_17	187	1.10	12.788	0.572	0.0569	0.0032	485.6	13.9	485.4	10.5	486.7	62.1	0.0
ws_1_14_11	70	0.71	12.547	0.472	0.0670	0.0047	560.0	17.1	494.3	9.0	836.8	73.1	11.7
CH-1-14, Camp Hill Gneiss													
	32.82607°N, 85.61992°W; foliated, medium- to coarse-grained, hornblende-muscovite-biotite granitic gneiss												
CH_1_14_8	260	0.72	13.97	0.82	0.057	0.003	453.0	14.4	445.7	12.6	490.5	58.0	1.6
CH_1_14_0	430	0.63	13.70	0.51	0.058	0.002	466.7	9.5	454.2	8.2	528.8	37.8	2.7
CH_1_14_2	123	0.49	13.53	0.48	0.062	0.004	497.1	14.5	459.7	7.9	673.1	69.0	7.5
CH_1_14_4	323	0.62	13.48	0.54	0.058	0.003	472.8	12.4	461.3	8.9	528.8	56.7	2.4
CH_1_14_1	302	0.57	13.21	0.54	0.056	0.003	467.2	12.6	470.4	9.3	451.4	59.5	-0.7
CH_1_14_9	279	0.60	13.18	0.59	0.057	0.003	474.7	13.1	471.4	10.2	490.5	58.0	0.7
CH_1_14_6	209	0.72	12.87	0.63	0.055	0.002	470.2	11.5	482.4	11.4	411.2	40.7	-2.6
CH_1_14_17	18	0.44	12.87	0.99	0.058	0.010	490.5	36.7	482.4	17.9	529.0	189.0	1.7
CH_1_14_7	112	0.53	12.85	0.55	0.056	0.005	477.6	18.9	483.1	10.0	451.4	99.1	-1.2
CH_1_14_5	104	0.37	12.52	0.56	0.059	0.004	508.1	16.2	495.4	10.7	566.1	73.8	2.5
CH_1_14_10	119	0.48	12.41	0.63	0.057	0.004	498.0	17.0	499.6	12.2	490.5	77.4	-0.3

TABLE A1
(continued)

Sample name	U (ppm)	Th/U	$^{238}U/^{206}Pb$	2 sigma abs	$^{207}Pb/^{206}Pb$	2 sigma abs	207/235 age Ma	1 sigma abs err Ma	206/238 age† Ma	1 sigma abs err Ma	207/206 age Ma	1 sigma abs err Ma	disc†† %
CH-1-14, Camp Hill Gneiss													
32.82607°N, 85.61992°W; foliated, medium- to coarse-grained, hornblende-muscovite-biotite granitic gneiss													
CH_1_14_18	28	0.40	12.39	0.83	0.056	0.007	491.7	27.6	500.4	16.1	451.0	139.0	-1.8
CH_1_14_3	242	0.59	12.36	0.53	0.054	0.003	478.6	13.4	501.5	10.3	370.0	62.6	-4.8
CH_1_14_11	78	0.36	12.25	0.57	0.058	0.005	510.0	19.6	505.9	11.3	528.8	94.5	0.8
CH_1_14_14	43	0.40	12.15	0.53	0.055	0.004	492.3	16.5	509.9	10.7	411.2	81.3	-3.6
CH_1_14_13	78	0.57	12.14	0.74	0.053	0.004	478.3	18.5	510.3	15.0	327.8	85.6	-6.7
CH_1_14_15	38	0.36	11.95	0.61	0.058	0.005	520.0	20.4	518.1	12.7	528.8	94.5	0.4
CH_1_14_12	60	0.61	11.61	0.59	0.059	0.004	539.0	17.7	532.6	13.0	566.1	73.8	1.2
CH_1_14_16	50	0.32	11.17	0.61	0.052	0.004	503.3	18.7	552.7	14.5	284.4	88.0	-9.8
CH_1_14_19	49	0.34	10.74	0.44	0.054	0.005	534.6	21.0	573.9	11.2	370.0	104.0	-7.4
RCA-FL6, Felsic layer of the Ropes Creek Amphibolite													
32.62476°N, 85.68619°W; fine- to medium-grained, biotite-hornblende quartzofeldspathic gneiss													
rca_fl6_27	216	0.74	17.83	1.49	0.046	0.007	308.9	23.1	351.8	14.3	0.0	140.0	-13.9
rca_fl6_26	320	0.89	15.11	1.16	0.053	0.005	400.4	20.1	413.1	15.4	328.0	107.0	-3.2
rca_fl6_11	298	0.84	14.90	0.89	0.060	0.002	448.2	12.4	418.7	12.1	602.6	36.1	6.6
rca_fl6_19	362	0.97	14.33	0.92	0.057	0.003	443.8	14.9	434.9	13.5	490.5	58.0	2.0
rca_fl6_17	384	1.04	14.25	1.01	0.058	0.003	452.1	16.0	437.2	15.0	528.8	56.7	3.3
rca_fl6_7	366	0.59	14.12	0.74	0.055	0.003	436.3	13.4	441.1	11.2	411.2	61.0	-1.1
rca_fl6_25	284	0.86	14.10	0.93	0.063	0.005	487.2	20.0	441.7	14.1	707.3	84.4	9.3
rca_fl6_31	273	0.71	13.95	1.83	0.050	0.011	407.6	43.0	446.3	28.3	194.0	256.0	-9.5
rca_fl6_23	222	0.78	13.85	0.88	0.056	0.004	449.7	17.4	449.4	13.8	451.4	79.3	0.1
rca_fl6_13	446	0.95	13.85	0.77	0.058	0.003	462.6	14.1	449.4	12.1	528.8	56.7	2.9
rca_fl6_15	295	0.71	13.83	0.80	0.058	0.003	463.2	14.4	450.0	12.6	528.8	56.7	2.8
rca_fl6_29	278	0.69	13.79	1.12	0.054	0.005	438.2	21.9	451.3	17.7	370.0	104.0	-3.0
rca_fl6_14	193	0.79	13.76	0.87	0.057	0.004	458.6	17.4	452.2	13.8	490.5	77.4	1.4
rca_fl6_24	184	0.79	13.72	0.90	0.054	0.004	440.0	17.7	453.5	14.4	370.0	83.4	-3.1
rca_fl6_22	169	0.70	13.70	0.92	0.053	0.003	433.9	15.5	454.2	14.7	327.8	64.2	-4.7
rca_fl6_2	229	0.82	13.64	0.80	0.057	0.002	461.8	12.7	456.1	12.9	490.5	38.7	1.2
rca_fl6_33	108	0.62	13.57	1.23	0.052	0.007	430.6	28.5	458.4	20.1	284.0	154.0	-6.5
rca_fl6_6	121	0.69	13.57	0.85	0.057	0.003	463.8	15.2	458.4	13.9	490.5	58.0	1.2
rca_fl6_28	127	0.74	13.53	1.26	0.056	0.007	458.3	28.7	459.7	20.7	451.0	139.0	-0.3
rca_fl6_3	84	0.72	13.53	0.81	0.056	0.002	458.3	12.9	459.7	13.3	451.4	39.7	-0.3
rca_fl6_18	174	0.90	13.53	0.86	0.058	0.003	471.4	15.5	459.7	14.1	528.8	56.7	2.5
rca_fl6_5	65	0.55	13.50	0.78	0.055	0.002	452.5	12.5	460.7	12.8	411.2	40.7	-1.8

TABLE A1
(continued)

Sample name	U (ppm)	Th/U	$^{238}U/^{206}Pb$	2 sigma abs	$^{207}Pb/^{206}Pb$	2 sigma abs	207/235 age Ma	1 sigma abs err Ma	206/238 age† Ma	1 sigma abs err Ma	207/206 age Ma	1 sigma abs err Ma	disc†† %
RCA-FL6, Felsic layer of the Ropes Creek Amphibolite													
	32.62476°N, 85.68619°W; fine- to medium-grained, biotite-hornblende quartzofeldspathic gneiss												
rca_fl6_1	116	0.75	13.50	0.76	0.059	0.003	478.7	14.5	460.7	12.5	566.1	55.4	3.8
rca_fl6_10	71	0.78	13.44	0.81	0.058	0.003	473.9	15.0	462.6	13.5	528.8	56.7	2.4
rca_fl6_9	39	0.62	13.35	0.77	0.055	0.003	456.6	14.6	465.6	13.0	411.2	61.0	-2.0
rca_fl6_8	49	0.56	13.35	0.71	0.058	0.003	476.4	14.1	465.6	11.9	528.8	56.7	2.3
rca_fl6_12	23	0.63	13.23	0.87	0.055	0.003	459.9	15.8	469.7	14.9	411.2	61.0	-2.1
rca_fl6_34	10	0.43	13.21	1.20	0.045	0.010	390.8	38.9	470.4	20.6	0.0	200.0	-20.4
rca_fl6_32	22	0.43	13.18	1.02	0.061	0.007	501.0	27.4	471.4	17.6	638.0	123.0	5.9
rca_fl6_36	27	0.50	13.16	1.52	0.057	0.008	475.3	34.5	472.1	26.3	491.0	155.0	0.7
rca_fl6_4	34	0.41	13.16	0.73	0.058	0.002	481.9	12.5	472.1	12.6	528.8	37.8	2.0
rca_fl6_30	17	0.60	13.12	1.15	0.058	0.007	483.1	28.7	473.5	20.0	529.0	132.0	2.0
rca_fl6_16	23	0.45	13.07	0.79	0.056	0.003	471.2	15.2	475.3	13.8	451.4	59.5	-0.9
rca_fl6_35	15	0.52	12.95	1.56	0.062	0.016	514.5	57.5	479.5	27.8	673.0	276.0	6.8
rca_fl6_21	10	0.47	12.89	0.78	0.058	0.004	489.9	17.8	481.7	14.0	528.8	75.6	1.7
rca_fl6_20	18	0.60	12.45	0.73	0.053	0.004	468.8	17.9	498.0	14.1	327.8	85.6	-6.2
rca_fl6_39	11	0.47	12.39	0.97	0.057	0.005	498.6	23.2	500.4	18.8	490.5	96.7	-0.4
rca_fl6_38	21	0.59	12.05	1.12	0.054	0.007	488.3	30.9	513.9	23.0	370.0	146.0	-5.2
rca_fl6_37	27	0.62	11.66	1.25	0.049	0.010	463.9	42.9	530.4	27.3	147.0	239.0	-14.3
WA-1-14, Waverly Gneiss													
	32.73951°N, 85.58507°W; foliated, medium-grained, muscovite-hornblende-biotite quartzofeldspathic gneiss												
wa_1_14_3$	945	0.02	17.04	1.25	0.053	0.003	362.2	14.1	367.6	13.1	327.8	64.2	-1.5
wa_1_14_28$	556	0.4221	15.65	2.23	0.060	0.011	430.7	40.8	399.3	27.6	603.0	198.0	7.3
wa_1_14_21$	303	0.44	15.55	1.35	0.054	0.006	397.1	23.2	401.8	16.9	370.0	125.0	-1.2
wa_1_14_17$	360	0.46	15.48	2.04	0.060	0.007	434.6	31.1	403.5	25.8	603.0	126.0	7.2
wa_1_14_0$	357	0.28	15.29	0.91	0.054	0.002	402.7	11.7	408.4	11.8	370.0	41.7	-1.4
wa_1_14_14$	360	0.46	15.24	1.16	0.053	0.005	397.6	19.9	409.7	15.1	328.0	107.0	-3.0
wa_1_14_25$	246	0.4444	14.93	1.54	0.059	0.007	441.5	28.1	417.9	20.9	566.0	129.0	5.3
wa_1_14_7$	327	0.39	14.88	0.89	0.053	0.003	405.5	13.8	419.3	12.1	327.8	64.2	-3.4
wa_1_14_18$	332	0.4673	14.86	1.50	0.062	0.008	461.3	30.4	419.8	20.5	673.0	138.0	9.0
wa_1_14_37	146	0.3096	14.81	1.51	0.062	0.008	462.5	30.5	421.2	20.8	673.0	138.0	8.9
wa_1_14_34	147	0.29	14.56	1.38	0.055	0.006	425.6	25.1	428.2	19.6	411.0	122.0	-0.6
wa_1_14_26	116	0.5319	14.47	1.95	0.054	0.008	421.3	34.5	430.8	28.1	370.0	167.0	-2.3
wa_1_14_36	43	0.3448	14.43	1.19	0.053	0.005	415.9	21.4	431.9	17.2	328.0	107.0	-3.8
wa_1_14_33	37	0.61	14.37	1.40	0.054	0.009	423.7	33.4	433.7	20.4	370.0	188.0	-2.4

TABLE A1
(continued)

Sample name	U (ppm)	Th/U	$^{238}U/^{206}Pb$	2 sigma abs	$^{207}Pb/^{206}Pb$	2 sigma abs	207/235 age Ma	1 sigma abs err Ma	206/238 age† Ma	1 sigma abs err Ma	207/206 age Ma	1 sigma abs err Ma	disc†† %
WA-1-14, Waverly Gneiss													
32.73951°N, 85.58507°W; foliated, medium-grained, muscovite-hornblende-biotite quartzofeldspathic gneiss													
wa_1_14_10	19	0.25	14.25	0.83	0.055	0.003	433.1	14.1	437.2	12.3	411.2	61.0	-0.9
wa_1_14_8	31	0.13	14.14	1.08	0.055	0.003	435.8	16.6	440.5	16.3	411.2	61.0	-1.1
wa_1_14_24	154	0.3891	14.08	2.18	0.086	0.025	620.1	76.4	442.3	33.1	1337.0	281.0	28.7
wa_1_14_15	36	0.1344	13.95	1.30	0.053	0.005	427.6	23.1	446.3	20.1	328.0	107.0	-4.4
wa_1_14_38	20	0.3012	13.93	1.05	0.050	0.006	408.1	23.8	446.9	16.3	194.0	139.0	-9.5
wa_1_14_20	28	0.3058	13.87	1.58	0.061	0.008	481.1	33.3	448.8	24.7	638.0	141.0	6.7
wa_1_14_12	13	0.18	13.81	0.86	0.055	0.003	444.3	14.9	450.7	13.6	411.2	61.0	-1.4
wa_1_14_32	17	0.2105	13.79	1.22	0.057	0.006	457.8	25.3	451.3	19.3	491.0	116.0	1.4
wa_1_14_35	21	0.18	13.77	1.23	0.055	0.005	445.3	23.0	451.9	19.5	411.0	102.0	-1.5
wa_1_14_5	20	0.22	13.68	0.90	0.057	0.002	460.8	13.8	454.8	14.4	490.5	38.7	1.3
wa_1_14_1	29	0.00	13.66	0.93	0.058	0.003	467.8	16.0	455.4	15.0	528.8	56.7	2.7
wa_1_14_9	20	0.27	13.62	1.00	0.055	0.002	449.3	14.9	456.7	16.2	411.2	40.7	-1.6
wa_1_14_2	27	0.55	13.57	0.83	0.054	0.002	444.0	12.9	458.4	13.5	370.0	41.7	-3.2
wa_1_14_39	50	0.5988	13.51	1.11	0.049	0.003	411.6	17.3	460.3	18.3	146.8	71.8	-11.8
wa_1_14_4	40	0.41	13.37	0.84	0.054	0.003	449.3	15.2	465.0	14.1	370.0	62.6	-3.5
wa_1_14_6	33	0.24	13.07	0.87	0.054	0.003	457.6	16.0	475.3	15.2	370.0	62.6	-3.9
wa_1_14_30	22	0.41	12.89	1.18	0.057	0.005	483.2	24.4	481.7	21.2	490.5	96.7	0.3
wa_1_14_22	45	0.3968	12.82	1.81	0.047	0.007	415.3	35.0	484.2	32.9	48.2	177.9	-16.6
wa_1_14_13	50	0.41	12.74	0.88	0.056	0.004	480.9	19.0	487.1	16.2	451.4	79.3	-1.3
wa_1_14_29	44	0.34	12.69	1.59	0.061	0.008	516.1	36.7	489.0	29.5	638.0	141.0	5.3
wa_1_14_31	29	0.33	12.63	1.13	0.056	0.006	484.2	26.9	491.2	21.2	451.0	119.0	-1.4
wa_1_14_11	49	0.42	12.50	0.88	0.055	0.004	481.3	19.4	496.1	16.8	411.2	81.3	-3.1
CM-AL-3, Felsic layer in the Agricola Schist													
32.80378°N, 85.79555°W; boudinaged													
CM_AL_3_7	12300	4.57	23.75	2.54	0.057	0.003	290.1	15.0	265.9	13.9	490.5	58.0	8.3
CM_AL_3_6	4950	13.48	16.81	1.19	0.058	0.003	395.0	14.3	372.5	12.8	528.8	56.7	5.7
CM_AL_3_9	7550	0.01	16.42	1.40	0.061	0.004	419.8	18.5	381.1	15.8	638.3	70.5	9.2
CM_AL_3_18	3210	21.01	16.21	1.50	0.056	0.003	395.4	17.5	385.9	17.3	451.4	59.5	2.4
CM_AL_3_17	4380	15.22	16.03	1.52	0.057	0.003	404.9	18.1	390.1	17.9	490.5	58.0	3.7
CM_AL_3_1	3660	20.88	15.92	1.55	0.057	0.003	407.3	18.6	392.7	18.5	490.5	58.0	3.6
CM_AL_3_8	4600	12.58	15.90	1.19	0.055	0.003	395.8	15.2	393.2	14.3	411.2	61.0	0.7
CM_AL_3_5	13600	4.55	15.90	1.52	0.059	0.003	419.4	18.6	393.2	18.2	566.1	55.4	6.2
CM_AL_3_3	4240	13.89	15.80	1.50	0.058	0.004	415.7	20.0	395.6	18.2	528.8	75.6	4.8

TABLE A1

(continued)

Sample name	U (ppm)	Th/U	$^{238}U/^{206}Pb$	2 sigma abs	$^{207}Pb/^{206}Pb$	2 sigma abs	207/235 age Ma	1 sigma abs err Ma	206/238 age† Ma	1 sigma abs err Ma	207/206 age Ma	1 sigma abs err Ma	disc†† %
CM-AL-3, Felsic layer in the Agricola Schist													
32.80378°N, 85.79555°W; boudinaged													
CM_AL_3_19	14000	4.27	15.72	1.83	0.055	0.002	399.6	20.1	397.6	22.4	411.2	40.7	0.5
CM_AL_3_21	7470	8.99	15.63	1.32	0.056	0.003	407.5	16.8	399.8	16.4	451.4	59.5	1.9
CM_AL_3_4	4910	15.06	15.55	1.57	0.056	0.003	409.2	19.2	401.8	19.7	451.4	59.5	1.8
CM_AL_3_13	3490	18.42	15.50	1.20	0.057	0.003	416.3	16.0	403.0	15.1	490.5	58.0	3.2
CM_AL_3_11	3170	21.79	15.48	1.32	0.058	0.003	422.7	17.2	403.5	16.7	528.8	56.7	4.5
CM_AL_3_14	14400	3.85	15.46	1.74	0.058	0.002	423.2	20.4	404.0	22.0	528.8	37.8	4.5
CM_AL_3_12	7590	9.28	15.34	1.60	0.056	0.003	413.8	19.9	407.1	20.6	451.4	59.5	1.6
CM_AL_3_16	8350	7.30	15.34	1.51	0.057	0.003	419.9	19.2	407.1	19.4	490.5	58.0	3.0
CM_AL_3_10	7120	8.55	15.20	1.27	0.056	0.003	416.9	17.0	410.7	16.6	451.4	59.5	1.5
CM_AL_3_15	750	0.01	12.92	1.29	0.088	0.008	672.2	33.2	480.6	23.1	1381.6	87.3	28.5
CM_AL_3_22	4700	0.04	12.11	1.29	0.088	0.005	704.6	30.7	511.5	26.2	1381.6	54.6	27.4
CM_AL_3_26	6200	0.01	11.82	1.02	0.055	0.002	503.1	18.6	523.5	21.7	411.2	40.7	-4.1
CM_AL_3_23	7350	0.00	11.36	1.42	0.055	0.003	519.0	27.7	543.9	32.6	411.2	61.0	-4.8
CM_AL_3_2$$	54	0.79	6.67	0.49	0.076	0.005	958.6	30.6	900.5	30.9	1094.2	65.9	6.1
CM_AL_3_24$$	167	0.18	6.58	1.08	0.073	0.004	942.1	53.1	912.0	69.8	1013.0	55.5	3.2
CM-AL-4, Agricola Schist													
32.82488°N, 85.73900°W; medium- to coarse-grained, muscovite-garnet-biotite quartzofeldspathic schist													
-10%< Discordance <10%													
CM_AL_4_131	514	0.04	13.33	2.13	0.064	0.003	515.6	33.7	466.3	35.9	740.7	49.6	9.6
CM_AL_4_85	96	0.55	9.25	0.42	0.071	0.003	732.8	16.2	661.8	14.3	956.5	43.2	9.7
CM_AL_4_121	90	0.12	9.07	0.80	0.067	0.004	712.9	27.3	674.2	28.2	836.8	62.2	5.4
CM_AL_4_113	125	0.58	8.67	0.63	0.073	0.004	782.1	24.8	703.7	24.2	1013.0	55.5	10.0
CM_AL_4_117	102	0.31	8.63	0.48	0.069	0.005	754.3	24.3	706.8	18.6	897.8	74.8	6.3
CM_AL_4_33	234	0.48	8.50	0.35	0.073	0.003	793.0	16.0	717.0	14.0	1013.0	41.6	9.6
CM_AL_4_51	251	0.32	8.42	0.67	0.073	0.003	798.2	24.8	723.5	27.2	1013.0	41.6	9.4
CM_AL_4_74	161	0.37	8.20	0.74	0.067	0.003	765.9	27.1	741.8	31.6	836.8	46.6	3.1
CM_AL_4_108	119	0.26	8.00	0.70	0.074	0.004	834.5	29.3	759.3	31.3	1040.6	54.6	9.0
CM_AL_4_122	358	0.12	7.69	1.07	0.071	0.004	833.5	42.7	788.1	51.6	956.5	57.6	5.4
CM_AL_4_127	544	0.18	7.41	1.04	0.067	0.004	821.7	43.0	816.1	53.8	836.8	62.2	0.7
CM_AL_4_142	94	0.59	7.41	0.55	0.074	0.007	878.9	35.4	816.1	28.4	1040.6	95.5	7.1
CM_AL_4_56	251	0.19	7.35	0.97	0.075	0.004	891.6	42.2	822.3	50.9	1067.6	53.6	7.8
CM_AL_4_125	77	0.35	7.09	0.33	0.078	0.004	936.9	21.2	850.6	18.5	1146.0	50.9	9.2
CM_AL_4_30	371	0.12	6.98	0.34	0.071	0.003	889.7	19.1	863.1	19.7	956.5	43.2	3.0

TABLE A1
(continued)

Sample name	U (ppm)	Th/U	$^{238}U/^{206}Pb$	2 sigma abs	$^{207}Pb/^{206}Pb$	2 sigma abs	207/235 age Ma	1 sigma abs err Ma	206/238 age† Ma	1 sigma abs err Ma	207/206 age Ma	1 sigma abs err Ma	disc†† %
CM-AL-4, Agricola Schist													
32.82488°N, 85.73900°W; medium- to coarse-grained, muscovite-garnet-biotite quartzofeldspathic schist													
CM_AL_4_52	162	0.44	6.76	0.46	0.074	0.003	933.9	24.2	889.3	28.3	1040.6	40.9	4.8
CM_AL_4_34	586	0.11	6.72	0.25	0.070	0.003	903.9	17.0	894.3	15.5	927.4	44.0	1.1
CM_AL_4_90	475	0.28	6.58	0.52	0.074	0.003	950.5	27.4	912.0	33.6	1040.6	40.9	4.1
CM_AL_4_50	97	0.31	6.54	0.28	0.071	0.003	928.8	18.3	917.2	18.3	956.5	43.2	1.2
CM_AL_4_132	65	0.22	6.47	0.33	0.076	0.004	977.6	23.0	926.5	22.0	1094.2	52.7	5.2
CM_AL_4_78	930	0.12	6.41	0.62	0.070	0.003	932.4	32.3	934.5	42.1	927.4	44.0	-0.2
CM_AL_4_35	69	0.49	6.40	0.34	0.070	0.003	933.4	20.8	935.9	23.1	927.4	44.0	-0.3
CM_AL_4_134	775	0.24	6.37	0.81	0.070	0.003	936.3	41.0	940.0	55.6	927.4	44.0	-0.4
CM_AL_4_28	75	0.91	6.36	0.36	0.074	0.003	971.6	21.8	941.4	24.8	1040.6	40.9	3.1
CM_AL_4_126	69	0.36	6.33	0.56	0.072	0.004	957.5	32.4	945.5	38.9	985.0	56.5	1.3
CM_AL_4_136	127	0.31	6.29	0.51	0.073	0.004	970.0	30.6	951.1	35.8	1013.0	55.5	1.9
CM_AL_4_77	89	0.97	6.29	0.30	0.074	0.004	978.5	22.6	951.1	21.1	1040.6	54.6	2.8
CM_AL_4_62	199	0.30	6.29	0.38	0.079	0.004	1020.1	25.4	951.1	26.7	1171.2	50.1	6.8
CM_AL_4_47	221	0.30	6.29	0.47	0.080	0.003	1028.2	27.0	951.1	33.0	1196.1	37.0	7.5
CM_AL_4_19	26	0.40	6.27	0.39	0.070	0.003	946.0	23.2	953.9	27.6	927.4	44.0	-0.8
CM_AL_4_144	71	0.76	6.17	0.72	0.077	0.003	1016.0	39.5	968.3	52.5	1120.3	38.9	4.7
CM_AL_4_118	100	0.32	6.10	0.56	0.069	0.004	954.0	33.6	978.6	41.7	897.8	59.8	-2.6
CM_AL_4_20	1370	0.16	6.10	0.63	0.070	0.004	963.0	36.7	978.6	46.9	927.4	58.7	-1.6
CM_AL_4_45	276	0.44	6.10	0.67	0.070	0.003	963.0	36.7	978.6	49.9	927.4	44.0	-1.6
CM_AL_4_114	103	0.27	6.10	0.48	0.074	0.004	997.9	30.3	978.6	35.7	1040.6	54.6	1.9
CM_AL_4_63	375	0.21	6.10	0.41	0.076	0.004	1014.9	27.4	978.6	30.5	1094.2	52.7	3.6
CM_AL_4_53	33	0.36	6.08	0.30	0.078	0.005	1033.8	26.2	981.6	22.5	1146.0	63.7	5.0
CM_AL_4_22	294	0.25	6.02	0.51	0.072	0.003	988.9	29.8	990.7	38.9	985.0	42.4	-0.2
CM_AL_4_6	684	0.27	6.02	0.69	0.073	0.004	997.6	40.4	990.7	52.6	1013.0	55.5	0.7
CM_AL_4_16	26	0.44	6.00	0.26	0.077	0.003	1034.0	18.9	993.7	20.0	1120.3	38.9	3.9
CM_AL_4_93	76	0.34	5.99	0.28	0.072	0.005	992.1	26.5	995.3	21.6	985.0	70.7	-0.3
CM_AL_4_98	332	0.53	5.99	0.43	0.075	0.002	1018.1	24.6	995.3	33.1	1067.6	26.8	2.2
CM_AL_4_32	32	0.39	5.85	0.34	0.070	0.004	989.2	25.8	1017.3	27.3	927.4	58.7	-9.7
CM_AL_4_89	324	0.13	5.81	0.61	0.072	0.004	1011.5	38.0	1023.8	49.7	985.0	56.5	-3.9
CM_AL_4_75	114	0.30	5.78	0.37	0.072	0.004	1014.8	27.2	1028.7	30.4	985.0	56.5	-4.4
CM_AL_4_8	411	0.32	5.68	0.24	0.072	0.003	1026.0	19.2	1045.4	20.4	985.0	42.4	-6.1
CM_AL_4_39	116	0.32	5.62	0.44	0.072	0.003	1032.9	28.7	1055.7	38.1	985.0	42.4	-7.2
CM_AL_4_115	157	0.24	5.62	0.38	0.072	0.003	1032.9	25.7	1055.7	32.9	985.0	42.4	-7.2

TABLE A1
(continued)

Sample name	U (ppm)	Th/U	$^{238}U/^{206}Pb$	2 sigma abs	$^{207}Pb/^{206}Pb$	2 sigma abs	207/235 age Ma	1 sigma abs err Ma	206/238 age† Ma	1 sigma abs err Ma	207/206 age Ma	1 sigma abs err Ma	disc†† %
CM-AL-4, Agricola Schist													
32.82488°N, 85.73900°W; medium- to coarse-grained, muscovite-garnet-biotite quartzofeldspathic schist													
CM_AL_4_72	376	0.26	5.52	0.58	0.072	0.003	1044.6	36.9	1073.3	51.9	985.0	42.4	-9.0
CM_AL_4_66	115	0.37	5.92	0.46	0.073	0.004	1008.3	30.4	1006.2	36.2	1013.0	55.5	0.7
CM_AL_4_87	710	0.31	5.75	0.53	0.073	0.004	1027.0	34.6	1033.6	44.0	1013.0	55.5	-2.0
CM_AL_4_54	138	0.43	5.62	0.41	0.073	0.004	1041.9	29.7	1055.7	35.5	1013.0	55.5	-4.2
CM_AL_4_139	538	0.38	5.56	0.62	0.073	0.004	1048.9	40.6	1066.2	54.8	1013.0	55.5	-5.3
CM_AL_4_76	147	0.49	5.32	0.57	0.073	0.004	1078.0	40.0	1110.4	54.6	1013.0	55.5	-9.6
CM_AL_4_49	229	0.26	5.95	0.50	0.074	0.004	1013.8	32.0	1001.5	39.0	1040.6	54.6	3.8
CM_AL_4_119	456	0.27	5.88	0.73	0.074	0.004	1021.4	43.6	1012.5	58.2	1040.6	54.6	2.7
CM_AL_4_26	275	0.36	5.87	0.29	0.074	0.003	1022.5	20.6	1014.1	23.2	1040.6	40.9	2.5
CM_AL_4_44	104	1.03	5.80	0.31	0.074	0.003	1030.2	21.7	1025.4	25.3	1040.6	40.9	1.5
CM_AL_4_68	274	0.20	5.75	0.53	0.074	0.004	1035.9	34.7	1033.6	44.0	1040.6	54.6	0.7
CM_AL_4_55	48	0.71	5.73	0.29	0.074	0.005	1038.1	27.4	1037.0	24.2	1040.6	68.2	0.3
CM_AL_4_120	336	0.27	5.81	0.44	0.075	0.004	1037.8	30.1	1023.8	35.8	1067.6	53.6	4.1
CM_AL_4_71	389	0.27	5.71	0.42	0.075	0.004	1049.2	29.7	1040.3	35.3	1067.6	53.6	2.6
CM_AL_4_88	150	0.28	5.71	0.46	0.075	0.005	1049.2	34.2	1040.3	38.7	1067.6	67.0	2.6
CM_AL_4_116	201	0.96	5.35	0.54	0.075	0.004	1092.2	38.2	1104.6	51.2	1067.6	53.6	-3.5
CM_AL_4_21	175	0.38	5.32	0.26	0.075	0.003	1096.0	21.2	1110.4	24.9	1067.6	40.2	-4.0
CM_AL_4_67	542	0.30	5.56	0.62	0.076	0.004	1075.4	40.9	1066.2	54.8	1094.2	52.7	2.6
CM_AL_4_105	475	0.16	5.52	0.34	0.076	0.004	1080.2	26.9	1073.3	30.4	1094.2	52.7	1.9
CM_AL_4_80	400	0.12	5.46	0.57	0.076	0.004	1087.5	39.0	1084.2	52.1	1094.2	52.7	0.9
CM_AL_4_1	81	0.40	5.43	0.35	0.076	0.004	1091.2	27.8	1089.7	32.3	1094.2	52.7	0.4
CM_AL_4_97	265	0.46	5.26	0.53	0.076	0.003	1112.6	36.6	1122.0	51.9	1094.2	39.5	-2.5
CM_AL_4_27	129	0.68	5.13	0.37	0.076	0.003	1129.5	28.0	1148.0	37.9	1094.2	39.5	-4.9
CM_AL_4_2	88	0.36	5.56	0.26	0.077	0.005	1084.1	26.7	1066.2	23.0	1120.3	64.8	4.8
CM_AL_4_37	173	0.15	5.52	0.27	0.077	0.004	1088.9	23.8	1073.3	24.2	1120.3	51.8	4.2
CM_AL_4_137	241	0.31	5.49	0.66	0.077	0.004	1092.6	43.8	1078.7	59.7	1120.3	51.8	3.7
CM_AL_4_138	157	0.14	5.43	0.47	0.077	0.004	1099.9	33.9	1089.7	43.4	1120.3	51.8	2.7
CM_AL_4_130	395	0.34	5.10	0.52	0.077	0.003	1142.5	37.4	1154.2	53.9	1120.3	38.9	-3.0
CM_AL_4_135	157	0.22	5.62	0.57	0.078	0.004	1085.6	37.9	1055.7	49.4	1146.0	50.9	7.9
CM_AL_4_57	168	0.74	5.43	0.35	0.078	0.004	1108.6	27.8	1089.7	32.3	1146.0	50.9	4.9
CM_AL_4_42	875	0.40	5.41	0.38	0.078	0.002	1111.1	25.3	1093.4	35.3	1146.0	25.5	4.6
CM_AL_4_140	351	0.31	4.98	0.52	0.078	0.004	1167.8	40.4	1179.6	56.3	1146.0	50.9	-2.9
CM_AL_4_110	168	0.23	4.93	0.58	0.078	0.004	1174.8	44.7	1190.6	63.9	1146.0	50.9	-3.9

TABLE A1
(continued)

Sample name	U (ppm)	Th/U	^{238}U/^{206}Pb	2 sigma abs	^{207}Pb/^{206}Pb	2 sigma abs	207/235 age Ma	1 sigma abs err Ma	206/238 age† Ma	1 sigma abs err Ma	207/206 age Ma	1 sigma abs err Ma	disc†† %
CM-AL-4, Agricola Schist													
32.82488°N, 85.73900°W; medium- to coarse-grained, muscovite-garnet-biotite quartzofeldspathic schist													
CM_AL_4_129	233	0.35	5.56	0.59	0.079	0.004	1101.3	39.5	1066.2	52.1	1171.2	50.1	9.0
CM_AL_4_84	597	0.37	5.52	0.52	0.079	0.004	1106.1	36.0	1073.3	46.6	1171.2	50.1	8.4
CM_AL_4_59	560	0.10	5.41	0.44	0.079	0.005	1119.7	35.0	1093.4	40.9	1171.2	62.6	6.6
CM_AL_4_143	344	0.21	4.81	0.60	0.079	0.004	1201.0	47.4	1217.6	69.2	1171.2	50.1	-4.0
CM_AL_4_23	285	0.38	5.43	0.30	0.080	0.003	1125.8	22.7	1089.7	27.7	1196.1	37.0	8.9
CM_AL_4_43	297	0.19	5.15	0.45	0.080	0.004	1162.1	34.8	1144.0	45.8	1196.1	49.3	4.4
CM_AL_4_61	189	0.22	4.90	0.50	0.080	0.004	1196.8	39.9	1197.2	55.7	1196.1	49.3	-0.1
CM_AL_4_128	555	0.33	5.35	0.80	0.081	0.005	1144.4	55.5	1104.6	75.9	1220.6	60.7	9.5
CM_AL_4_83	469	0.36	4.78	0.43	0.081	0.005	1223.1	38.8	1224.6	50.2	1220.6	60.7	-0.3
CM_AL_4_109	264	0.29	5.10	0.42	0.082	0.004	1186.1	33.5	1154.2	43.5	1244.6	47.8	7.3
CM_AL_4_18	348	0.53	4.74	0.29	0.082	0.003	1237.9	25.5	1234.0	34.4	1244.6	35.8	0.9
CM_AL_4_41	375	0.59	4.48	0.22	0.082	0.003	1278.6	22.3	1298.8	28.9	1244.6	35.8	-4.4
CM_AL_4_133	62	0.35	4.95	0.44	0.083	0.004	1215.6	35.8	1186.2	48.2	1268.3	47.0	6.5
CM_AL_4_82	300	0.27	4.90	0.60	0.083	0.004	1222.8	46.8	1197.2	66.9	1268.3	47.0	5.6
CM_AL_4_112	209	0.43	4.65	0.43	0.083	0.004	1260.4	37.6	1255.7	52.8	1268.3	47.0	1.0
CM_AL_4_94	97	0.21	4.59	0.42	0.084	0.004	1278.4	37.5	1270.6	52.8	1291.7	46.3	1.6
CM_AL_4_95	106	0.30	4.55	0.37	0.084	0.005	1284.8	36.7	1280.7	47.2	1291.7	57.9	0.9
CM_AL_4_124	149	0.64	4.83	0.51	0.085	0.005	1250.1	43.4	1213.0	58.4	1314.7	57.0	7.7
CM_AL_4_48	276	0.62	4.13	0.58	0.085	0.004	1365.2	55.6	1397.8	88.2	1314.7	45.6	-6.3
CM_AL_4_65	155	0.61	4.20	0.48	0.086	0.004	1361.4	46.3	1376.8	70.8	1337.3	45.0	-3.0
Discordance >10% or <-10%													
CM_AL_4_46	613	0.03	13.95	1.07	0.080	0.012	591.4	37.8	446.3	16.5	1196.0	148.0	24.5
CM_AL_4_3	195	0.08	12.61	1.26	0.067	0.003	557.9	23.5	492.0	23.7	836.8	46.6	11.8
CM_AL_4_4	412	0.28	10.52	0.50	0.074	0.002	688.2	13.7	585.4	13.3	1040.6	27.3	14.9
CM_AL_4_96	626	0.19	10.42	1.01	0.069	0.003	658.4	25.7	590.7	27.4	897.8	44.9	10.3
CM_AL_4_7	1110	0.05	10.35	0.66	0.075	0.004	703.1	21.1	594.6	18.1	1067.6	53.6	15.4
CM_AL_4_9	329	0.08	9.96	0.92	0.072	0.003	701.9	25.7	616.8	27.2	985.0	42.4	12.1
CM_AL_4_92	1110	0.12	9.52	0.91	0.073	0.004	732.2	28.7	643.9	29.3	1013.0	55.5	12.1
CM_AL_4_14	491	0.36	9.01	0.57	0.075	0.003	775.9	20.3	678.5	20.4	1067.6	40.2	12.6
CM_AL_4_29	69	0.50	8.77	1.00	0.071	0.003	760.9	32.6	696.1	37.6	956.5	43.2	8.5
CM_AL_4_107	128	0.26	8.77	0.92	0.074	0.005	783.3	34.1	696.1	34.6	1040.6	68.2	11.1
CM_AL_4_86	2	0.10	6.94	0.96	0.109	0.034	1170.0	118.0	867.8	56.2	1782.0	284.0	25.8
CM_AL_4_73	28	0.00	6.48	0.34	0.557	0.032	2592.3	36.4	925.1	22.6	4399.0	42.0	64.3
CM_AL_4_79	230	0.22	6.33	0.56	0.140	0.015	1419.8	53.1	945.5	38.9	2226.4	92.8	33.4

TABLE A1

(continued)

Sample name	U (ppm)	Th/U	$^{238}U/^{206}Pb$	2 sigma abs	$^{207}Pb/^{206}Pb$	2 sigma abs	207/235 age Ma	1 sigma abs err Ma	206/238 age† Ma	1 sigma abs err Ma	207/206 age Ma	1 sigma abs err Ma	disc†† %
CM-AL-4, Agricola Schist													
32.82488°N, 85.73900°W; medium- to coarse-grained, muscovite-garnet-biotite quartzofeldspathic schist													
Discordance >10% or <-10%													
CM_AL_4_64	304	0.26	5.75	0.63	0.070	0.003	1000.1	37.4	1033.6	52.3	927.4	44.0	-11.5
CM_AL_4_69	311	0.35	5.59	0.66	0.070	0.003	1018.2	40.4	1060.9	57.7	927.4	44.0	-14.4
CM_AL_4_104	283	0.56	5.56	0.34	0.081	0.006	1118.1	32.6	1066.2	30.0	1220.6	72.8	12.6
CM_AL_4_60	55	0.28	5.46	0.45	0.072	0.004	1051.7	32.6	1084.2	41.1	985.0	56.5	-10.1
CM_AL_4_100	167	0.49	5.41	0.56	0.072	0.004	1057.8	38.6	1093.4	52.1	985.0	56.5	-11.0
CM_AL_4_38	124	0.41	5.29	0.36	0.073	0.004	1081.7	29.1	1116.2	34.9	1013.0	55.5	-10.2
CM_AL_4_11	171	0.34	5.24	0.26	0.071	0.003	1069.6	21.5	1125.9	25.6	956.5	43.2	-17.7
CM_AL_4_58	96	0.71	5.24	0.49	0.073	0.003	1088.1	34.1	1125.9	48.3	1013.0	41.6	-11.1
CM_AL_4_102	219	0.22	5.21	0.38	0.084	0.004	1188.0	30.5	1131.9	37.9	1291.7	46.3	12.4
CM_AL_4_25	228	0.27	5.13	0.17	0.071	0.003	1083.7	17.9	1148.0	17.4	956.5	43.2	-20.0
CM_AL_4_36	599	0.58	5.10	0.24	0.073	0.003	1106.2	21.0	1154.2	24.9	1013.0	41.6	-13.9
CM_AL_4_141	213	0.32	5.08	0.64	0.089	0.005	1246.9	49.5	1158.4	66.8	1403.3	53.8	17.5
CM_AL_4_40	109	0.34	4.93	0.39	0.075	0.004	1147.7	32.8	1190.6	43.0	1067.6	53.6	-11.5
CM_AL_4_24	210	0.21	4.83	0.58	0.075	0.003	1161.8	43.8	1213.0	66.4	1067.6	40.2	-13.6
CM_AL_4_70	149	0.21	4.76	0.68	0.088	0.012	1285.8	72.0	1229.3	79.9	1382.0	131.0	11.0
CM_AL_4_99	93	0.22	4.76	0.41	0.089	0.005	1294.1	37.6	1229.3	48.2	1403.3	53.8	12.4
CM_AL_4_10	266	0.27	4.74	0.31	0.077	0.003	1193.3	26.7	1234.0	36.7	1120.3	38.9	-10.1
CM_AL_4_31	471	0.68	4.30	0.14	0.079	0.003	1281.3	18.2	1347.9	19.8	1171.2	37.6	-15.1
Th/U<0.1													
CM_AL_4_5	729	0.02	9.55	0.68	0.067	0.003	686.9	21.0	642.0	21.8	836.8	46.6	6.5
CM_AL_4_15	1690	0.07	9.51	0.63	0.065	0.003	673.9	19.9	644.5	20.3	773.4	48.6	4.4
CM_AL_4_106	220	0.07	9.31	0.67	0.063	0.004	669.0	23.5	657.7	22.5	707.3	67.5	1.7
CM_AL_4_101	502	0.02	8.29	0.65	0.065	0.003	743.9	24.0	734.2	27.2	773.4	48.6	1.3
CM_AL_4_123	364	0.03	7.69	0.71	0.071	0.004	833.5	30.7	788.1	34.2	956.5	57.6	5.4
CM_AL_4_13	269	0.07	7.35	0.87	0.077	0.004	907.3	38.8	822.3	45.7	1120.3	51.8	9.4
CM_AL_4_103	859	0.04	7.30	0.91	0.067	0.002	830.1	36.3	827.6	48.4	836.8	31.1	0.3
CM_AL_4_111	1120	0.01	7.06	0.49	0.070	0.003	874.6	23.9	853.9	27.8	927.4	44.0	2.4
CM_AL_4_91	551	0.02	6.89	0.47	0.071	0.003	897.4	23.9	873.7	27.9	956.5	43.2	2.6
CM_AL_4_17	279	0.03	6.45	0.75	0.075	0.004	971.2	40.0	929.1	50.3	1067.6	53.6	4.3
CM_AL_4_12	490	0.02	6.37	0.65	0.078	0.004	1003.8	36.4	940.0	44.6	1146.0	50.9	6.4
CM_AL_4_81	670	0.01	5.81	0.61	0.073	0.004	1020.4	38.1	1023.8	49.7	1013.0	55.5	-1.1

TABLE A1
(continued)

Sample name	U (ppm)	Th/U	$^{238}U/^{206}Pb$	2 sigma abs	$^{207}Pb/^{206}Pb$	2 sigma abs	207/235 age Ma	1 sigma abs err Ma	206/238 age† Ma	1 sigma abs err Ma	207/206 age Ma	1 sigma abs err Ma	disc†† %
CM-AL-4, Agricola Schist													
32.81725°N, 85.75417°W; medium- to coarse-grained quartzofeldspathic muscovite-garnet-biotite schist													
-10%< Discordance <10%													
AG1_14_95	1610	0.11	13.50	0.56	0.064	0.003	510.5	12.6	460.7	9.2	740.7	49.6	9.8
AG1_14_22	106	0.55	12.58	0.35	0.059	0.002	506.2	8.7	493.1	6.6	566.1	36.9	2.6
AG1_14_21	27	0.79	9.87	0.28	0.064	0.002	648.3	10.1	622.1	8.4	740.7	33.1	4.0
AG1_14_87	118	0.11	9.66	0.63	0.065	0.003	666.2	19.5	635.0	19.7	773.4	48.6	4.7
AG1_14_92	178	0.15	8.88	0.71	0.067	0.002	723.8	22.1	687.9	26.1	836.8	31.1	5.0
AG1_14_125	740	0.15	8.50	0.63	0.064	0.002	722.8	20.8	717.0	25.1	740.7	33.1	0.8
AG1_14_30	470	0.13	8.50	0.36	0.069	0.003	762.4	16.3	717.0	14.4	897.8	44.9	6.0
AG1_14_71	194	0.17	8.33	0.69	0.067	0.003	757.5	25.1	730.8	28.6	836.8	46.6	3.5
AG1_14_37	65	0.36	8.10	0.20	0.069	0.002	788.5	10.4	750.4	8.8	897.8	29.9	4.8
AG1_14_79	97	0.46	8.05	0.44	0.068	0.002	783.9	17.0	754.8	19.5	867.6	30.5	3.7
AG1_14_73	187	0.12	7.87	0.74	0.071	0.003	820.4	29.0	771.1	34.2	956.5	43.2	6.0
AG1_14_94	206	0.30	7.79	0.47	0.070	0.003	818.2	20.8	778.6	22.1	927.4	44.0	4.8
AG1_14_96	328	0.43	7.75	0.56	0.071	0.003	829.1	23.7	782.3	26.6	956.5	43.2	5.6
AG1_14_9	232	0.25	7.46	0.72	0.069	0.003	834.5	30.1	810.9	36.8	897.8	44.9	2.8
AG1_14_136	71	0.27	7.40	0.19	0.072	0.003	863.6	14.2	817.1	9.9	985.0	42.4	5.4
AG1_14_35	110	0.55	7.25	0.24	0.073	0.003	883.7	15.6	833.0	12.9	1013.0	41.6	5.7
AG1_14_75	101	0.49	7.23	0.31	0.071	0.002	869.0	15.0	835.1	16.8	956.5	28.8	3.9
AG1_14_111	187	0.10	7.19	0.67	0.070	0.003	864.0	29.8	839.5	36.7	927.4	44.0	2.8
AG1_14_70	117	0.31	7.16	0.26	0.066	0.002	832.6	13.4	842.8	14.3	805.4	31.7	-1.2
AG1_14_1	193	0.40	7.14	0.17	0.070	0.002	868.1	10.9	845.0	9.4	927.4	29.3	2.7
AG1_14_85	275	0.62	7.14	0.40	0.071	0.002	876.4	18.4	845.0	22.2	956.5	28.8	3.6
AG1_14_118	202	0.41	7.05	0.21	0.070	0.002	875.5	12.1	855.1	11.9	927.4	29.3	2.3
AG1_14_132	57	0.33	7.04	0.55	0.065	0.002	833.5	23.9	856.2	31.3	773.4	32.4	-2.7
AG1_14_15	87	0.47	6.94	0.19	0.074	0.002	917.9	11.6	867.8	11.1	1040.6	27.3	5.5
AG1_14_160	288	0.11	6.93	0.24	0.071	0.002	894.0	13.3	868.9	14.1	956.5	28.8	2.8
AG1_14_102	515	0.28	6.92	0.33	0.069	0.002	878.0	16.4	870.1	19.4	897.8	29.9	0.9
AG1_14_159	115	0.40	6.86	0.19	0.074	0.003	925.0	14.9	877.2	11.4	1040.6	40.9	5.2
AG1_14_32	90	0.24	6.85	0.28	0.074	0.002	925.8	14.9	878.4	16.8	1040.6	27.3	5.1
AG1_14_14	139	0.44	6.84	0.23	0.070	0.002	893.3	13.1	879.6	13.8	927.4	29.3	1.5
AG1_14_7	472	2.67	6.78	0.24	0.073	0.002	923.8	13.6	886.9	14.7	1013.0	27.8	4.0
AG1_14_26	60	0.60	6.76	0.21	0.071	0.003	908.8	15.7	889.3	12.9	956.5	43.2	2.1
AG1_14_134	66	0.79	6.75	0.24	0.071	0.002	909.7	13.6	890.6	14.8	956.5	28.8	2.1

TABLE A1
(continued)

Sample name	U (ppm)	Th/U	$^{238}U/^{206}Pb$	2 sigma abs	$^{207}Pb/^{206}Pb$	2 sigma abs	207/235 age Ma	1 sigma abs err Ma	206/238 age† Ma	1 sigma abs err Ma	207/206 age Ma	1 sigma abs err Ma	disc†† %
CM-AL-4, Agricola Schist													
32.81725°N, 85.75417°W; medium- to coarse-grained quartzofeldspathic muscovite-garnet-biotite schist													
-10%< Discordance <10%													
AG1_14_40	702	0.19	6.71	0.25	0.070	0.003	904.8	17.0	895.5	15.6	927.4	44.0	1.0
AG1_14_2	87	0.38	6.66	0.20	0.071	0.003	917.8	15.7	901.8	12.6	956.5	43.2	1.7
AG1_14_18	93	0.29	6.66	0.26	0.072	0.003	926.3	17.3	901.8	16.4	985.0	42.4	2.6
AG1_14_120	110	0.22	6.65	0.30	0.071	0.003	918.7	18.7	903.1	19.0	956.5	43.2	1.7
AG1_14_81	77	0.38	6.59	0.19	0.073	0.003	941.2	15.4	910.7	12.2	1013.0	41.6	3.2
AG1_14_104	102	0.45	6.59	0.16	0.074	0.002	949.5	11.2	910.7	10.3	1040.6	27.3	4.1
AG1_14_29	102	0.46	6.58	0.20	0.071	0.002	925.1	12.6	912.0	12.9	956.5	28.8	1.4
AG1_14_8	341	0.89	6.56	0.25	0.078	0.002	985.2	14.5	914.6	16.2	1146.0	25.5	7.2
AG1_14_67	398	0.62	6.54	0.18	0.071	0.002	928.8	12.0	917.2	11.8	956.5	28.8	1.2
AG1_14_97	122	0.29	6.48	0.27	0.077	0.003	984.8	18.0	925.1	18.0	1120.3	38.9	6.1
AG1_14_23	40	0.42	6.44	0.24	0.076	0.003	980.5	17.1	930.5	16.1	1094.2	39.5	5.1
AG1_14_65	95	0.62	6.33	0.26	0.077	0.004	999.6	21.1	945.5	18.1	1120.3	51.8	5.4
AG1_14_57	48	0.52	6.31	0.16	0.072	0.003	959.4	15.1	948.3	11.2	985.0	42.4	1.2
AG1_14_49	86	0.41	6.31	0.18	0.075	0.002	985.0	12.3	948.3	12.6	1067.6	26.8	3.7
AG1_14_103	227	0.24	6.29	0.33	0.076	0.003	995.4	20.8	951.1	23.2	1094.2	39.5	4.5
AG1_14_12	79	0.44	6.27	0.18	0.072	0.002	963.4	12.4	953.9	12.7	985.0	28.3	1.0
AG1_14_93	98	1.16	6.26	0.21	0.074	0.003	981.5	16.6	955.4	14.9	1040.6	40.9	2.7
AG1_14_126	587	0.28	6.25	0.19	0.073	0.002	974.0	12.8	956.8	13.5	1013.0	27.8	1.8
AG1_14_109	49	0.59	6.20	0.16	0.072	0.002	970.4	11.8	963.9	11.6	985.0	28.3	0.7
AG1_14_78	167	0.50	6.20	0.18	0.073	0.002	979.0	12.5	963.9	13.0	1013.0	27.8	1.5
AG1_14_74	110	0.17	6.20	0.16	0.073	0.003	979.0	15.2	963.9	11.6	1013.0	41.6	1.5
AG1_14_89	264	0.25	6.19	0.23	0.074	0.003	988.6	17.4	965.4	16.7	1040.6	40.9	2.3
AG1_14_13	188	0.65	6.15	0.19	0.074	0.002	992.7	13.0	971.2	13.9	1040.6	27.3	2.2
AG1_14_55	84	0.51	6.13	0.14	0.072	0.003	977.5	14.9	974.2	10.3	985.0	42.4	0.3
AG1_14_107	70	0.65	6.12	0.27	0.072	0.002	978.5	16.4	975.6	20.0	985.0	28.3	0.3
AG1_14_59	75	0.32	6.10	0.48	0.073	0.003	989.3	28.1	978.6	35.7	1013.0	41.6	1.1
AG1_14_41	161	0.37	6.09	0.18	0.074	0.002	998.9	12.7	980.1	13.4	1040.6	27.3	1.9
AG1_14_20	229	0.59	6.07	0.25	0.072	0.003	983.7	18.5	983.1	18.8	985.0	42.4	0.1
AG1_14_83	100	0.58	6.06	0.18	0.073	0.002	993.4	12.8	984.6	13.6	1013.0	27.8	0.9
AG1_14_129	267	0.32	6.04	0.27	0.074	0.004	1004.2	22.4	987.6	20.5	1040.6	54.6	1.7
AG1_14_11	65	0.55	6.04	0.17	0.077	0.002	1029.7	12.4	987.6	12.9	1120.3	25.9	4.1
AG1_14_84	90	0.51	6.03	0.17	0.076	0.002	1022.4	12.4	989.1	12.9	1094.2	26.3	3.3

TABLE A1
(continued)

Sample name	U (ppm)	Th/U	$^{238}U/^{206}Pb$	2 sigma abs	$^{207}Pb/^{206}Pb$	2 sigma abs	207/235 age Ma	1 sigma abs err Ma	206/238 age† Ma	1 sigma abs err Ma	207/206 age Ma	1 sigma abs err Ma	disc†† %
CM-AL-4, Agricola Schist													
32.81725°N, 85.75417°W; medium- to coarse-grained quartzofeldspathic muscovite-garnet-biotite schist													
-10%< Discordance <10%													
AG1_14_53	1110	0.16	6.02	0.20	0.073	0.002	997.6	13.7	990.7	15.3	1013.0	27.8	0.7
AG1_14_44	131	0.40	6.02	0.14	0.073	0.002	997.6	11.4	990.7	10.7	1013.0	27.8	0.7
AG1_14_19	203	0.46	6.02	0.22	0.076	0.003	1023.4	17.3	990.7	16.8	1094.2	39.5	3.2
AG1_14_153	132	0.27	6.01	0.20	0.072	0.002	990.0	13.7	992.2	15.3	985.0	28.3	-0.2
AG1_14_34	13	0.76	6.01	0.24	0.075	0.003	1016.0	18.1	992.2	18.4	1067.6	40.2	2.3
AG1_14_105	224	0.31	5.99	0.32	0.074	0.003	1009.5	21.4	995.3	24.6	1040.6	40.9	1.4
AG1_14_128	633	0.25	5.98	0.21	0.069	0.002	966.4	14.2	996.8	16.2	897.8	29.9	-3.1
AG1_14_80	61	0.33	5.97	0.20	0.073	0.003	1003.0	16.9	998.3	15.5	1013.0	41.6	0.5
AG1_14_66	930	0.28	5.96	0.16	0.074	0.002	1012.7	12.2	999.9	12.4	1040.6	27.3	1.3
AG1_14_52	118	1.96	5.92	0.25	0.070	0.003	981.7	18.9	1006.2	19.7	927.4	44.0	-8.5
AG1_14_62	261	0.13	5.86	0.14	0.070	0.002	988.1	11.8	1015.7	11.2	927.4	29.3	-9.5
AG1_14_131	147	0.30	5.85	0.19	0.070	0.002	989.2	13.7	1017.3	15.3	927.4	29.3	-9.7
AG1_14_149	63	0.31	5.91	0.18	0.072	0.003	1000.6	16.4	1007.7	14.2	985.0	42.4	-2.3
AG1_14_139	138	0.44	5.84	0.18	0.072	0.003	1008.2	16.6	1018.9	14.5	985.0	42.4	-3.4
AG1_14_106	180	0.49	5.79	0.17	0.072	0.002	1013.7	13.0	1027.0	13.9	985.0	28.3	-4.3
AG1_14_58	147	0.61	5.68	0.14	0.072	0.002	1026.0	12.0	1045.4	11.9	985.0	28.3	-6.1
AG1_14_51	93	0.46	5.50	0.16	0.072	0.002	1047.0	13.1	1076.9	14.4	985.0	28.3	-9.3
AG1_14_110	195	0.36	5.77	0.17	0.073	0.002	1024.8	13.0	1030.3	14.0	1013.0	27.8	-1.7
AG1_14_98	564	0.14	5.77	0.19	0.073	0.002	1024.8	13.8	1030.3	15.7	1013.0	27.8	-1.7
AG1_14_140	213	0.92	5.66	0.26	0.073	0.002	1037.3	17.4	1048.8	22.2	1013.0	27.8	-3.5
AG1_14_158	440	0.25	5.62	0.16	0.073	0.002	1041.9	12.9	1055.7	13.9	1013.0	27.8	-4.2
AG1_14_114	554	0.34	5.46	0.19	0.073	0.002	1060.8	14.6	1084.2	17.4	1013.0	27.8	-7.0
AG1_14_133	99	0.52	5.34	0.16	0.073	0.002	1075.5	13.5	1106.5	15.2	1013.0	27.8	-9.2
AG1_14_145	162	1.00	5.76	0.22	0.074	0.002	1034.7	15.2	1032.0	18.2	1040.6	27.3	0.8
AG1_14_117	132	0.79	5.68	0.17	0.074	0.002	1043.8	13.1	1045.4	14.4	1040.6	27.3	-0.5
AG1_14_108	141	1.56	5.48	0.23	0.074	0.003	1067.4	19.3	1080.5	20.9	1040.6	40.9	-3.8
AG1_14_88	55	0.37	5.31	0.19	0.074	0.002	1088.3	15.0	1112.3	18.3	1040.6	27.3	-6.9
AG1_14_143	347	1.30	5.19	0.25	0.074	0.002	1103.6	18.6	1135.9	25.1	1040.6	27.3	-9.2
AG1_14_99	48	1.00	5.93	0.18	0.075	0.003	1024.6	16.2	1004.6	14.1	1067.6	40.2	5.9
AG1_14_86	153	0.51	5.91	0.18	0.075	0.002	1026.8	13.1	1007.7	14.2	1067.6	26.8	5.6
AG1_14_82	280	0.21	5.85	0.16	0.075	0.002	1033.4	12.4	1017.3	12.9	1067.6	26.8	4.7
AG1_14_76	361	0.14	5.52	0.37	0.075	0.002	1071.4	23.9	1073.3	33.1	1067.6	26.8	-0.5

TABLE A1
(continued)

Sample name	U (ppm)	Th/U	$^{238}U/^{206}Pb$	2 sigma abs	$^{207}Pb/^{206}Pb$	2 sigma abs	207/235 age Ma	1 sigma abs err Ma	206/238 age† Ma	1 sigma abs err Ma	207/206 age Ma	1 sigma abs err Ma	disc†† %
CM-AL-4, Agricola Schist													
32.81725°N, 85.75417°W; medium- to coarse-grained quartzofeldspathic muscovite-garnet-biotite schist													
-10%< Discordance <10%													
AG1_14_69	60	0.85	5.93	0.18	0.076	0.003	1033.2	16.1	1004.6	14.1	1094.2	39.5	8.2
AG1_14_61	187	0.23	5.54	0.16	0.076	0.003	1077.8	16.2	1069.7	14.2	1094.2	39.5	2.2
AG1_14_64	163	0.30	5.21	0.11	0.076	0.002	1119.0	11.4	1131.9	11.0	1094.2	26.3	-3.4
AG1_14_54	190	0.25	5.04	0.12	0.076	0.002	1141.6	12.2	1166.8	12.7	1094.2	26.3	-6.6
AG1_14_5	452	1.06	5.73	0.15	0.077	0.002	1064.1	12.2	1037.0	12.5	1120.3	25.9	7.4
AG1_14_43	347	0.47	5.65	0.17	0.077	0.002	1073.4	13.2	1050.5	14.6	1120.3	25.9	6.2
AG1_14_91	221	0.44	5.68	0.17	0.078	0.002	1078.5	13.1	1045.4	14.4	1146.0	25.5	8.8
AG1_14_147	140	0.32	5.51	0.13	0.078	0.003	1098.8	15.1	1075.1	11.7	1146.0	38.2	6.2
AG1_14_141	153	0.60	5.36	0.15	0.078	0.002	1117.4	12.9	1102.8	14.2	1146.0	25.5	3.8
AG1_14_148	72	0.90	5.22	0.17	0.078	0.002	1135.4	14.2	1129.9	16.9	1146.0	25.5	1.4
AG1_14_60	92	0.68	5.16	0.11	0.078	0.003	1143.3	15.1	1141.9	11.2	1146.0	38.2	0.4
AG1_14_154	404	0.33	4.85	0.28	0.078	0.003	1186.3	24.3	1208.5	31.8	1146.0	38.2	-5.5
AG1_14_36	138	0.30	5.58	0.17	0.079	0.003	1098.9	16.3	1062.7	14.9	1171.2	37.6	9.3
AG1_14_138	361	0.32	5.21	0.21	0.079	0.003	1145.4	19.0	1131.9	20.9	1171.2	37.6	3.4
AG1_14_152	394	0.53	5.03	0.15	0.079	0.003	1169.7	16.8	1168.9	15.9	1171.2	37.6	0.2
AG1_14_115	967	0.33	4.70	0.14	0.079	0.002	1217.4	13.9	1243.5	16.8	1171.2	25.1	-6.2
AG1_14_6	339	0.60	5.40	0.21	0.080	0.002	1129.5	15.8	1095.2	19.6	1196.1	24.7	8.4
AG1_14_48	239	0.36	4.80	0.18	0.080	0.003	1211.4	18.8	1219.9	20.8	1196.1	37.0	-2.0
AG1_14_33	94	0.66	5.05	0.18	0.081	0.003	1184.4	18.0	1164.7	19.0	1220.6	36.4	4.6
AG1_14_47	258	0.49	4.34	0.16	0.081	0.003	1292.8	19.1	1336.7	22.3	1220.6	36.4	-9.5
AG1_14_90	193	0.44	5.01	0.15	0.082	0.003	1198.6	16.6	1173.2	16.1	1244.6	35.8	5.7
AG1_14_42	376	0.14	4.95	0.23	0.082	0.003	1207.1	20.9	1186.2	25.2	1244.6	35.8	4.7
AG1_14_156	184	0.49	4.94	0.14	0.082	0.002	1208.5	13.2	1188.4	15.4	1244.6	23.9	4.5
AG1_14_3	560	0.35	4.83	0.16	0.082	0.002	1224.5	14.6	1213.0	18.3	1244.6	23.9	2.5
AG1_14_155	300	0.65	5.07	0.17	0.083	0.002	1198.7	14.5	1160.5	17.8	1268.3	23.5	8.5
AG1_14_146	268	0.42	4.69	0.11	0.083	0.002	1254.2	12.1	1245.9	13.3	1268.3	23.5	1.8
AG1_14_68	99	0.53	4.59	0.11	0.083	0.003	1269.7	15.7	1270.6	13.8	1268.3	35.3	-0.2
AG1_14_157	425	0.75	4.46	0.13	0.083	0.002	1290.7	13.8	1304.1	17.2	1268.3	23.5	-2.8
AG1_14_16	374	0.53	4.78	0.27	0.084	0.004	1249.1	26.5	1224.6	31.5	1291.7	46.3	5.2
AG1_14_150	94	0.67	4.71	0.12	0.084	0.003	1259.7	15.8	1241.1	14.4	1291.7	34.7	3.9
AG1_14_56	63	0.69	4.63	0.10	0.084	0.002	1272.1	11.7	1260.6	12.4	1291.7	23.2	2.4
AG1_14_63	124	0.47	4.54	0.09	0.084	0.003	1286.4	14.9	1283.3	11.5	1291.7	34.7	0.7
AG1_14_144	199	0.65	4.50	0.14	0.084	0.003	1292.9	17.3	1293.6	18.2	1291.7	34.7	-0.1

TABLE A1

(continued)

Sample name	U (ppm)	Th/U	$^{238}U/^{206}Pb$	2 sigma abs	$^{207}Pb/^{206}Pb$	2 sigma abs	207/235 age Ma	1 sigma abs err Ma	206/238 age† Ma	1 sigma abs err Ma	207/206 age Ma	1 sigma abs err Ma	disc†† %
CM-AL-4, Agricola Schist													
32.81725°N, 85.75417°W; medium- to coarse-grained quartzofeldspathic muscovite-garnet-biotite schist													
-10%< Discordance <10%													
AG1_14_124	148	0.57	4.62	0.18	0.086	0.003	1290.8	19.1	1263.1	22.3	1337.3	33.7	5.5
AG1_14_116	172	0.43	4.60	0.14	0.086	0.003	1294.0	16.9	1268.1	17.5	1337.3	33.7	5.2
AG1_14_45	103	0.71	4.49	0.11	0.086	0.003	1311.8	15.7	1296.2	14.4	1337.3	33.7	3.1
AG1_14_119	126	1.04	4.59	0.23	0.087	0.003	1304.1	22.3	1270.6	28.9	1359.6	33.2	6.5
AG1_14_142	54	0.36	4.35	0.16	0.087	0.003	1343.8	18.8	1333.9	22.2	1359.6	33.2	1.9
AG1_14_77	120	0.84	3.98	0.17	0.088	0.002	1419.5	18.5	1445.0	27.6	1381.6	21.8	-4.6
AG1_14_112	94	1.04	3.57	0.14	0.099	0.003	1597.4	19.9	1591.9	27.7	1604.5	28.3	0.8
AG1_14_46	109	0.44	1.94	0.06	0.194	0.006	2734.8	20.7	2679.9	33.9	2775.6	25.4	3.4
Discordance >10% or <-10%													
AG1_14_24	50	0.73	6.42	0.19	0.083	0.004	1038.8	18.4	933.2	12.9	1268.3	47.0	10.2
AG1_14_137	190	0.49	5.83	0.23	0.078	0.004	1061.2	21.3	1020.5	18.6	1146.0	50.9	11.0
AG1_14_72	420	0.27	5.77	0.17	0.080	0.002	1084.9	12.9	1030.3	14.0	1196.1	24.7	13.9
AG1_14_17	290	0.30	5.63	0.30	0.071	0.002	1022.7	19.4	1054.0	25.9	956.5	28.8	-10.2
AG1_14_39	428	0.13	5.62	0.47	0.070	0.002	1014.8	28.4	1055.7	40.7	927.4	29.3	-13.8
AG1_14_135	125	0.49	5.58	0.25	0.071	0.003	1028.5	19.9	1062.7	21.9	956.5	43.2	-11.1
AG1_14_50	193	0.30	5.49	0.30	0.084	0.003	1151.6	22.5	1078.7	27.1	1291.7	34.7	16.5
AG1_14_127	211	0.84	5.46	0.20	0.088	0.007	1187.8	30.7	1084.2	18.3	1381.6	76.4	21.5
AG1_14_113	223	0.38	5.41	0.38	0.091	0.010	1217.9	46.3	1093.4	35.3	1446.0	105.0	24.4
AG1_14_130	155	0.47	5.27	0.16	0.072	0.002	1075.1	13.6	1120.0	15.6	985.0	28.3	-13.7
AG1_14_27	163	0.49	5.26	0.28	0.083	0.003	1173.0	22.4	1122.0	27.4	1268.3	35.3	11.5
AG1_14_151	346	0.39	5.26	0.18	0.072	0.003	1076.3	17.9	1122.0	17.6	985.0	42.4	-13.9
AG1_14_122	200	0.72	5.00	0.14	0.075	0.003	1138.0	16.7	1175.3	15.0	1067.6	40.2	-10.1
AG1_14_28	54	0.71	4.91	0.20	0.074	0.002	1141.3	16.8	1195.0	22.2	1040.6	27.3	-14.8
Th/U<0.1													
AG1_14_10	655	0.08	14.68	0.43	0.058	0.002	441.4	8.1	424.8	6.0	528.8	37.8	3.8
AG1_14_25	287	0.01	12.36	1.24	0.059	0.003	513.3	22.7	501.5	24.2	566.1	55.4	2.3
AG1_14_38	259	0.08	11.98	0.44	0.055	0.003	497.8	12.9	516.8	9.1	411.2	61.0	-3.8
AG1_14_123	1480	0.05	11.63	0.61	0.058	0.003	531.2	15.2	531.7	13.4	528.8	56.7	-0.1
AG1_14_100	151	0.04	8.40	0.85	0.066	0.004	745.0	31.1	725.1	34.7	805.4	63.4	2.7
AG1_14_101	177	0.03	8.20	1.01	0.069	0.006	781.8	41.1	741.8	43.2	897.8	89.7	5.1
AG1_14_4	1137	0.04	7.65	0.28	0.073	0.003	852.4	15.9	792.0	13.6	1013.0	41.6	7.1
AG1_14_31	296	0.02	6.29	0.19	0.074	0.002	978.5	12.7	951.1	13.4	1040.6	27.3	2.8
AG1_14_121	481	0.09	5.40	0.21	0.079	0.003	1121.0	18.4	1095.2	19.6	1171.2	37.6	6.5

TABLE A1
(continued)

Sample name	U (ppm)	Th/U	$^{238}U/^{206}Pb$	2 sigma abs	$^{207}Pb/^{206}Pb$	2 sigma abs	207/235 age Ma	1 sigma abs err Ma	206/238 age† Ma	1 sigma abs err Ma	207/206 age Ma	1 sigma abs err Ma	disc†† %
CMTBC, button schist from the uppermost Emuckfaw Group													
32.75511°N, 85.88691°W; quartzofeldspathic garnet-chlorite-muscovite-biotite schist													
Zircon interiors (detrial grains)													
cmtbc_39	2870	0.05	20.79	1.17	0.058	0.002	330.3	9.3	302.9	8.3	528.8	37.8	8.3
cmtbc_59		0.55	18.28	0.94	0.059	0.002	373.6	9.6	343.3	8.6	566.1	36.9	8.1
cmtbc_51	1570	0.52	17.04	0.70	0.056	0.002	379.3	8.6	367.6	7.3	451.4	39.7	3.1
cmtbc_57		2.19	16.95	0.95	0.056	0.002	381.0	10.6	369.5	10.1	451.4	39.7	3.0
cmtbc_31	3720	1.04	15.82	0.73	0.057	0.002	409.4	9.8	395.1	8.8	490.5	38.7	3.5
cmtbc_58		2.25	15.75	0.99	0.057	0.003	410.9	13.9	396.8	12.1	490.5	58.0	3.4
cmtbc_19	504	0.42	15.58	0.61	0.060	0.003	432.3	11.2	401.0	7.6	602.6	54.1	7.2
cmtbc_48	612	1.76	15.34	0.78	0.059	0.003	431.9	12.6	407.1	10.0	566.1	55.4	5.7
cmtbc_32	4280	1.30	14.99	0.56	0.055	0.002	415.5	8.9	416.3	7.5	411.2	40.7	-0.2
cmtbc_4	850	0.58	14.93	0.47	0.057	0.002	429.3	8.3	417.9	6.4	490.5	38.7	2.6
cmtbc_16	808	0.78	14.22	0.85	0.058	0.003	452.9	14.4	438.1	12.7	528.8	56.7	3.3
cmtbc_15	656	0.48	13.97	0.72	0.058	0.003	459.4	13.5	445.7	11.1	528.8	56.7	3.0
cmtbc_40	867	0.79	16.31	0.77	0.062	0.002	427.8	10.0	383.6	8.8	673.1	34.5	10.3
cmtbc_20	986	0.27	19.76	0.86	0.060	0.002	355.0	8.2	318.3	6.8	602.6	36.1	10.3
cmtbc_43	422	0.08	16.45	0.73	0.062	0.002	424.8	9.5	380.4	8.2	673.1	34.5	10.4
cmtbc_37	4500	0.02	14.64	0.84	0.065	0.003	484.8	14.2	425.9	11.8	773.4	48.6	12.1
cmtbc_47	612	0.79	15.80	1.00	0.064	0.004	450.4	16.2	395.6	12.1	740.7	66.1	12.2
cmtbc_45	531	0.52	15.90	0.81	0.069	0.007	476.0	21.6	393.2	9.7	898.0	105.0	17.4
cmtbc_52	3690	1.10	14.71	0.71	0.083	0.007	584.1	21.6	424.0	9.9	1268.3	82.3	27.4
cmtbc_60		1.93	15.36	0.99	0.102	0.013	659.8	34.6	406.6	12.7	1660.0	118.0	38.4
cmtbc_3	1271	1.23	20.58	0.76	0.099	0.004	516.4	11.1	305.9	5.5	1604.5	37.7	40.8
Zircon interiors (detrial grains)													
-10%< Discordance <10%													
cmtbc_55		0.04	9.78	0.94	0.064	0.003	652.7	25.7	627.6	28.7	740.7	49.6	3.8
cmtbc_13	686	0.20	8.61	0.49	0.070	0.003	763.2	19.1	708.3	19.1	927.4	44.0	7.2
cmtbc_34	6160	0.20	8.59	0.51	0.072	0.003	779.7	19.7	709.9	20.0	985.0	42.4	9.0
cmtbc_29		0.12	8.37	0.38	0.066	0.002	746.9	14.4	727.5	15.6	805.4	31.7	2.6
cmtbc_54	4390	0.10	7.60	0.38	0.070	0.002	832.1	16.4	796.9	18.7	927.4	29.3	4.2
cmtbc_6	764	0.06	7.03	0.29	0.075	0.003	918.3	17.4	857.4	16.6	1067.6	40.2	6.6
cmtbc_41	258	0.34	6.76	0.59	0.074	0.002	933.9	27.9	889.3	36.3	1040.6	27.3	4.8
cmtbc_44	85	0.60	6.69	0.29	0.072	0.003	923.6	18.2	898.0	18.2	985.0	42.4	2.8
cmtbc_30		0.18	6.51	0.35	0.073	0.003	948.7	20.9	921.2	23.1	1013.0	41.6	2.9
cmtbc_14	539	0.30	6.39	0.25	0.070	0.003	934.3	17.7	937.3	17.1	927.4	44.0	-0.3

Table A1

(continued)

Sample name	U (ppm)	Th/U	$^{238}U/^{206}Pb$	2 sigma abs	$^{207}Pb/^{206}Pb$	2 sigma abs	207/235 age Ma	1 sigma abs err Ma	206/238 age[†] Ma	1 sigma abs err Ma	207/206 age Ma	1 sigma abs err Ma	disc[††] %
CMTBC, button schist from the uppermost Emuckfaw Group													
32.75511°N, 85.88691°W; quartzofeldspathic garnet-chlorite-muscovite-biotite schist													
Zircon interiors (detrial grains)													
-10%< Discordance <10%													
cmtbc_17	1105	0.11	6.31	0.30	0.073	0.002	968.0	17.1	948.3	21.0	1013.0	27.8	2.0
cmtbc_25		0.53	5.75	0.36	0.071	0.003	1009.2	24.2	1033.6	29.9	956.5	43.2	-8.1
cmtbc_7	309	0.26	5.49	0.20	0.075	0.003	1075.0	17.9	1078.7	18.1	1067.6	40.2	-1.0
cmtbc_8	341	0.53	5.43	0.24	0.078	0.003	1108.6	19.8	1089.7	22.2	1146.0	38.2	4.9
cmtbc_1	286	0.56	5.41	0.32	0.080	0.003	1128.3	23.9	1093.4	29.7	1196.1	37.0	8.6
cmtbc_42	162	0.66	5.36	0.28	0.074	0.003	1082.0	22.0	1102.8	26.5	1040.6	40.9	-6.0
cmtbc_28		0.86	4.94	0.18	0.082	0.003	1208.5	18.2	1188.4	19.8	1244.6	35.8	4.5
cmtbc_18	1066	0.23	4.78	0.22	0.081	0.003	1223.1	21.0	1224.6	25.7	1220.6	36.4	-0.3
cmtbc_22	1500	0.12	4.49	0.15	0.085	0.003	1303.2	17.8	1296.2	19.6	1314.7	34.2	1.4
cmtbc_24	2130	0.84	3.66	0.16	0.092	0.004	1519.1	24.3	1557.1	30.2	1466.5	41.3	-6.2
cmtbc_50	147	0.60	2.17	0.11	0.172	0.007	2516.7	30.2	2443.2	51.5	2576.4	34.0	5.2
Discordance >10% or <-10%													
cmtbc_46	1010	0.84	13.39	0.82	0.107	0.019	754.0	50.0	464.3	13.7	1748.0	163.0	38.4
cmtbc_33	5710	0.06	13.37	0.59	0.073	0.004	569.7	15.3	465.0	9.9	1013.0	55.5	18.4
cmtbc_2	166	1.14	13.21	0.65	0.086	0.008	650.2	25.3	470.4	11.2	1337.3	89.9	27.7
cmtbc_27		0.10	12.82	0.56	0.068	0.003	557.1	13.3	484.2	10.2	867.6	45.7	13.1
cmtbc_35	3680	0.04	12.55	0.68	0.066	0.003	553.5	15.1	494.2	12.9	805.4	47.6	10.7
cmtbc_56		0.04	11.40	0.82	0.067	0.003	602.4	19.2	542.0	18.7	836.8	46.6	10.0
cmtbc_23	3222	0.17	10.79	0.45	0.076	0.003	688.8	14.4	571.4	11.4	1094.2	39.5	17.0
cmtbc_21	2670	0.01	8.00	0.48	0.076	0.003	849.8	20.7	759.3	21.5	1094.2	39.5	10.6
cmtbc_9	1449	0.35	7.86	0.41	0.083	0.003	912.1	19.1	772.0	19.0	1268.3	35.3	15.4
cmtbc_49	1280	0.04	7.36	0.34	0.088	0.004	988.7	20.5	821.3	17.8	1381.6	43.7	16.9
cmtbc_12	232	0.70	7.36	0.41	0.210	0.029	1620.4	60.3	821.3	21.5	2905.0	112.0	49.3
cmtbc_10	1490	0.70	7.04	0.40	0.086	0.004	1002.3	23.4	856.2	22.8	1337.3	45.0	14.6
cmtbc_38	2320	0.05	5.71	0.33	0.080	0.003	1091.9	23.0	1040.3	27.8	1196.1	37.0	13.0
cmtbc_36	1355	0.48	5.63	0.20	0.082	0.003	1118.0	17.3	1054.0	17.3	1244.6	35.8	15.3
cmtbc_26		0.46	5.32	0.23	0.071	0.002	1059.6	17.0	1110.4	22.0	956.5	28.8	-16.1

TABLE A1
(continued)

Sample name	U (ppm)	Th/U	$^{238}U/^{206}Pb$	2 sigma abs	$^{207}Pb/^{206}Pb$	2 sigma abs	207/235 age Ma	1 sigma abs err Ma	206/238 age† Ma	1 sigma abs err Ma	207/206 age Ma	1 sigma abs err Ma	disc†† %
Zircon Standards													
Z_91500_1	77	2.64	5.60	0.18	0.075	0.002	1061.9	13.8	1059.2	15.7	1067.6	26.8	0.8
Z_91500_2	92	2.77	5.59	0.19	0.076	0.003	1071.9	17.2	1060.9	16.6	1094.2	39.5	3.0
Z_91500_3	78	2.68	5.59	0.19	0.075	0.002	1063.1	14.2	1060.9	16.6	1067.6	26.8	0.6
Z_91500_4	76	3.06	5.57	0.15	0.074	0.002	1056.6	12.5	1064.4	13.2	1040.6	27.3	-2.3
Z_91500_5	84	2.48	5.59	0.21	0.074	0.002	1054.3	15.2	1060.9	18.4	1040.6	27.3	-2.0
Z_91500_6	79	2.62	5.56	0.21	0.073	0.002	1048.9	15.3	1066.2	18.6	1013.0	27.8	-5.3
Z_91500_7	81	2.58	5.55	0.20	0.076	0.003	1076.6	17.7	1068.0	17.7	1094.2	39.5	2.4
Z_91500_8	81	2.75	5.56	0.16	0.075	0.002	1066.7	13.0	1066.2	14.1	1067.6	26.8	0.1
Z_91500_9	80	2.70	5.61	0.20	0.076	0.003	1069.5	17.6	1057.4	17.4	1094.2	39.5	3.4
Z_91500_10	80	2.79	5.59	0.18	0.076	0.002	1071.9	13.8	1060.9	15.7	1094.2	26.3	3.0
Z_91500_11	79	2.70	5.61	0.18	0.076	0.002	1069.5	13.7	1057.4	15.6	1094.2	26.3	3.4
Z_91500_12	81	2.51	5.60	0.18	0.076	0.003	1070.7	16.8	1059.2	15.7	1094.2	39.5	3.2
Z_91500_13	79	3.09	5.59	0.16	0.074	0.002	1054.3	12.9	1060.9	14.0	1040.6	27.3	-2.0
Z_91500_14	82	2.44	5.57	0.17	0.076	0.003	1074.2	16.5	1064.4	15.0	1094.2	39.5	2.7
Z_91500_15	82	3.07	5.59	0.34	0.072	0.004	1036.4	26.8	1060.9	29.7	985.0	56.5	-7.7
Z_91500_16	80	2.71	5.56	0.22	0.075	0.003	1066.7	18.6	1066.2	19.4	1067.6	40.2	0.1
Z_91500_17	80	2.65	5.56	0.16	0.073	0.003	1048.9	16.4	1066.2	14.1	1013.0	41.6	-5.3
Z_91500_18	80	2.56	5.55	0.20	0.076	0.002	1076.6	14.8	1068.0	17.7	1094.2	26.3	2.4
Z_91500_19	79	3.04	5.56	0.19	0.074	0.002	1057.8	14.3	1066.2	16.8	1040.6	27.3	-2.5
Z_91500_20	81	2.45	5.61	0.16	0.076	0.002	1069.5	12.8	1057.4	13.9	1094.2	26.3	3.4
Z_91500_1	79	2.67	5.57	0.25	0.075	0.005	1065.5	26.5	1064.4	22.0	1067.6	67.0	0.3
Z_91500_2	73	2.63	5.58	0.17	0.075	0.003	1064.3	16.6	1062.7	14.9	1067.6	40.2	0.5
Z_91500_3	83	2.76	5.58	0.12	0.074	0.002	1055.5	11.3	1062.7	10.5	1040.6	27.3	-2.1
Z_91500_4	83	2.62	5.60	0.23	0.082	0.004	1121.6	21.6	1059.2	20.1	1244.6	47.8	14.9
Z_91500_5	76	2.71	5.56	0.15	0.074	0.003	1057.8	16.0	1066.2	13.3	1040.6	40.9	-2.5
Z_91500_6	86	2.60	5.52	0.19	0.076	0.003	1080.2	17.4	1073.3	17.0	1094.2	39.5	1.9
Z_91500_7	76	2.60	5.57	0.19	0.077	0.003	1082.9	17.2	1064.4	16.7	1120.3	38.9	5.0
Z_91500_8	83	2.66	5.55	0.18	0.075	0.003	1067.8	17.0	1068.0	16.0	1067.6	40.2	0.0
Z_91500_9	84	2.49	5.57	0.23	0.076	0.004	1074.2	22.2	1064.4	20.3	1094.2	52.7	2.7
Z_91500_10	80	2.75	5.58	0.16	0.074	0.003	1055.5	16.3	1062.7	14.0	1040.6	40.9	-2.1
Z_91500_11	81	2.90	5.58	0.23	0.073	0.003	1046.5	19.0	1062.7	20.2	1013.0	41.6	-4.9
Z_91500_12	76	2.70	5.59	0.13	0.076	0.002	1071.9	11.6	1060.9	11.4	1094.2	26.3	3.0
Z_91500_13	80	2.60	5.57	0.13	0.075	0.002	1065.5	11.7	1064.4	11.5	1067.6	26.8	0.3
Z_91500_14	85	2.88	5.59	0.18	0.074	0.003	1054.3	17.0	1060.9	15.7	1040.6	40.9	-2.0
Z_91500_15	77	2.51	5.58	0.18	0.076	0.003	1073.0	16.9	1062.7	15.8	1094.2	39.5	2.9

TABLE A1
(continued)

Sample name	U (ppm)	Th/U	$^{238}U/^{206}Pb$	2 sigma abs	$^{207}Pb/^{206}Pb$	2 sigma abs	207/235 age Ma	1 sigma abs err Ma	206/238 age† Ma	1 sigma abs err Ma	207/206 age Ma	1 sigma abs err Ma	disc†† %
Zircon Standards													
Z_91500_16	77	2.65	5.57	0.20	0.074	0.003	1056.6	17.8	1064.4	17.6	1040.6	40.9	-2.3
Z_91500_17	79	2.39	5.58	0.17	0.074	0.003	1055.5	16.6	1062.7	14.9	1040.6	40.9	-2.1
Z_91500_18	80	2.80	5.59	0.18	0.077	0.003	1080.5	16.8	1060.9	15.7	1120.3	38.9	5.3
Z_91500_19	84	2.78	5.58	0.12	0.076	0.003	1073.0	14.9	1062.7	10.5	1094.2	39.5	2.9
Z_91500_20	84	2.75	5.58	0.16	0.079	0.002	1098.9	12.8	1062.7	14.0	1171.2	25.1	9.3
Z_91500_21	81	2.71	5.58	0.17	0.074	0.002	1055.5	13.4	1062.7	14.9	1040.6	27.3	-2.1
Z_91500_22	79	2.81	5.58	0.19	0.074	0.003	1055.5	17.4	1062.7	16.7	1040.6	40.9	-2.1
Z_91500_23	72	2.46	5.59	0.21	0.074	0.003	1054.3	18.1	1060.9	18.4	1040.6	40.9	-2.0
Z_91500_24	85	2.76	5.58	0.26	0.071	0.002	1028.5	17.6	1062.7	22.8	956.5	28.8	-11.1
Z_91500_25	81	2.72	5.57	0.25	0.076	0.004	1074.2	22.9	1064.4	22.0	1094.2	52.7	2.7
Z_91500_26	78	2.61	5.56	0.16	0.077	0.003	1084.1	16.1	1066.2	14.1	1120.3	38.9	4.8
Z_91500_27	69	2.52	5.57	0.18	0.074	0.003	1056.6	17.0	1064.4	15.9	1040.6	40.9	-2.3
Z_91500_28	92	2.98	5.57	0.23	0.075	0.003	1065.5	19.0	1064.4	20.3	1067.6	40.2	0.3
Z_91500_29	87	2.76	5.59	0.21	0.076	0.005	1071.9	25.1	1060.9	18.4	1094.2	65.9	3.0
Z_91500_30	82	2.69	5.55	0.14	0.077	0.004	1085.3	19.3	1068.0	12.4	1120.3	51.8	4.7
Z_91500_31	72	2.70	5.56	0.31	0.072	0.004	1039.9	25.6	1066.2	27.4	985.0	56.5	-8.2
Z_91500_32	88	2.83	5.56	0.16	0.089	0.006	1183.0	25.6	1066.2	14.1	1403.3	64.6	24.0
Z_91500_33	72	2.72	5.56	0.18	0.072	0.003	1039.9	17.2	1066.2	15.9	985.0	42.4	-8.2
Z_91500_34	78	2.57	5.58	0.19	0.073	0.003	1046.5	17.4	1062.7	16.7	1013.0	41.6	-4.9
Z_91500_35	82	2.53	5.57	0.22	0.074	0.003	1056.6	18.6	1064.4	19.4	1040.6	40.9	-2.3
Z_91500_36	79	2.53	5.57	0.16	0.075	0.003	1065.5	16.2	1064.4	14.1	1067.6	40.2	0.3
Z_91500_37	84	2.58	5.60	0.15	0.077	0.003	1079.3	15.7	1059.2	13.1	1120.3	38.9	5.5
Z_91500_38	83	2.74	5.57	0.16	0.078	0.003	1091.5	16.1	1064.4	14.1	1146.0	38.2	7.1
Z_91500_1	81	2.84	5.49	0.29	0.076	0.004	1083.8	24.8	1078.7	26.2	1094.2	52.7	1.4
Z_91500_2	85	2.79	5.71	0.39	0.073	0.004	1031.6	28.4	1040.3	32.8	1013.0	55.5	-2.7
Z_91500_3	79	2.65	5.68	0.61	0.075	0.005	1052.6	41.4	1045.4	51.8	1067.6	67.0	2.1
Z_91500_4	91	3.31	5.48	0.29	0.077	0.004	1093.8	24.8	1080.5	26.3	1120.3	51.8	3.6
Z_91500_5	69	2.80	5.56	0.24	0.076	0.004	1075.4	22.6	1066.2	21.2	1094.2	52.7	2.6
Z_91500_6	94	3.11	5.56	0.46	0.073	0.004	1048.9	32.4	1066.2	40.7	1013.0	55.5	-5.3
Z_91500_7	92	2.88	5.59	0.47	0.075	0.004	1063.1	32.8	1060.9	41.1	1067.6	53.6	0.6
Z_91500_8	91	2.66	5.63	0.18	0.073	0.003	1040.7	16.9	1054.0	15.5	1013.0	41.6	-4.0
Z_91500_9	84	2.49	5.59	0.25	0.077	0.003	1080.5	19.7	1060.9	21.9	1120.3	38.9	5.3
Z_91500_10	89	2.74	5.56	0.27	0.076	0.005	1075.4	27.1	1066.2	23.9	1094.2	65.9	2.6
Z_91500_11	71	2.83	5.62	0.41	0.073	0.004	1041.9	29.7	1055.7	35.5	1013.0	55.5	-4.2
Z_91500_12	84	2.88	5.59	0.24	0.077	0.004	1080.5	22.4	1060.9	21.0	1120.3	51.8	5.3

TABLE A1
(continued)

Sample name	U (ppm)	Th/U	$^{238}U/^{206}Pb$	2 sigma abs	$^{207}Pb/^{206}Pb$	2 sigma abs	207/235 age Ma	1 sigma abs err Ma	206/238 age† Ma	1 sigma abs err Ma	207/206 age Ma	1 sigma abs err Ma	disc†† %
Zircon Standards													
Z_91500_13	84	2.61	5.55	0.27	0.073	0.004	1050.1	24.0	1068.0	23.9	1013.0	55.5	-5.4
Z_91500_14	80	2.59	5.62	0.66	0.076	0.004	1068.3	42.5	1055.7	57.2	1094.2	52.7	3.5
Z_91500_15	91	2.74	5.52	0.73	0.081	0.006	1123.0	51.5	1073.3	65.4	1220.6	72.8	12.1
Z_91500_16	53	1.88	5.75	0.69	0.075	0.006	1044.6	47.0	1033.6	57.3	1067.6	80.4	3.2
Z_91500_17	62	2.40	5.46	0.72	0.077	0.005	1096.2	49.3	1084.2	65.8	1120.3	64.8	3.2
Z_91500_18	88	2.71	5.56	0.24	0.073	0.002	1048.9	16.7	1066.2	21.2	1013.0	27.8	-5.3
Z_91500_19	90	2.63	5.59	0.22	0.075	0.004	1063.1	21.8	1060.9	19.2	1067.6	53.6	0.6
Z_91500_20	68	2.34	5.62	0.35	0.078	0.005	1085.6	29.8	1055.7	30.3	1146.0	63.7	7.9
Z_91500_21	93	2.71	5.52	0.52	0.074	0.004	1062.6	35.8	1073.3	46.6	1040.6	54.6	-3.1
Z_91500_22	64	2.79	5.52	0.46	0.078	0.004	1097.6	32.8	1073.3	41.2	1146.0	50.9	6.3
Z_91500_23	81	4.29	5.62	0.54	0.075	0.003	1059.6	34.2	1055.7	46.8	1067.6	40.2	1.1
Z_91500_24	89	2.73	5.49	0.45	0.076	0.004	1083.8	32.4	1078.7	40.7	1094.2	52.7	1.4
Z_91500_25	90	2.50	5.68	0.48	0.075	0.004	1052.6	32.7	1045.4	40.8	1067.6	53.6	2.1
Z_91500_26	80	2.52	5.62	0.41	0.072	0.003	1032.9	27.2	1055.7	35.5	985.0	42.4	-7.2
Z_91500_27	82	2.69	5.59	0.41	0.078	0.004	1089.1	29.9	1060.9	35.9	1146.0	50.9	7.4
Z_91500_28	78	3.03	5.52	0.34	0.073	0.006	1053.6	33.7	1073.3	30.4	1013.0	83.3	-6.0
Z_91500_29	66	2.88	5.57	0.31	0.078	0.005	1091.5	28.4	1064.4	27.3	1146.0	63.7	7.1
Z_91500_30	81	2.81	5.56	0.59	0.076	0.005	1075.4	41.4	1066.2	52.1	1094.2	65.9	2.6
Z_91500_31	84	2.69	5.65	0.35	0.074	0.003	1047.3	24.2	1050.5	30.0	1040.6	40.9	-1.0
Z_91500_32	93	2.64	5.59	0.31	0.073	0.004	1045.4	25.4	1060.9	27.1	1013.0	55.5	-4.7
Z_91500_33	86	2.84	5.57	0.22	0.071	0.003	1029.7	18.7	1064.4	19.4	956.5	43.2	-11.3
Z_91500_34	54	2.72	5.68	0.61	0.074	0.006	1043.8	43.9	1045.4	51.8	1040.6	81.8	-0.5
Z_91500_35	92	3.32	5.52	0.34	0.078	0.007	1097.6	36.5	1073.3	30.4	1146.0	89.2	6.3
Z_91500_36	85	2.70	5.62	0.54	0.076	0.004	1068.3	36.2	1055.7	46.8	1094.2	52.7	3.5
Z_91500_37	91	2.67	5.59	0.41	0.081	0.004	1114.5	29.9	1060.9	35.9	1220.6	48.5	13.1
Z_R33_1	418	2.37	14.90	0.96	0.054	0.002	411.3	12.6	418.7	13.1	370.0	41.7	-1.8
Z_R33_2	118	1.42	14.84	0.62	0.059	0.002	443.6	9.7	420.4	8.5	566.1	36.9	5.2
Z_R33_3	217	1.07	15.13	1.14	0.053	0.002	400.0	13.9	412.6	15.1	327.8	42.8	-3.2
Z_R33_4	148	1.27	14.86	0.93	0.056	0.002	424.7	12.5	419.8	12.7	451.4	39.7	1.2
Z_R33_5	121	1.02	14.95	0.76	0.056	0.003	422.6	12.8	417.4	10.3	451.4	59.5	1.2
Z_R33_6	555	2.23	14.81	1.40	0.055	0.003	419.7	18.8	421.2	19.3	411.2	61.0	-0.4
Z_R33_7	289	1.32	14.86	0.91	0.056	0.003	424.7	14.1	419.8	12.4	451.4	59.5	1.2
Z_R33_8	1870	1.58	14.79	1.07	0.053	0.003	407.5	15.4	421.8	14.8	327.8	64.2	-3.5
R33_1	194	1.59	14.84	0.46	0.056	0.002	425.2	8.2	420.4	6.3	451.4	39.7	1.1
R33_2	353	0.96	14.35	0.39	0.056	0.002	437.0	8.0	434.3	5.7	451.4	39.7	0.6

TABLE A1
(continued)

Sample name	U (ppm)	Th/U	$^{238}U/^{206}Pb$	2 sigma abs	$^{207}Pb/^{206}Pb$	2 sigma abs	207/235 age Ma	1 sigma abs err Ma	206/238 age† Ma	1 sigma abs err Ma	207/206 age Ma	1 sigma abs err Ma	disc†† %
Zircon Standards													
R33_3	293	1.36	14.79	0.61	0.056	0.002	426.4	9.5	421.8	8.4	451.4	39.7	1.1
R33_4	190	1.55	14.81	0.57	0.057	0.002	432.1	9.2	421.2	7.9	490.5	38.7	2.5
R33_5	102	2.00	14.27	0.49	0.054	0.002	426.2	8.8	436.6	7.3	370.0	41.7	-2.5
R33_6	104	1.62	14.64	0.54	0.056	0.003	429.9	11.4	425.9	7.6	451.4	59.5	0.9
R33_7	115	1.26	14.84	0.48	0.056	0.002	425.2	8.4	420.4	6.6	451.4	39.7	1.1
R33_8	236	1.70	14.86	0.38	0.056	0.002	424.7	7.6	419.8	5.2	451.4	39.7	1.2
R33_9	38	2.55	15.41	0.64	0.057	0.003	418.3	11.5	405.3	8.2	490.5	58.0	3.1
R33_10	243	1.17	14.60	0.47	0.056	0.002	430.9	8.4	427.1	6.7	451.4	39.7	0.9
R33_11	162	1.90	14.60	0.47	0.056	0.002	430.9	8.4	427.1	6.7	451.4	39.7	0.9
R33_12	105	1.47	14.75	0.39	0.055	0.002	421.1	7.8	422.9	5.4	411.2	40.7	-0.4
R33_13	58	2.14	15.41	0.47	0.055	0.002	406.2	7.9	405.3	6.0	411.2	40.7	0.2
R33_14	256	1.48	14.93	0.42	0.054	0.002	410.7	7.9	417.9	5.7	370.0	41.7	-1.8
R33_15	174	2.30	15.36	0.33	0.057	0.002	419.4	7.1	406.6	4.2	490.5	38.7	3.1
R33_16	424	0.89	14.88	0.38	0.054	0.001	411.8	5.3	419.3	5.2	370.0	20.9	-1.8
R33_17	70	1.98	14.95	0.42	0.055	0.002	416.5	7.9	417.4	5.7	411.2	40.7	-0.2
R33_18	254	1.37	14.81	0.72	0.054	0.002	413.4	10.4	421.2	9.9	370.0	41.7	-1.9
r33_0	17	3.31	15.36	1.23	0.059	0.008	431.4	27.7	406.6	15.8	566.0	148.0	5.7
r33_1	22	2.28	14.43	1.10	0.056	0.007	435.0	25.9	431.9	15.9	451.0	139.0	0.7
r33_2	70	1.56	15.08	0.96	0.053	0.005	401.1	18.9	413.9	12.8	328.0	107.0	-3.2
r33_3	89	1.29	15.04	0.99	0.055	0.003	414.4	14.5	415.0	13.2	411.2	61.0	-0.1
r33_4	94	1.53	14.68	0.99	0.055	0.004	422.7	17.1	424.8	13.9	411.2	81.3	-0.5
r33_5	86	1.37	15.17	1.04	0.058	0.004	429.8	17.0	411.5	13.7	528.8	75.6	4.3
r33_6	84	1.30	13.66	0.88	0.053	0.004	434.9	17.6	455.4	14.2	327.8	85.6	-4.7
r33_7	100	1.79	14.43	0.92	0.056	0.004	435.0	16.9	431.9	13.3	451.4	79.3	0.7
r33_8	70	1.80	12.97	0.91	0.057	0.004	480.8	19.0	478.8	16.2	490.5	77.4	0.4
r33_9	38	1.80	14.86	1.08	0.054	0.005	412.3	19.9	419.8	14.8	370.0	104.0	-1.8
r33_10	16	2.54	14.66	1.07	0.050	0.010	391.2	34.6	425.4	15.0	194.0	232.0	-8.7
r33_11	25	2.54	14.64	1.01	0.048	0.008	378.6	28.5	425.9	14.2	98.2	197.2	-12.5
r33_12	23	3.29	15.34	1.83	0.062	0.009	449.6	34.1	407.1	23.5	673.0	155.0	9.5
r33_13	92	1.21	15.15	1.12	0.053	0.003	399.5	15.4	412.1	14.8	327.8	64.2	-3.2
r33_14	56	1.54	14.43	1.15	0.053	0.004	415.9	18.7	431.9	16.6	327.8	85.6	-3.8
r33_15	69	1.46	14.45	0.96	0.062	0.005	471.7	19.7	431.4	13.9	673.1	86.2	8.5
r33_16	76	1.40	14.79	0.94	0.060	0.004	450.9	16.8	421.8	13.0	602.6	72.1	6.5
r33_17	76	1.68	13.32	0.99	0.056	0.004	464.1	19.2	466.7	16.7	451.4	79.3	-0.6

TABLE A1
(continued)

Sample name	U (ppm)	Th/U	$^{238}U/^{206}Pb$	2 sigma abs	$^{207}Pb/^{206}Pb$	2 sigma abs	207/235 age Ma	1 sigma abs err Ma	206/238 age† Ma	1 sigma abs err Ma	207/206 age Ma	1 sigma abs err Ma	disc†† %
Zircon Standards													
Z_Temora2_1	156	1.99	14.49	0.53	0.055	0.002	427.2	9.0	430.2	7.6	411.2	40.7	-0.7
Z_Temora2_2	113	2.64	14.86	0.55	0.055	0.003	418.5	11.3	419.8	7.5	411.2	61.0	-0.3
Z_Temora2_3	214	2.41	14.93	0.69	0.056	0.002	423.1	10.1	417.9	9.4	451.4	39.7	1.2
Z_Temora2_4	2190	1.24	14.31	0.76	0.057	0.003	444.3	13.5	435.4	11.2	490.5	58.0	2.0
Z_Temora2_5	146	2.00	14.99	0.56	0.056	0.002	421.7	8.9	416.3	7.5	451.4	39.7	1.3
Z_Temora2_6	99	3.06	14.99	0.43	0.056	0.002	421.7	7.9	416.3	5.8	451.4	39.7	1.3
Z_Temora2_7	272	1.86	14.97	0.54	0.056	0.002	422.2	8.8	416.9	7.3	451.4	39.7	1.3
Z_Temora2_8	2530	1.41	14.90	0.53	0.052	0.002	398.7	8.6	418.8	7.2	284.4	44.0	-5.0
Z_Temora2_9	168	1.77	14.95	0.34	0.056	0.002	422.6	7.3	417.4	4.6	451.4	39.7	1.2
Z_Temora2_10	99	2.74	15.11	0.57	0.054	0.002	406.6	8.9	413.1	7.6	370.0	41.7	-1.6
Z_Temora2_11	290	2.62	14.93	0.49	0.054	0.002	410.7	8.4	417.9	6.6	370.0	41.7	-1.8
Z_Temora2_12	3090	1.27	14.01	0.51	0.054	0.002	432.6	9.2	444.5	7.8	370.0	41.7	-2.7
Z_Temora2_13	137	2.48	14.08	0.71	0.056	0.004	443.8	15.7	442.3	10.8	451.4	79.3	0.3
Z_Temora2_14	143	2.83	13.91	0.43	0.055	0.002	441.7	8.6	447.5	6.7	411.2	40.7	-1.3
Z_Temora2_15	258	2.34	14.41	0.69	0.055	0.002	429.2	10.5	432.5	10.0	411.2	40.7	-0.8
Z_Temora2_16	3020	1.22	14.47	0.71	0.054	0.002	421.3	10.6	430.8	10.2	370.0	41.7	-2.3
Z_Temora2_17	167	1.92	14.77	0.74	0.054	0.004	414.3	15.2	422.3	10.2	370.0	83.4	-1.9
Z_Temora2_18	95	2.96	14.47	0.40	0.055	0.002	427.7	8.0	430.8	5.8	411.2	40.7	-0.7
Z_Temora2_19	204	2.77	14.86	0.60	0.057	0.002	430.9	9.4	419.8	8.2	490.5	38.7	2.6
Z_Temora2_20	2730	1.23	14.27	0.47	0.052	0.004	413.2	14.2	436.6	7.0	284.4	88.0	-5.7
Z_Temora2_1	270	3.05	15.11	1.57	0.054	0.003	406.6	19.7	413.1	20.8	370.0	62.6	-1.6
Z_Temora2_2	264	2.07	14.88	0.58	0.056	0.004	424.3	14.1	419.3	7.9	451.4	79.3	1.2
Z_Temora2_3	121	2.27	14.95	1.01	0.057	0.002	428.8	13.3	417.4	13.7	490.5	38.7	2.7
Z_Temora2_4	333	3.72	14.75	0.61	0.054	0.003	414.8	11.8	422.9	8.5	370.0	62.6	-1.9
Z_Temora2_5	292	2.15	14.25	1.18	0.055	0.002	433.1	15.9	437.2	17.5	411.2	40.7	-0.9
Z_Temora2_6	250	3.51	14.20	1.47	0.054	0.002	427.9	19.2	438.7	22.0	370.0	41.7	-2.5
Z_Temora2_7	198	2.16	14.77	1.77	0.057	0.002	433.0	22.0	422.3	24.5	490.5	38.7	2.5
Z_Temora2_8	514	2.00	15.34	1.39	0.055	0.003	407.7	17.8	407.1	17.9	411.2	61.0	0.1
Z_Temora2_9	268	2.24	15.58	0.53	0.056	0.002	408.6	8.3	401.0	6.6	451.4	39.7	1.8
Z_Temora2_10	230	3.16	15.08	0.61	0.057	0.002	425.8	9.3	413.9	8.1	490.5	38.7	2.8
Z_Temora2_11	462	2.27	15.80	0.90	0.059	0.004	421.6	15.3	395.6	10.9	566.1	73.8	6.2
Z_Temora2_12	469	1.53	15.72	1.48	0.059	0.006	423.3	24.0	397.6	18.1	566.0	111.0	6.1
Z_Temora2_13	263	3.76	14.84	0.77	0.054	0.002	412.7	10.8	420.4	10.6	370.0	41.7	-1.9
Z_Temora2_14	168	2.17	14.99	0.99	0.054	0.003	409.3	14.5	416.3	13.3	370.0	62.6	-1.7
Z_Temora2_15	166	2.29	14.95	0.85	0.056	0.003	422.6	13.5	417.4	11.5	451.4	59.5	1.2

TABLE A1
(continued)

Sample name	U (ppm)	Th/U	$^{238}U/^{206}Pb$	2 sigma abs	$^{207}Pb/^{206}Pb$	2 sigma abs	207/235 age Ma	1 sigma abs err Ma	206/238 age† Ma	1 sigma abs err Ma	207/206 age Ma	1 sigma abs err Ma	disc†† %
Zircon Standards													
Z_Temora2_16	1900	1.70	13.48	1.05	0.053	0.002	439.7	15.4	461.3	17.3	327.8	42.8	-4.9
Z_Temora2_17	249	2.55	14.41	1.52	0.055	0.003	429.2	20.8	432.5	22.1	411.2	61.0	-0.8
Z_Temora2_18	151	1.90	14.45	1.46	0.056	0.004	434.5	21.9	431.4	21.1	451.4	79.3	0.7
Z_Temora2_19	204	2.81	15.20	0.92	0.055	0.004	410.8	16.0	410.7	12.0	411.2	81.3	0.0
Z_Temora2_20	700	2.00	14.22	1.56	0.056	0.002	440.2	20.6	438.1	23.2	451.4	39.7	0.5
Z_Temora2_21	196	2.09	14.12	1.10	0.056	0.002	442.8	15.4	441.1	16.6	451.4	39.7	0.4
Z_Temora2_22	189	3.45	14.53	0.70	0.054	0.003	419.9	12.6	429.1	10.0	370.0	62.6	-2.2
Z_Temora2_23	161	2.23	14.93	1.29	0.057	0.003	429.3	17.7	417.9	17.5	490.5	58.0	2.7
Z_Temora2_24	670	1.82	14.41	1.22	0.054	0.003	422.8	17.5	432.5	17.7	370.0	62.6	-2.3
Z_Plesovice_1	892	11.46	20.62	0.81	0.061	0.014	347.2	34.2	305.3	5.9	638.0	247.0	12.1
Z_Plesovice_2	932	11.67	18.83	1.88	0.051	0.003	322.1	16.0	333.6	16.2	239.8	67.8	-3.6
Z_Plesovice_3	1570	10.37	19.57	0.57	0.054	0.003	327.3	8.8	321.3	4.6	370.0	62.6	1.8
Z_Plesovice_4	980	10.08	18.12	2.43	0.050	0.003	327.3	20.6	346.3	22.6	193.9	69.7	-5.8
Z_Plesovice_5	700	10.65	17.09	2.31	0.050	0.003	344.0	21.6	366.6	24.1	193.9	69.7	-6.6
Z_Plesovice_6	730	10.24	17.45	2.01	0.052	0.002	349.4	17.9	359.2	20.1	284.4	44.0	-2.8
Z_Plesovice_7	1220	8.82	18.83	2.41	0.056	0.003	348.8	20.5	333.6	20.8	451.4	59.5	4.4
Z_Plesovice_8	900	9.88	18.18	2.41	0.051	0.002	331.9	19.6	345.2	22.3	239.8	45.2	-4.0
Z_Plesovice_9	857	10.30	18.90	0.64	0.054	0.002	337.1	7.2	332.4	5.5	370.0	41.7	1.4
Z_Plesovice_10	838	10.42	18.87	1.74	0.054	0.002	337.6	14.3	332.9	15.0	370.0	41.7	1.4
Z_Plesovice_11	1320	8.75	19.23	0.63	0.055	0.002	337.4	7.0	326.8	5.2	411.2	40.7	3.1
Z_Plesovice_12	1150	8.53	18.52	1.44	0.053	0.002	337.6	12.4	339.0	12.8	327.8	42.8	-0.4
Z_Plesovice_13	903	10.47	17.73	1.51	0.051	0.002	339.1	13.5	353.7	14.7	239.8	45.2	-4.3
Z_Plesovice_14	874	10.27	16.81	2.15	0.054	0.003	372.2	21.7	372.5	23.1	370.0	62.6	-0.1
Z_Plesovice_15	1200	8.80	18.55	1.62	0.054	0.002	342.5	13.8	338.5	14.4	370.0	41.7	1.2
Z_Plesovice_16	812	11.03	18.52	1.85	0.055	0.002	348.4	15.7	339.0	16.5	411.2	40.7	2.7
Z_Plesovice_17	846	11.62	17.76	1.83	0.053	0.002	349.8	16.2	353.1	17.7	327.8	42.8	-0.9
Z_Plesovice_18	857	10.83	18.15	1.84	0.053	0.002	343.4	15.8	345.7	17.1	327.8	42.8	-0.7
Z_Plesovice_19	1070	8.67	18.45	1.91	0.055	0.003	349.5	17.3	340.3	17.2	411.2	61.0	2.6
Z_Plesovice_20	900	9.35	17.83	1.72	0.058	0.003	376.1	17.2	351.8	16.5	528.8	56.7	6.5
Z_Plesovice_21	1370	8.00	18.42	1.93	0.053	0.003	339.1	17.2	340.8	17.4	327.8	64.2	-0.5
Z_Plesovice_22	1360	7.69	18.66	1.78	0.055	0.003	346.1	16.1	336.5	15.6	411.2	61.0	2.8
Z_Plesovice_23	1260	8.33	17.51	1.69	0.052	0.003	348.4	16.6	358.0	16.8	284.4	66.0	-2.8
Z_Plesovice_24	1031	9.27	18.32	1.04	0.056	0.002	357.0	10.1	342.6	9.5	451.4	39.7	4.0
Z_Plesovice_1	886	9.15	18.38	0.98	0.052	0.003	334.3	11.2	341.5	8.9	284.4	66.0	-2.2

TABLE A1
(continued)

Sample name	U (ppm)	Th/U	$^{238}U/^{206}Pb$	2 sigma abs	$^{207}Pb/^{206}Pb$	2 sigma abs	207/235 age Ma	1 sigma abs err Ma	206/238 age† Ma	1 sigma abs err Ma	207/206 age Ma	1 sigma abs err Ma	disc†† %
Zircon Standards													
Z_Plesovice_2	1073	10.30	18.18	0.89	0.051	0.002	331.9	8.9	345.2	8.2	239.8	45.2	-4.0
Z_Plesovice_3	2320	7.03	18.38	0.68	0.054	0.002	345.2	7.7	341.5	6.2	370.0	41.7	1.1
Z_Plesovice_4	759	9.89	18.15	0.63	0.053	0.002	343.4	7.5	345.7	5.8	327.8	42.8	-0.7
Z_Plesovice_5	930	9.02	18.45	0.89	0.055	0.002	349.5	8.9	340.3	8.0	411.2	40.7	2.6
Z_Plesovice_6	1183	10.16	18.35	0.47	0.051	0.001	329.3	4.5	342.1	4.3	239.8	22.6	-3.9
Z_Plesovice_7	2390	7.31	18.66	0.59	0.053	0.002	335.4	7.0	336.5	5.2	327.8	42.8	-0.3
Z_Plesovice_8	755	9.00	18.80	0.57	0.053	0.002	333.3	6.9	334.1	4.9	327.8	42.8	-0.2
Z_Plesovice_9	797	9.10	18.62	0.90	0.057	0.003	357.4	10.8	337.2	7.9	490.5	58.0	5.6
Z_Plesovice_10	1241	11.00	18.08	0.82	0.053	0.003	344.5	10.6	347.0	7.7	327.8	64.2	-0.7
Z_Plesovice_11	2540	6.66	18.76	0.53	0.055	0.002	344.6	6.7	334.8	4.6	411.2	40.7	2.8
Z_Plesovice_12	775	8.67	18.76	0.60	0.053	0.002	333.9	7.0	334.8	5.2	327.8	42.8	-0.3
Z_Plesovice_13	850	8.10	18.45	0.68	0.054	0.003	344.1	9.7	340.3	6.1	370.0	62.6	1.1
Z_Plesovice_14	1273	10.60	18.15	0.79	0.055	0.003	354.4	10.4	345.7	7.3	411.2	61.0	2.4
Z_Plesovice_15	1950	6.73	18.38	0.51	0.052	0.002	334.3	6.8	341.5	4.6	284.4	44.0	-2.2
Z_Plesovice_16	731	9.44	18.42	0.44	0.053	0.002	339.1	6.4	340.8	4.0	327.8	42.8	-0.5
Z_Plesovice_17	875	8.65	18.32	0.60	0.053	0.002	340.7	7.2	342.6	5.5	327.8	42.8	-0.6
Z_Plesovice_18	1002	9.99	18.62	0.87	0.053	0.003	336.0	10.5	337.2	7.7	327.8	64.2	-0.4
Z_Plesovice_19	2620	6.88	18.38	0.64	0.055	0.002	350.6	7.5	341.5	5.8	411.2	40.7	2.6
Z_Plesovice_20	1068	6.40	18.87	0.68	0.053	0.002	332.2	7.4	332.9	5.9	327.8	42.8	-0.2

Notes:
$Overgrowth around zircon
$$Inherited zircon
† Common lead corrected
†† Discordance was calculated based on $^{207}Pb/^{206}Pb$ versus $^{206}Pb/^{238}U$ for zircons >1000 Ma, and based on $^{207}Pb/^{235}U$ versus $^{206}Pb/^{238}U$ for zircons <1000 Ma, abs = absolute, err = error, disc = discordance

REFERENCES

Abbott, R. N., and Greenwood, J. P., 2001, Retrograde metamorphism of eclogite in the southern Appalachian Mountains, U.S.A.–A case involving seamount subduction?: Journal of Metamorphic Geology, v. 19, n. 4, p. 433–443, https://doi.org/10.1046/j.0263-4929.2001.00321.x

Abrahams, J., ms, 2014, Geology of the Dadeville Quadrangle and the Tallassee synform in characterizing the Dog River window: Auburn, Alabama, Auburn University, M.S. thesis, 141 p.

Adams, M., Stewart, K., Trupe, C., and Willard, R., 1995, Tectonic significance of high-pressure metamorphic rocks and dextral strike-slip faulting along the Taconic suture, *in* Hibbard, J. P., van Staal, C. R., and Cawood, P. A., editors, Current Perspectives in the Appalachian-Caledonian Orogen: Geological Association of Canada, Special Paper, v. 41, p. 21–42.

Anderson, E. D., and Moecher, D. P., 2009, Formation of high-pressure metabasites in the southern Appalachian Blue Ridge via Taconic continental subduction beneath the Laurentian margin: Tectonics, v. 28, n. 5, TC5012, https://doi.org/10.1029/2008TC002319

Barineau, C., Tull, J. F., and Holm-Denoma, C. S., 2015, A Laurentian margin back-arc: The Ordovician Wedowee-Emuckfaw-Dahlonega basin, *in* Holmes, A. E., editor, Diverse Excursions in the Southeast: Paleozoic to Present: Geological Society of America Field Guide 39, p. 21–78, https://doi.org/10.1130/2015.0039(02)

Bayona, G., and Thomas, W. A., 2006, Influence of pre-existing plate-margin structures on foredeep filling: Insights from the Taconian (Blountian) clastic wedge, Southeastern USA: Sedimentary Geology, v. 191, n. 1–2, p. 115–133, https://doi.org/10.1016/j.sedgeo.2006.02.001

Bentley, R. D., and Neathery, T. L., 1970, Geology of the Brevard fault zone and related rocks of the Inner Piedmont of Alabama: Alabama Geological Society 8th Annual Fieldtrip Guidebook, p. 1–80.

Bittner, E. I., and Neilson, M. J., 1990, Structural and metamorphic development of the Dadeville Complex, emphasizing the Dadeville and Agricola shear zones, *in* Steltenpohl, M. G., Neilson, M. J., and Kish, S. A., editors, Geology of the southern Inner Piedmont, Alabama and southwest Georgia, Geological Society of America Southeastern section 39th Annual Meeting Fieldtrip Guidebook: Tuscaloosa, Alabama, Geological Survey of Alabama, p. 91–99.

Black, L. P., Kamo, S. L., Allen, C. M., Davis, D. W., Aleinikoff, J. N., Valley, J. W., Mundil, R., Campbell, I. H., Korsch, R. J., Williams, I. S., and Foudoulis, C., 2004, Improved $^{206}Pb/^{238}U$ microprobe geochronology by the monitoring of a trace-element-related matrix effect; SHRIMP, ID-TIMS, ELA-ICP-MS and oxygen isotope documentation for a series of zircon standards: Chemical Geology, v. 205, n. 1–2, p. 115–140, https://doi.org/10.1016/j.chemgeo.2004.01.003

Bream, B. R., ms, 2003, Tectonic Implications of Geochronology and Geochemistry of Para- and Ortho-Gneisses from the Southern Appalachian Crystalline Core: Knoxville, Tennessee, University of Tennessee, Ph. D. thesis, 262 p.

Bream, B. R., Hatcher, R. D., Miller, C. F., and Fullagar, P. D., 2004, Detrital zircon ages and Nd isotopic data from the southern Appalachian crystalline core, Georgia, South Carolina, North Carolina, and Tennessee: New provenance constraints for part of the Laurentian margin, *in* Tollo, R. P., Corriveau, L., McLelland, J., and Bartholomew, M. J., editors, Proterozoic tectonic evolution of the Grenville orogen in North America: Geological Society of America Memoir 197, p. 459–475, https://doi.org/10.1130/0-8137-1197-5.459

Brueckner, H. K., Van Roermund, H. L. M., and Pearson, N. J., 2004, An Archean (?) to Paleozoic evolution for a garnet peridotite lens with sub-Baltic shield affinity within the Seve Nappe Complex of Jämtland, Sweden, Central Scandinavian Caledonides: Journal of Petrology, v. 45, p. 415–437, https://doi.org/10.1093/petrology/egg088

Codegone, G., Festa, A., and Dilek, Y., 2012, Formation of Taconic mélanges and broken formations in the Hamburg Klippe, central Appalachian orogenic belt, eastern Pennsylvania: Tectonophysics, v. 568–569, p. 215–229, https://doi.org/10.1016/j.tecto.2012.03.017

Collins, N. C., ms, 2011, Geochemical systematics among amphibolitic rocks in the central Blue Ridge province of southwestern North Carolina: Tampa, Florida, University of South Florida, M.S. thesis, 98 p.

Corrie, S. L., and Kohn, M. J., 2007, Resolving the timing of orogenesis in the Western Blue Ridge, southern Appalachians, via *in situ* ID-TIMS monazite geochronology: Geology, v. 35, n. 7, p. 627–630, https://doi.org/10.1130/G23601A.1

Dickson, H., Bollen, E. M., and Stowell, H. H., 2019, The timing of metamorphism in the southern Appalachian: Filling in the gaps using garnet Sm-Nd geochronology: Geological Society of America Abstracts with Programs, v. 51, n. 3, https://doi.org/10.1130/abs/2019SE-326887

Drake Jr., A. A., Sinha, A. K., Laird, J., and Guy, R. E., 1989, The Taconic orogen, *in* Hatcher, R. D., Thomas, W. A., and Viele, G. W., editors, The Appalachian-Ouachita orogen in the United States (Geology of North America, v. F-2): Boulder, Colorado, Geological Society of America, p. 101–177, https://doi.org/10.1130/DNAG-GNA-F2.101

Drummond, M. S., Neilson, M. J., Allison, D. T., and Tull, J. F., 1997, Igneous petrogenesis and tectonic setting of granitic rocks from the eastern Blue Ridge and Inner Piedmont, Alabama Appalachians, *in* Sinha, A. K., Whalen, J. B., and Hogan, J. P., editors, The Nature of Magmatism in the Appalachian Orogen: Boulder, Colorado, Geological Society of America Memoir 191, p. 147–164, https://doi.org/10.1130/0-8137-1191-6.147

Ettensohn, F. R., 2004, Modeling the nature and development of major Paleozoic clastic wedges in the Appalachian Basin, USA: Journal of Geodynamics, v. 37, n. 3–5, p. 657–681, https://doi.org/10.1016/j.jog.2004.02.009

Farris, D. W., Tull, J., Mueller, P., and Davis, B., 2017, Is the Dadeville Complex part of the “missing” southern Appalachian Taconic arc?, *in* Barineau, C., and Tull, J., editors, A Taconic Backarc and arc terrane in the southern Appalachians: Correlating geologic units of the Blue Ridge and western Inner

Piedmont of Georgia and Alabama: Georgia Geological Society 51st Annual Fieldtrip Guidebook, p. 41–56.
Goldberg, S. A., and Steltenpohl, M. G., 1990, Lithology, metamorphism, and geochronology of the Opelika Complex, *in* Steltenpohl, M. G., Neilson, M. J., and Kish, S. A., editors, Geology of the southern Inner Piedmont, Alabama and southwest Georgia, Geological Society of America Southeastern section 39th Annual Meeting Fieldtrip Guidebook: Tuscaloosa, Alabama, Geological Survey of Alabama, p. 17–28.
Guerrero, J. C., Herrmann, A. D., and Haynes, J. T., 2016, Provenance study of Ordovician sandstones along the southeastern Appalachian Mountains: Geological Society of America Abstracts with Programs. v. 48, n. 7, https://doi.org/10.1130/abs/2016AM-287696
Hall, G. D., and Salpas, P. A., 1990, Geochemistry of thin-layered amphibolites of the Ropes Creek Amphibolite, *in* Steltenpohl, M. G., Neilson, M. J., and Kish, S. A., editors, Geology of the southern Inner Piedmont, Alabama and southwest Georgia, Geological Society of America Southeastern section 39th Annual Meeting Fieldtrip Guidebook: Tuscaloosa, Alabama, Geological Survey of Alabama, p. 79–89.
Harstad, R. P., 2017, Geology of the 1:24,000 Roanoke East Quadrangle and investigations of the Long Island Creek Gneiss within the southernmost Appalachians, Alabama and Georgia: Auburn, Alabama, Auburn University, M.S. thesis, 81 p.
Hatcher Jr., R. D., 1978, Tectonics of the western Piedmont and Blue Ridge, Southern Appalachians: Review and speculation: American Journal of Science, v. 278, n. 3, p. 276–304, https://doi.org/10.2475/ajs.278.3.276
_______1989, Tectonic synthesis of the U.S. Appalachians, *in* Hatcher, R. D., Thomas, W. A., and Viele, G. W., editors, The Appalachian-Ouachita orogen in the United States (Geology of North America, v. F-2): Boulder, Colorado, Geological Society of America, p. 511–535, https://doi.org/10.1130/DNAG-GNA-F2.511
_______2010, The Appalachian orogen: A brief summary, *in* Tollo, R. P., Bartholomew, M. J., Hibbard, J. P., and Karabinos, P. M., editors, From Rodinia to Pangea: The Lithotectonic Record of the Appalachian Region: Geological Society of America Memoir 206, p. 1–19, https://doi.org/10.1130/2010.1206(01)
Hatcher, R. D., and Merschat, A. J., 2006, The Appalachian Inner Piedmont: An exhumed strike-parallel, tectonically forced orogenic channel: Geological Society, London, Special Publications, v. 268, p. 517–541, https://doi.org/10.1144/GSL.SP.2006.268.01.24
Hatcher Jr., R. D., Thomas, W. A., Geiser, P. A., Snoke, A. W., Mosher, S., and Wiltschko, D. V., 1989, Alleghanian orogen, *in* Hatcher, R. D., Thomas, W. A., and Viele, G. W., editors, The Appalachian-Ouachita Orogen in the United States: Geological Society of America, Geology of North America, v. F-2, p. 233–318, https://doi.org/10.1130/DNAG-GNA-F2.233
Hatcher Jr., R. D., Huebner, M. T., Rehrer, J. R., Acker, L. L., Fullagar, P. D., Liu, A., and Goad, P. L., 2017, Geologic and kinematic insights from far-traveled horses in the Brevard fault zone, southern Appalachians, *in* Law, R. D., Thigpen, J. R., Merschat, A. J., and Stowell, H. H., editors, Linkages and Feedbacks in Orogenic Systems: Geological Society of America Memoir 213, p. 313–351, https://doi.org/10.1130/2017.1213(13)
Hawkins, J. F., Steltenpohl, M. G., Zou, H., Mueller, P. M., and Schwartz, J. J., 2013, New constraints on Ordovician magmatism in the southernmost exposures of the eastern Blue Ridge in Alabama: Geological Society of America Abstracts with Programs, v. 45, n. 2, p. 62.
Haynes, J. T., 1994, The Ordovician Deicke and Millbrig K-Bentonite Beds of the Cincinnati Arch and the Southern Valley and Ridge Province, *in* Haynes, J. T., editor, The Ordovician Deicke and Millbrig K-Bentonite Beds of the Cincinnati Arch and the Southern Valley and Ridge Province: Geological Society of America Special Paper 290, p. 1–80, https://doi.org/10.1130/SPE290-p1
Hibbard, J. P., Van Staal, C. R., and Rankin, D. W., 2007, A comparative analysis of pre-Silurlan crustal building blocks of the northern and the southern Appalachian orogen: American Journal of Science, v. 307, n. 1, p. 23–45, https://doi.org/10.2475/01.2007.02
Hibbard, J. P., Miller, B. V., Hames, W. E., Standard, I. D., Allen, J. S., Lavallee, S. B., and Boland, I. B., 2012, Kinematics, U-Pb geochronology, and $^{40}Ar/^{39}Ar$ thermochronology of the Gold Hill shear zone, North Carolina: The Cherokee orogeny in Carolinia, southern Appalachians: Geological Society of America Bulletin, v. 124, n. 5–6, p. 643–656, https://doi.org/10.1130/B30579.1
Higgins, M. W., Atkins, R. L., Crawford, T. J., Crawford III, R. F., Brooks, R., and Cook, R. B., 1988, The structure, stratigraphy, tectonostratigraphy, and evolution of the southernmost part of the Appalachian Orogen: U.S. Geological Survey Professional Paper 1475, p. 180, https://doi.org/10.3133/pp1475
Hirahara, Y., Kimura, J. I., Senda, R., Miyazaki, T., Kawabata, H., Takahashi, T., Chang, Q., Vaglarov, B. S., Sato, T., and Kodaira, S., 2015, Geochemical variations in Japan Sea back-arc basin basalts formed by high-temperature adiabatic melting of mantle metasomatized by sediment subduction components: Geochemistry, Geophysics, Geosystems, v. 16, n. 5, p. 1324–1347, https://doi.org/10.1002/2015GC005720
Hochstaedter, A., Gill, J., Peters, R., Broughton, P., Holden, P., and Taylor, B., 2001, Across-arc geochemical trends in the Izu-Bonin arc: Contributions from the subducting slab: Geochemistry, Geophysics, Geosystems, v. 2, n. 7, https://doi.org/10.1029/2000GC000105
Holm-Denoma, C. S., and Das, R., 2010, Bimodal volcanism as evidence for Paleozoic extensional accretionary tectonism in the southern Appalachians: GSA Bulletin, v. 122, n. 7–8, p. 1220–1234, https://doi.org/10.1130/B30051.1
Huebner, M. T., Hatcher Jr., R. D., and Merschat, A. J., 2017, Confirmation of the southwest continuation of the Cat Square terrane, southern Appalachian Inner Piedmont, with implications for middle Paleozoic collisional orogenesis: American Journal of Science, v. 317, n. 2, p. 95–176, https://doi.org/10.2475/02.2017.01

Huff, W. D., Bergström, S. M., and Kolata, D. R., 1992, Gigantic Ordovician volcanic ash fall in North America and Europe: Biological, tectonomagmatic, and event-stratigraphic significance: Geology, v. 20, n. 10, p. 875–878, https://doi.org/10.1130/0091-7613(1992)020<0875:GOVAFI>2.3.CO;2

Huff, W. D., Kolata, D. R., Bergström, S. M., and Zhang, Y. S., 1996, Large-magnitude Middle Ordovician volcanic ash falls in North America and Europe: Dimensions, emplacement and post-emplacement characteristics: Journal of Volcanology and Geothermal Research, v. 73, n. 3–4, p. 285–301, https://doi.org/10.1016/0377-0273(96)00025-X

Karabinos, P., Samson, S. D., Hepburn, J. C., and Stoll, H. M., 1998, Taconian orogeny in the New England Appalachians: Collision between Laurentia and the Shelburne Falls arc: Geology, v. 26, n. 3, p. 215–218, https://doi.org/10.1130/0091-7613(1998)026<0215:TOITNE>2.3.CO;2

Kimura, J.-I., and Yoshida, T., 2006, Contributions of Slab Fluid, Mantle Wedge and Crust to the Origin of Quaternary Lavas in the NE Japan Arc: Journal of Petrology, v. 47, n. 11, p. 2185–2232, https://doi.org/10.1093/petrology/egl041

Klonowska, I., Janák, M., Majka, J., Petrík, I., Froitzheim, N., Gee, D. G., and Sasinková, V., 2017, Microdiamond on Åreskutan confirms regional UHP metamorphism in the Seve Nappe Complex of the Scandinavian Caledonides: Journal of Metamorphic Geology, v. 35, n. 5, p. 541–564, https://doi.org/10.1111/jmg.12244

Kohn, M. J., and Malloy, M. A., 2004, Formation of monazite via prograde metamorphic reactions among common silicates: implications for age determinations: Geochimica et Cosmochimica Acta, v. 68, p. 101–113, https://doi.org/10.1016/S0016-7037(03)00258-8

Majka, J., Rosén, Å., Janák, M., Froitzheim, N., Klonowska, I., Manecki, M., Sasinková, V., and Yoshida, K., 2014, Microdiamond discovered in the Seve Nappe (Scandinavian Caledonides) and its exhumation by the "vacuum-cleaner" mechanism: Geology, v. 42, n. 12, p. 1107–1110, https://doi.org/10.1130/G36108.1

McDowell, S. M., Miller, C. F., Fullagar, P. D., Bream, B. R., and Mapes, R. W., 2002, The Persimmon Creek Gneiss, eastern Blue Ridge, North Carolina–Georgia: Evidence for the missing Taconic arc?: Southeastern Geology, v. 41, n. 2, p. 103–117.

Merschat, A. J., and Hatcher Jr., R. D., 2007, The Cat Square terrane: Possible Siluro-Devonian remnant ocean basin in the Inner Piedmont, southern Appalachians, USA, *in* Hatcher Jr., R. D., Carlson, M. P., McBride, J. H., and Martínez Catalán, J. R., editors., 4-D Framework of Continental Crust: Geological Society of America Memoir 200, p. 553–565, https://doi.org/10.1130/2007.1200(27)

Merschat, A. J., Hatcher Jr., R. D., and Davis, T. L., 2005, The northern Inner Piedmont, southern Appalachians, USA: Kinematics of transpression and SW-directed mid-crustal flow: Journal of Structural Geology, v. 27, n. 7, p. 1252–1281, https://doi.org/10.1016/j.jsg.2004.08.005

Merschat, A. J., Hatcher Jr., R. D., Bream, B. R., Miller, C. F., Byars, H. E., Gatewood, M. P., and Wooden, J. L., 2010, Detrital zircon geochronology and provenance of southern Appalachian Blue Ridge and Inner Piedmont crystalline terranes, *in* Tollo, R. P., Bartholomew, M. J., Hibbard, J. P., and Karabinos, P. M., editors, From Rodinia to Pangea: The Lithotectonic Record of the Appalachian Region: Geological Society of America Memoir 206, p. 661–699, https://doi.org/10.1130/2010.1206(26)

Merschat, A. J., Bream, B. R., Huebner, M. T., Hatcher Jr., R. D., and Miller, C. F., 2017, Temporal and spatial distribution of Paleozoic metamorphism in the southern Appalachian Blue Ridge and Inner Piedmont delimited by ion microprobe U-Pb ages of metamorphic zircon, *in* Law, R. D., Thigpen, J. R., Merschat, A. J., and Stowell, H. H., editors, Linkages and Feedbacks in Orogenic Systems: Geological Society of America Memoir 213, p. 199–254, https://doi.org/10.1130/2017.1213(10)

Miller, B. V., Fetter, A. H., and Stewart, K. G., 2006, Plutonism in three orogenic pulses, Eastern Blue Ridge Province, southern Appalachians: GSA Bulletin, v. 118, n. 1–2, p. 171–184, https://doi.org/10.1130/B25580.1

Miller, B. V., Stewart, K. G., and Whitney, D. L., 2010, Three tectonothermal pulses recorded in eclogite and amphibolite of the Eastern Blue Ridge, southern Appalachians, *in* Tollo, R. P., Bartholomew, M. J., Hibbard, J. P., and Karabinos, P. M., editors, From Rodinia to Pangea: The Lithotectonic Record of the Appalachian Region: Geological Society of America Memoir 206, p. 701–724, https://doi.org/10.1130/2010.1206(27)

Min, K., Renne, P. R., and Huff, W. D., 2001, $^{40}Ar/^{39}Ar$ dating of Ordovician K-bentonites in Laurentia and Baltoscandia: Earth and Planetary Science Letters, v. 185, n. 1–2, p. 121–134, https://doi.org/10.1016/S0012-821X(00)00365-4

Moecher, D. P., Samson, S. D., and Miller, C. F., 2004, Precise time and conditions of peak Taconian granulite facies metamorphism in the Southern Appalachian Orogen, USA, with implications for zircon behavior during crustal melting events: The Journal of Geology, v. 112, n. 3, p. 289–304, https://doi.org/10.1086/382760

Neathery, T. L., 1968, Talc and anthophyllite asbestos deposits in Tallapoosa and Chambers Counties: Alabama: Geological Survey of Alabama Bulletin, v. 90, p. 98.

Neilson, M. J., and Stow, S. H., 1986, Geology and geochemistry of the mafic and ultramafic intrusive rocks, Dadeville belt, Alabama: GSA Bulletin, v. 97, n. 3, p. 296–304, https://doi.org/10.1130/0016-7606(1986)97<296:GAGOTM>2.0.CO;2

Neilson, M. J., Seal, T. L., and Kish, S. A., 1997, Two high-silica gneisses from the Dadeville Complex of Alabama's Inner Piedmont: Southeastern Geology, v. 36, n. 3, p. 123–132.

Osborne, W. E., Szabo, M. W., Copeland, J., Charles W., and Neathery, T. L., 1988, Geologic map of Alabama: Geological Survey of Alabama Special Map 221, scale 1:500,000.

Peterson, V., Ryan, J. G., and 1997–1998 Research Experiences for Undergraduates Site Program Participants, 2009, Petrogenesis and structure of the Buck Creek mafic-ultramafic suite, southern Appalachians: Constraints on ophiolite evolution and emplacement in collisional orogens: GSA Bulletin, v. 121, n. 3–4, p. 615–629, https://doi.org/10.1130/B26302.1

Pollock, J. C., Hibbard, J. P., and van Staal, C. R., 2012, A paleogeographical review of the peri-Gondwanan realm of the Appalachian orogen: Canadian Journal of Earth Sciences, v. 49, n. 1, p. 259–288, https://doi.org/10.1139/e11-049

Raymond, L. A., Merschat, A., and Vance, R. K., 2016, Metaultramafic schists and dismembered ophiolites of the Ashe Metamorphic Suite of northwestern North Carolina, USA: International Geology Review, v. 58, n. 7, p. 874–912, https://doi.org/10.1080/00206814.2015.1129515

Rehrer, J. R., ms, 2014, Characterizing the relationship of part of the Inner Piedmont and Pine Mountain window, Georgia, from detailed geologic mapping, geochemistry, geochronology, and structural analysis at the southwestern end of the Cat Square terrane: Knoxville, Tennessee, University of Tennessee, M. S. thesis, 196 p.

Sagul, D. A., ms, 2016, Constraining the age and petrogenesis of the Zana and Kowaliga gneisses, eastern Blue Ridge, Alabama: Gainesville, Florida, University of Florida, M. S. thesis, 150 p.

Seal, T. L., and Kish, S. A., 1990, The geology of the Dadeville Complex of the western Georgia and eastern Alabama Inner Piedmont: Initial petrographic, geochemical, and geochronological results, *in* Steltenpohl, M. G., Neilson, M. J., and Kish, S. A., editors, Geology of the southern Inner Piedmont, Alabama and southwest Georgia, Geological Society of America Southeastern section 39th Annual Meeting Fieldtrip Guidebook: Tuscaloosa, Alabama, Geological Survey of Alabama, p. 65–77.

Sears, J. W., Cook Jr., R. B., and Brown, D. E., 1981, Tectonic evolution of the western part of the Pine Mountain window and adjacent Inner Piedmont province, *in* Sears, J. W., editor, Contrasts in tectonic style between the Inner Piedmont terrane and the Pine Mountain Window: Alabama Geological Society 18th Annual Fieldtrip Guidebook, p. 1–13.

Sinha, A. K., Thomas, W. A., Hatcher Jr., R. D., and Harrison, T. M., 2012, Geodynamic evolution of the central Appalachian orogen: Geochronology and compositional diversity of magmatism from Ordovician through Devonian: American Journal of Science, v. 312, n. 8, p. 907–966, https://doi.org/10.2475/08.2012.03

Sláma, J., Košler, J., Condon, D. J., Crowley, J. L., Gerdes, A., Hanchar, J. M., Horstwood, M. S. A., Morris, G. A., Nasdala, L., Norberg, N., Schaltegger, U., Schoene, B., Tubrett, M. N., and Whitehouse, M. J., 2008, Plešovice zircon–A new natural reference material for U–Pb and Hf isotopic microanalysis: Chemical Geology, v. 249, n. 1–2, p. 1–35, https://doi.org/10.1016/j.chemgeo.2007.11.005

Spell, T. L., and Norrell, G. T., 1990, The Ropes Creek assemblage: Petrology, geochemistry, and tectonic setting of an ophiolitic thrust sheet in the Southern Appalachians: American Journal of Science, v. 290, n. 7, p. 811–842, https://doi.org/10.2475/ajs.290.7.811

Stacey, J. S., and Kramers, J. D., 1975, Approximation of terrestrial lead isotope evolution by a two-stage model: Earth and Planetary Science Letters, v. 26, n. 2, 207–221, https://doi.org/10.1016/0012-821X(75)90088-6

Steltenpohl, M. G., 2005, A primer on terranes of the southernmost Appalachians of Alabama and Georgia, *in* Steltenpohl, M. G., editor, New perspectives on southernmost Appalachian terranes, Alabama and Georgia: Alabama Geological Society 42nd Annual Fieldtrip Guidebook, p. 1–18.

Steltenpohl, M. G., Neilson, M. J., and Kish, S. A., 1990, Tectonometamorphic development in the southernmost Inner Piedmont terrane, Alabama, *in* Steltenpohl, M. G., Kish, S. A., and Neilson, M. J., editors, Geology of the southern Inner Piedmont, Alabama and southwest Georgia, Geological Society of America Southeastern section 39th Annual Meeting Fieldtrip Guidebook: Tuscaloosa, Alabama, Geological Survey of Alabama, p. 1–16.

Steltenpohl, M. G., Schwartz, J. J., and Miller, B. V., 2013, Late to post-Appalachian strain partitioning and extension in the Blue Ridge of Alabama and Georgia: Geosphere, v. 9, n. 3, p. 647–666, https://doi.org/10.1130/GES00738.1

Stevens, A., and Tull, J. F., 2017, Relationship between the Dadeville Complex and Opelika Group, Appalachian Inner Piedmont of Alabama and Georgia: Geological Society of America Abstracts with Programs, v. 49, n. 6, https://doi.org/10.1130/abs/2017AM-306857

Stewart, K. G., Adams, M. G., and Trupe, C. H., 1997, Paleozoic structural evolution of the Blue Ridge thrust complex, western North Carolina, *in* Stewart, K. G., Adams, M. G., and Trupe, C. H., editors, Paleozoic structure, metamorphism, and tectonics of the Blue Ridge of western North Carolina: Durham, North Carolina, Carolina Geological Society 1997 Field Trip Guidebook, p. 21–31.

Stow, S. H., Neilson, M. J., and Neathery, T. L., 1984, Petrography, geochemistry, and tectonic significance of the amphibolites of the Alabama Piedmont: American Journal of Science, v. 284, n. 4–5, p. 414–436, https://doi.org/10.2475/ajs.284.4-5.414

Sun, S. S., and McDonough, W. F., 1989, Chemical and isotopic systematics of oceanic basalts: Implications for mantle composition and processes, *in* Saunders, A. D., and Norry, M. J., editors, Magmatism in ocean basins: Geological Society, London, Special Publications, v. 42, p. 313–345, https://doi.org/10.1144/GSL.SP.1989.042.01.19

Swanson, S. E., and Veal, W. B., 2010, Mineralogy and petrogenesis of pegmatites in the Spruce Pine District, North Carolina, USA: Journal of Geosciences, v. 55, n. 1, p. 27–42, https://doi.org/10.3190/jgeosci.062

Tera, F., and Wasserburg, G. J., 1972, U-Th-Pb systematics in three Apollo 14 basalts and the problem of initial Pb in lunar rocks: Earth and Planetary Science Letters, v. 14, n. 3, p. 281–304, https://doi.org/10.1016/0012-821X(72)90128-8

Thomas, W. A., 1977, Evolution of Appalachian-Ouachita salients and recesses from reentrants and promontories in the continental margin: American Journal of Science, v. 277, n. 10, p. 1233–1278, https://doi.org/10.2475/ajs.277.10.1233

_______ 2006, Tectonic inheritance at a continental margin: GSA Today, v. 16, p. 4–11, https://doi.org/10.1130/1052-5173(2006)016[4:TIAACM]2.0.CO;2

Thompson, A. B., Schulmann, K., and Jezek, J., 1997, Extrusion tectonics and elevation of lower crustal metamorphic rocks in convergent orogens: Geology, v. 25, n. 6, p. 491–494, https://doi.org/10.1130/0091-7613(1997)025<0491:ETAEOL>2.3.CO;2

Tucker, R. D., 1992, U-Pb dating of Plinian-eruption ashfalls by the isotope dilution method: A reliable and precise tool for time-scale calibration and biostratigraphic correlation: Geological Society of America Abstracts with Programs, v. 24, n. 7, p. A198.

Tull, J. F., Barineau, C. I., Mueller, P. A., and Wooden, J. L., 2007, Volcanic arc emplacement onto the southernmost Appalachian Laurentian shelf: Characteristics and constraints: GSA Bulletin, v. 119, n. 3–4, p. 261–274, https://doi.org/10.1130/B25998.1

Tull, J. F., Barineau, C. I., and Holm-Denoma, C. S., 2012, Characteristics, extent, and tectonic significance of a Middle Ordovician back-arc basin in the southern Appalachian Blue Ridge, *in* Barineau, C. I., and Tull, J. F., editors, The Talladega slate belt and eastern Blue Ridge: Laurentian plate passive margin to back-arc basin tectonics in the southern Appalachian orogen: Alabama Geological Society 49th Annual Fieldtrip Guidebook, p. 12–26.

Tull, J. F., Holm-Denoma, C. S., and Barineau, C. I., 2014, Early to Middle Ordovician back-arc basin in the southern Appalachian Blue Ridge: Characteristics, extent, and tectonic significance: GSA, v. 126, n. 7–8, p. 990–1015, https://doi.org/10.1130/B30967.1

Tull, J. F., Mueller, P. A., Farris, D. W., and Davis, B. L., 2018, Taconic suprasubduction zone magmatism in southern Laurentia: Evidence from the Dadeville Complex: GSA Bulletin, v. 130, n. 7–8, p. 1339–1354, https://doi.org/10.1130/B31885.1

van Staal, C., Whalen, J. B., McNicoll, V. J., Pehrsson, S., Lissenberg, C. J., Zagorevski, A., Van Breemen, O., and Jenner, G. A., 2007, The Notre Dame arc and the Taconic orogeny in Newfoundland, *in* Hatcher Jr., R. D., Carlson, M. P., McBride, J. H., and Martínez Catalán, J. R., editors, 4-D Framework of Continental Crust: Geological Society of America Memoir 200, p. 511–552, https://doi.org/10.1130/2007.1200(26)

VanDervoort, D. S., ms, 2016, Geology of the Wadley South Quadrangle and geochronology of the Dadeville Complex, southernmost Appalachians of east Alabama: Auburn, Alabama, Auburn University, M. S. thesis, 127 p.

VanDervoort, D. S., Steltenpohl, M. G., and Schwartz, J. J., 2015, U-Pb ages from the Dadeville Complex, southernmost Appalachians, eastern Alabama: An accreted Taconic arc: Geological Society of America Abstracts with Programs, v. 47, n. 7, p. 159.

VanDervoort, D. S., Ma, C., Steltenpohl, M. G., and Schwartz, J. J., 2017, The early Paleozoic (Taconic) Dadeville arc complex, southernmost Appalachians of Alabama and Georgia: Implications for the crustal growth of eastern North America: Geological Society of America Abstracts with Programs, v. 49, n. 3, https://doi.org/10.1130/abs/2017SE-290572

Vermeesch, P., 2012, On the visualisation of detrital age distributions: Chemical Geology, v. 312–313, p. 190–194, https://doi.org/10.1016/j.chemgeo.2012.04.021

_________ 2018, IsoplotR: A free and open toolbox for geochronology: Geoscience Frontiers, v. 9, n. 5, p. 1479–1493, https://doi.org/10.1016/j.gsf.2018.04.001

Wiedenbeck, M., Allé, P., Corfu, F., Griffin, W. L., Meier, M., Oberli, F., von Quadt, A., Roddick, J. C., and Spiegel, W., 1995, Three natural zircon standards for U-Th-Pb, Lu-Hf, trace element and REE analyses: Geostandards Newsletter, v. 19, n. 1, p. 1–23, https://doi.org/10.1111/j.1751-908X.1995.tb00147.x

Wise, D. U., and Ganis, G. R., 2009, Taconic Orogeny in Pennsylvania: A ~15–20 m.y. Apennine-style Ordovician event viewed from its Martic hinterland: Journal of Structural Geology, v. 31, n. 9, p. 887–899, https://doi.org/10.1016/j.jsg.2008.03.011